

# POLITECNICO DI TORINO

Department of Mechanical and Aerospace Engineering (DIMEAS)

Master's degree in biomedical engineering



**Politecnico  
di Torino**

## **Design and characterization of an injectable hydrogels for cellular reprogramming**

### **Supervisors:**

Prof.ssa Valeria Chiono  
Prof.ssa Chiara Tonda-Turo

### **Correlator:**

Ph.D. Elena Marcello  
MSc Letizia Nicoletti

### **Candidate:**

Irene Guerriero

Academic year 2020/2021

## Acknowledgments

---

I would like to express my gratitude to my supervisor, Valeria Chiono, and co-supervisor, Chiara Tonda-Turo, for giving me the opportunity to do the master thesis with them and give my contribution to a big project as BIORECAR. Thank you for enriching this work by scientific and non-scientific contributions. A special thanks to my correlators, Elena Marcello and Letizia Nicoletti, for their constant guidance, the countless days spent in laboratory, the formal and informal meetings, and support throughout these months.

Thank you DIMEAS Lab, although the technical problems and burning issues experienced this year.

I would like to thank all the Cellular and Interdisciplinary laboratories members with whom I has the opportunity to work. They have welcomed me with familiarity and kindness from the start. Their logical assistance, advice and help in progress of this work were really important.

I would also like to thank my Master thesis colleagues, Francesca and Mimma, for the mutual support that we gave each other.

Special thanks to my friends spread throughout all over Italy and even the world, that are always by my side and give me reason to cheer.

I would like to thank my family, the strongest team I have ever seen play. No matter how fare we may be, we would always be close to each other's heart. I am thankful to you for strongly believe in me, but I have to say that I would not have been able to make it so far without you love, care, support, and every little or big things.

Thank you, Politecnico di Torino. Rather than saying goodbye to a period of my life that has meant so much for me, I will say thank you Politecnico of Turin for giving me the brain I need to keep expanding and the character I need to keep building.

## Abstract

---

During Myocardial infarction (MI), cardiomyocytes (CMs) irreversible death occurs, leading to the formation of a non-contractile fibrotic scar. To date, heart transplantation remains the only effective clinical therapy to restore heart function. An alternative promising strategy is the use of injectable hydrogels as minimally invasive systems for the release of bioactive agents for cardiac repair. *In situ* release of specific micro-RNAs (miRNAs) has been previously found to trigger direct reprogramming of human cardiac fibroblasts (CFs) into CMs, favoring heart regeneration.

Alginate-based injectable hydrogels are widely used in biomedical applications thanks to their promising results in supporting cardiac regeneration. However, alginate (ALG) presents some limitations such as low degradability *in vivo* and poor cell adhesion. Partial oxidation of ALG chains can overcome these drawbacks, leading to the formation of alginate dialdehyde (ADA). Specifically, through Schiff-base reaction, ADA can form covalent bonds with bioactive molecules containing amino groups, such as gelatin (GEL).

In this thesis project, an injectable ADA-GEL crosslinked hydrogel was designed for *in situ* controlled delivery of miRNAs-loaded nanoparticles (NPs), to mechanically sustain damaged myocardium and promote heart regeneration. The goal was to select an ADA-GEL hydrogel composition with biomimetic stiffness and injectable properties.

ADA was synthesized by ALG oxidation using sodium metaperiodate, obtaining an average degree of oxidation of 23% (mol%) and average yield of production of 68% (wt%). Chemical ADA-GEL crosslinking through Schiff-base formation was evaluated by mixing ADA and GEL at five different ratios (w/w%) (50:50, 70:30,

80:20, 90:10, 95:5). Due to the low crosslinking degree of the blend systems, hindering gel formation, calcium-Alginate ( $\text{Ca}^{2+}$ -alg) particles were used as ionic crosslinking agent. Different types of insoluble  $\text{Ca}^{2+}$ -alg particles were prepared by precipitation of an alginate solution (with final concentration of 0.05% w/v) by slowly adding a  $\text{CaCl}_2$  solution with four different molarities (3,4,5 or 6 M). Subsequently, ionically-crosslinked ADA hydrogels with a final polymer (ADA/ $\text{Ca}^{2+}$ -alg) content of 4 or 6% w/v were prepared by mixing a suspension of  $\text{Ca}^{2+}$ -alg particles with a solution of ADA. Through rheological characterization, the sample with 2% w/v ADA and 4% w/v  $\text{Ca}^{2+}$ -alg (obtained with 6M  $\text{CaCl}_2$  solution) was identified as optimal to develop injectable hydrogels with viscoelastic properties resembling those of the cardiac tissue.

DE-DOPE/PLGA-miRNA complexes (here defined as NPs) recently developed at Politecnico di Torino, were loaded into the ionically-crosslinked ADA hydrogels at a concentration of 13,4  $\mu\text{g}/\text{ml}$ . A controlled and prolonged release of miRNA, evaluated by Qubit fluorometric quantification, was confirmed reaching 100% of release after 9 days of incubation.

Optimization of GEL incorporation into the ADA- $\text{Ca}^{2+}$ -alg system was investigated by developing hydrogels with ADA:GEL composition of 90:10 and 80:20 (w/w%), maintaining the final polymer concentration constant at 6% w/v . Through preliminary rheological analysis, the 80:20 ratio was identified as the most appropriate to replicate the mechanical properties of the optimized ADA –  $\text{Ca}^{2+}$ -alg hydrogels.

Future studies will include the testing of *in vitro* cytocompatibility and direct reprogramming ability *in vitro*.

The work is part of BIORECAR ERC project (contract nr: 772168, [www.biorecar.polito.it](http://www.biorecar.polito.it)).

## Abbreviations

---

ADA	Alginate di-aldehyde
ALG	Alginate
ATR-FTIR	Attenuated Total Reflection - Fourier Transform Infrared Spectroscopy
Ca <sup>2+</sup> -Alg	Calcium – Alginate
CMs	Cardiomyocytes
CTE	Cardiac Tissue Engineering
DLS	Dynamic Light Scattering
ECM	Extra cellular matrix
ELS	Electrophoretic Light Scattering
FBs	Fibroblasts
GEL	Gelatin
HF	Heart failure
IS	Indicator solution
MI	Myocardial infarction
NMR	Nuclear Magnetic Resonance
NPs	Nanoparticles
SS	Stock solution
UV	Ultraviolet

## Contents

---

<b>I. INTRODUCTION.....</b>	<b>11</b>
1.1. MYOCARDIAL REGENERATIVE MEDICINE .....	11
1.1.1. Myocardial infarction: the clinical problem.....	11
1.1.2. Myocardial regeneration and repair .....	14
1.1.2.1. Cell-based therapies.....	15
1.1.2.2. Cell-free therapies.....	20
1.1.2.2.1. Endogenous cardiomyocyte proliferation.....	22
1.1.3. Cardiac tissue engineering (CTE): a biomaterial-based approach.....	26
1.1.3.4. Bioactive nanocarriers .....	27
1.1.3.1. Cardiac patches.....	30
1.1.3.2. Hydrogels .....	31
1.2.1.2. Cell-laden hydrogels.....	32
1.2.1.3. Injectable hydrogel-based gene delivery systems.....	33
1.2. HYDROGELS .....	35
1.2.1. Hydrogels for cardiac tissue repair.....	35
1.2.1.1. Acellular hydrogels.....	36
1.2.1.2. Cell-laden hydrogels.....	37
1.2.1.3. Injectable hydrogel-based gene delivery systems.....	38
1.2.2. Composition of injectable hydrogels .....	39
1.2.2.1. Chitosan.....	40
1.2.2.2 Fibrin .....	40
1.2.2.3. Decellularized ECM .....	41
1.2.2.4. Collagen.....	42
1.2.2.5. Gelatin .....	42

1.2.2.6. Alginate .....	44
1.3 ALGINATE IN CARDIAC REGENERATION.....	44
1.3.1. <i>Promising properties of alginate</i> .....	44
1.3.2. <i>Algisyl LVR</i> .....	47
1.3.3 <i>IK-5001</i> .....	49
1.3.4. <i>Commercial alternatives: VentriGel</i> .....	51
1.3.3. <i>Oxidized alginate (OA)</i> .....	52
1.4 THYMOSIN $\beta$ 4.....	56
1.4.1. <i>THYMOSIN B4 FOR CARDIAC APPLICATIONS</i> .....	56
<b>II. AIM OF THE WORK.....</b>	<b>60</b>
<b>III. MATERIALS AND METHODS .....</b>	<b>63</b>
3.1. MATERIALS .....	63
3.2. METHODS .....	63
3.2.1. <i>Alginate dialdehyde formulation protocol</i> .....	63
3.2.2. <i>Characterization of oxidized alginate</i> .....	64
3.2.2.1. Yield of production.....	64
3.2.2.3. Determination of the degree of oxidation .....	66
3.2.2.4. FTIR Analysis .....	68
3.2.2.5. NMR Analysis .....	69
3.2.3. <i>ADA/GEL hydrogel formulation</i> .....	70
3.2.3.1. Chemical crosslinking .....	70
3.2.3.2. Ionic crosslinking .....	71
3.2.3.2.1. $\text{Ca}^{2+}$ -Alg preparation .....	71
3.2.3.2.2. Alginate/ADA and $\text{Ca}^{+}$ -Alg formulation .....	73
3.2.3.2.3. <i>ADA/GEL</i> .....	75
3.2.4. <i>NPs-loaded hydrogel formation</i> .....	76
3.2.5. <i>Hydrogel characterization</i> .....	78
3.2.4.1. Oscillatory rheological measurements.....	78
3.2.4.3. Swelling and degradation study .....	80
3.2.4.4. NPs release from NPs-loaded hydrogels.....	80

3.2.4.5. miRNA release from NPs-loaded hydrogels.....	81
<b>IV. RESULTS AND DISCUSSION .....</b>	<b>83</b>
4.1. OXIDATION OF SODIUM ALGINATE .....	83
4.1.1. Oxidation degree and molecular weight of the modified alginate.....	83
4.1.2. Yield of ADA production.....	87
4.1.2. Formation of aldehyde groups.....	88
4.2. CHEMICALLY CROSSLINKED HYDROGELS.....	91
4.2.1. ADA/GEL hydrogels.....	91
4.3. IONICALLY CROSSLINKED HYDROGELS .....	96
4.3.1. Gelation mechanism and Ca <sup>2+</sup> -Alg particles preparation.....	96
4.3.2. ALG/ Ca <sup>2+</sup> -Alg hydrogels .....	100
4.3.3. ADA/ Ca <sup>2+</sup> -Alg hydrogels.....	104
4.4. NPS-LOADED HYDROGELS .....	109
4.4.1. NPs formation.....	109
4.4.2. In vitro stability studies .....	110
4.4.3. In vitro NPs release .....	111
4.4.4. In vitro miRNA release .....	112
4.5. OPTIMIZATION OF IONICALLY CROSSLINKED ADA/CA <sup>2+</sup> -ALG HYDROGELS....	114
4.5.1. Rheological characterization.....	115
4.5.2. In vitro swelling and degradation study .....	118
4.4. IONICALLY CROSSLINKED ADA/GEL HYDROGEL .....	120
<b>V. CONCLUSION .....</b>	<b>126</b>
<b>VI. FUTURE PERSPECTIVES .....</b>	<b>129</b>
<b>VII. BIBLIOGRAPHY .....</b>	<b>131</b>



# I. INTRODUCTION

---

## 1.1. Myocardial Regenerative Medicine

### *1.1.1. Myocardial infarction: the clinical problem*

Cardiovascular diseases (CVDs) are a set of pathologies that affect both the heart and blood vessels, thereby including coronary artery disease (CAD), that can evolve in an acute coronary syndrome (ACS), and coronary heart disease (CHD).<sup>1</sup>

CAD indicates the pathologic process affecting the coronary arteries (usually atherosclerosis) while CHD is a consequence of CAD and includes the diagnoses of myocardial infarction (MI).<sup>1</sup> MI is one of the main causes of mortality and morbidity worldwide: approximately 1.5 million cases occur annually in the US and it is associated with a 30% mortality rate and about 50% of the deaths occur prior to arrival at the hospital.<sup>2</sup>

From a pathologic perspective, MI is defined as cardiomyocyte irreversible death caused by an ischemic insult: a decrease or interruption of blood flows to the cardiac district causes cell necrosis. The first histological changes are diminished cellular glycogen, relaxed myofibrillis and sarcolemmal disruption, followed by mitochondrial abnormalities.<sup>3</sup>

Recently, the quantification of specific biomarkers, such as cardiac troponins, was introduced to detect cardiomyocytes death.<sup>4</sup> Cardiac troponin I (cTnI) and T (cTnT) are components of the contractile apparatus of myocardial cells and are expressed almost exclusively in the heart.<sup>3</sup> Myocardial injury is characterized by an increase of the blood levels of cTn above the 99th percentile upper reference limit (URL). However, elevated cTn values can also be associated to non-ischemic cardiomyocytes death, caused by some specific pathological conditions such as

chronic heart failure, renal failure or myocarditis, and to other causes including an increased cell wall permeability and the normal turnover of cardiomyocytes.<sup>4</sup>

For this reason, it is not clinically possible to identify the triggering mechanism. Anyway, when an acute myocardial injury is caused by myocardial ischaemia, a diagnosis of acute MI is appropriate.<sup>3</sup>

The Universal Definition of Myocardial Infarction (UDMI) classifies MI into 5 subtypes, of which type 1 and type 2 MI are the most common and relevant to practicing clinicians. Type 1 MI is caused by acute atherothrombotic mechanisms and type 2 MI is the consequence of a myocardial oxygen supply/demand mismatch. In particular, type 1 MI (76.4%) is much more prevalent than type 2 MI (23.6%).<sup>5,6</sup>

As the mammalian heart exhibits a minimal regenerative capacity, cardiac repair is characterized by the clearance of dead cardiomyocytes and by the formation of a collagen-based scar. The healing of the infarcted myocardium involves three distinct but overlapping phases: the inflammatory, the proliferative and the maturation phase (Figure 1.1). In all these phases, a crucial role is played by the dynamic changes in the extra cellular matrix (ECM) composition and the main effectors are fibroblasts, that are much less susceptible to ischemic injury.<sup>7,8</sup>

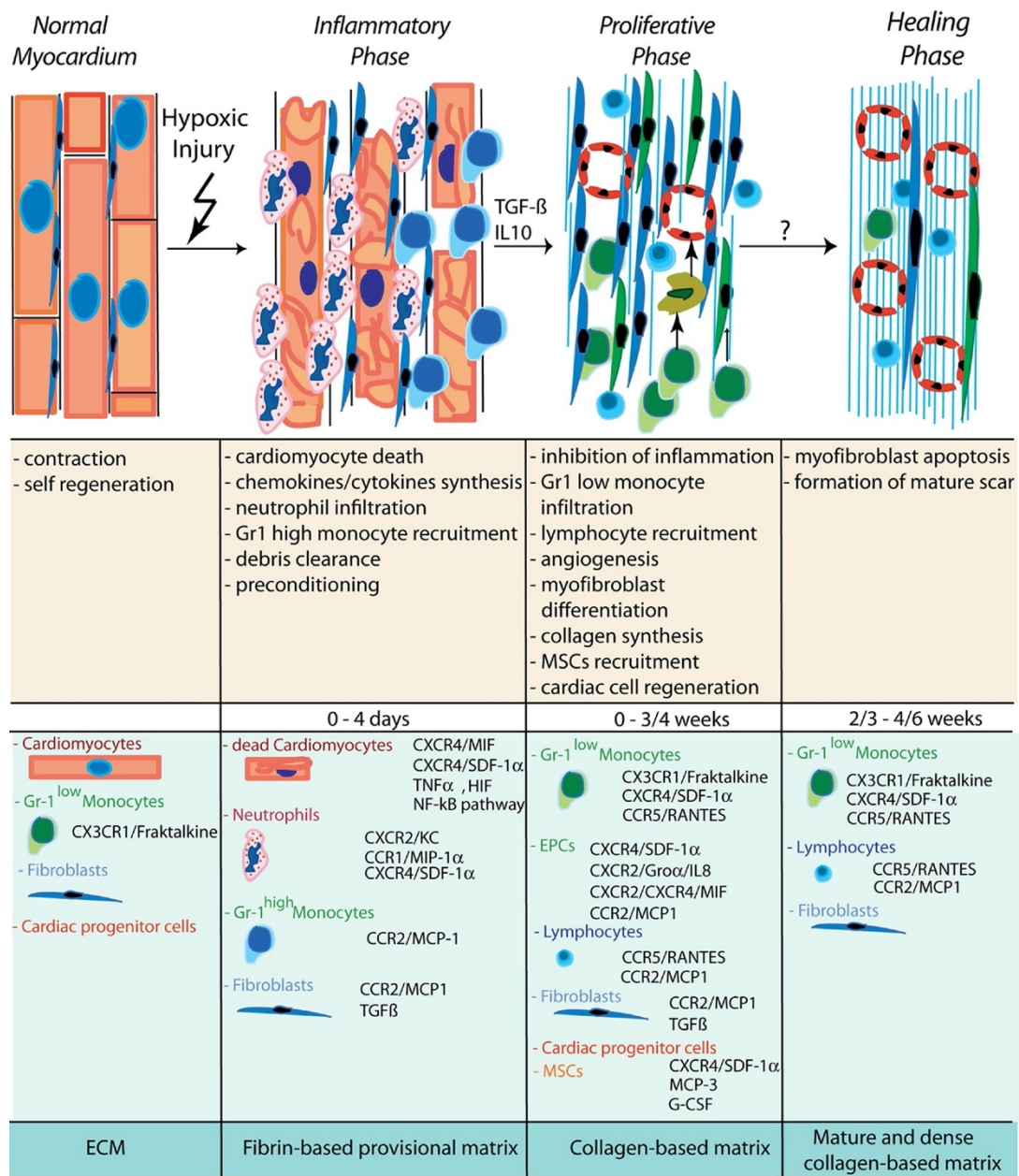


**Figure 1.1.** Phases of cardiac healing after myocardial infarction (MI): cellular and molecular events.

Source: Liehn, E.A. et al. / *Journal of the American College of Cardiology* 2011;23(58):2357-62.

During the first phase, the injured cells and the damaged ECM release signal substances called danger-associated molecular patterns (DAMPs), that are able to induce a pro-inflammatory phenotype in fibroblasts. They act as an important source of chemokines and cytokines to recruit circulating leukocytes (neutrophils and mononuclear cells), that clear the necrotic tissue.<sup>9</sup> The clearance of the infarcted area determines the release of anti-inflammatory mediators, marking the transition to the

proliferative phase. The dominant cells during this phase are phenotypically modulated fibroblasts called myofibroblasts, that migrate to the infarct border zone and secrete large amounts of structural ECM proteins.<sup>7,8</sup>

The apoptosis of the majority of the reparative cells marks the beginning of the maturation phase, in which a non-contractile fibrous scar, not containing cardiomyocytes, is formed to avoid fatal cardiac rupture.

During the entire process of infarct healing, a “post-infarction ventricular remodeling” occurs, consisting in the hypertrophy of the non-infarcted segments and the dilation and increased sphericity of the ventricle. The remodeling process worsens cardiac dysfunction, eventually leading to fatal heart failure (HF), where the heart is not capable of generating sufficient cardiac output to meet the body tissues needs (Figure 1.2).<sup>10,11</sup>

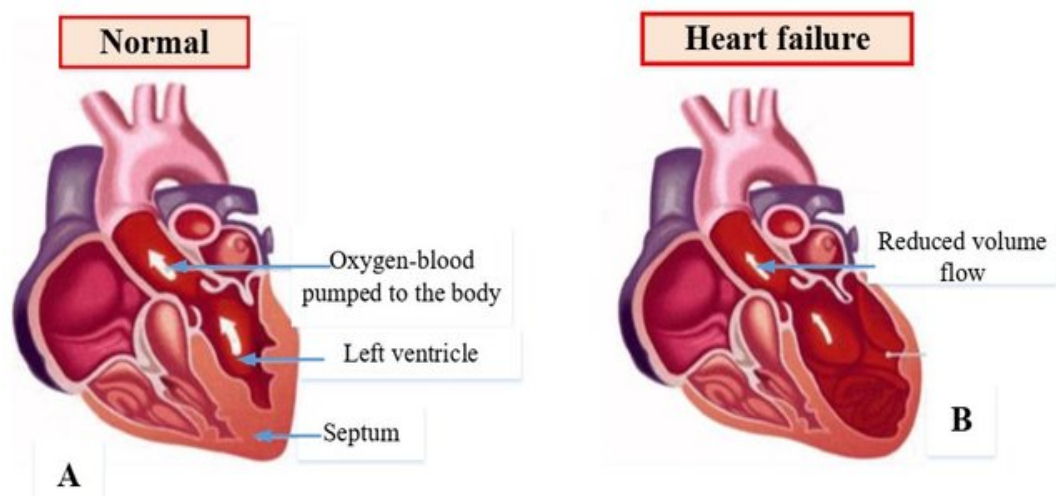


**Figure 1.2.** Normal and heart failure condition.  
*Source: Junejo, Ar et al. / IEEE, 2019; 7:120315-25.*

### 1.1.2. Myocardial regeneration and repair

Traditional therapies for myocardial regeneration are focused on preventing or delaying the progression of HF. These therapies comprise pharmacotherapy and the use of medical devices such as left ventricular assist devices (LVADs) and cardiac

resynchronization therapy with a pacemaker. The former aims at targeting the remodeling process in the failing heart and includes inhibitors of the renin-angiotensin system, the mineralocorticoid receptor, the sympathetic nervous system, and, most recently, the natriuretic system. The latter are used to treat the advanced remodeled heart at end-stage HF.<sup>10</sup> Although these therapies are capable of improving patients' quality of life, they do not restore the cardiac tissue and therefore are not able to stop the progression of HF. Nowadays, the only curative therapeutic option is heart transplantation, but it is limited by the restricted availability of donor organs and the need of an anti-rejection immunosuppressive therapy for the rest of the patient's life. As a result, there is an urgent need to identify alternative effective methods to regenerate the damaged myocardium.<sup>11</sup>

Several therapeutic approaches based on regenerative medicine techniques are under investigation, involving the administration of cells, growth factors, drugs or reprogramming factors. Recently, these therapeutical agents have been investigated in combination with biomaterial-based tissue engineering to increase the efficiency of the treatments, a combined use with, showing significant potential. To date, clinical efforts towards cardiac regeneration have focused on cell-based therapies, while methods for augmentation of intrinsic repair and cell reprogramming are under investigation in preclinical animal models.

#### *1.1.2.1. Cell-based therapies*

Cell-based therapies are characterized by the use of living cells as drug product to be delivered. Living cells are complex entities, capable of integrating signals from the surrounding environment and answering to the received inputs; hence, their use as therapeutic agents brings more benefits than small molecules and biologics.<sup>12</sup>

After myocardial infarction, cell delivery is used to stimulate cardiac regeneration, in order to achieve three main goals: (i) restore perfusion and

nutrient supply; (ii) restore lost cardiomyocytes and contractility; (iii) consequently, restore heart function.<sup>13</sup>

The way through which the cells are delivered to the myocardium determines their retention *in situ* and, in turn, the efficiency of the therapy. The delivery methods are three (Figure 1.3):

- (i) Intravenous administration (IV), which is the easiest and least invasive one but has shown poor cardiac engraftment since the delivered cells are infused directly into the circulation. This method can be effective only for cells capable of getting out of the bloodstream and home to the heart.<sup>13</sup>
- (ii) Intracoronary administration (IC), which is able to deliver the cells into perfused areas but not in the ischemic, non-perfused one. However, because of its feasibility, IC injection is the most common route.
- (iii) Intramyocardial injection (IM), that can be made during open heart surgeries or through mini-thoracotomies. This is the best method for supporting cardiac engraftment, as it is associated with a 11% retention rate, while IC and IV present rates of 3%.<sup>14</sup>

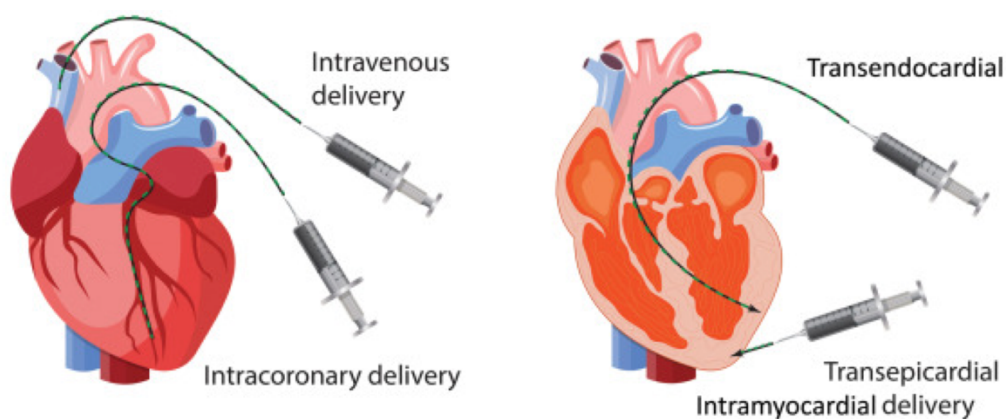


**Figure 1.3.** Route of cardiac administration.

Source: Parajuli, S.P. et al. / *Emerging technologies for Heart Disease*, 2020; 2:725-738

To optimize cell-based therapies, cell sources capable of yielding mature and functional cardiomyocytes (CMs) should be used.

First-generation cell-based therapies involved noncardiac cells, which include:

- Skeletal myoblasts: they were the first cells used because of their availability from autologous sources and their ability to proliferate *in vitro* and to regenerate skeletal muscle after an injury. Although animal and initial clinical trials showed positive effect, long-term follow-up studies showed unsuccessful results, as the skeletal myoblasts neither differentiate into CMs, nor integrate electromechanically with them.<sup>10,15</sup>
- Bone marrow mononuclear cells (BMMNCs): they represent the first stem cell population employed in clinical trials. The potential efficacy of therapies based on BMMNCs has not been assessed, because different trials showed controversial results.<sup>10</sup>
- Mesenchymal stem cells (MSCs): these stromal cells can be isolated from various tissues, such as bone marrow or adipose tissue, and *in vitro* studies have shown their capacity for self-renewal and multipotent differentiation into a wide variety of cells, including cardiomyocytes. Several preclinical studies demonstrated that these cells improved cardiac function when transplanted into the fibrotic tissue, but outputs from clinical trials were contradictory.<sup>16</sup>

The next generation of cell-based therapies uses resident cardiac stem cells (CSCs). This population of non-cardiomyocytes are undifferentiated cells but with multipotent capacity, since they can differentiate *in vitro* into cardiomyocytes, endothelial and smooth muscle cells. Transplantation of CSCs into ischemic myocardium has shown improved heart function, in terms of reduction in myocardial remodeling and increased formation of large blood vessels. However, their usage is limited by their poor numbers in the myocardium.<sup>13</sup>

Nevertheless, CSCs have a limited capacity to differentiate into cardiomyocytes once transplanted into the myocardium. For this reason, current research has been focused on the use of pluripotent stem cells to be differentiated *in vitro* CMs, which can be subsequently transplanted *in vivo*.<sup>10</sup>

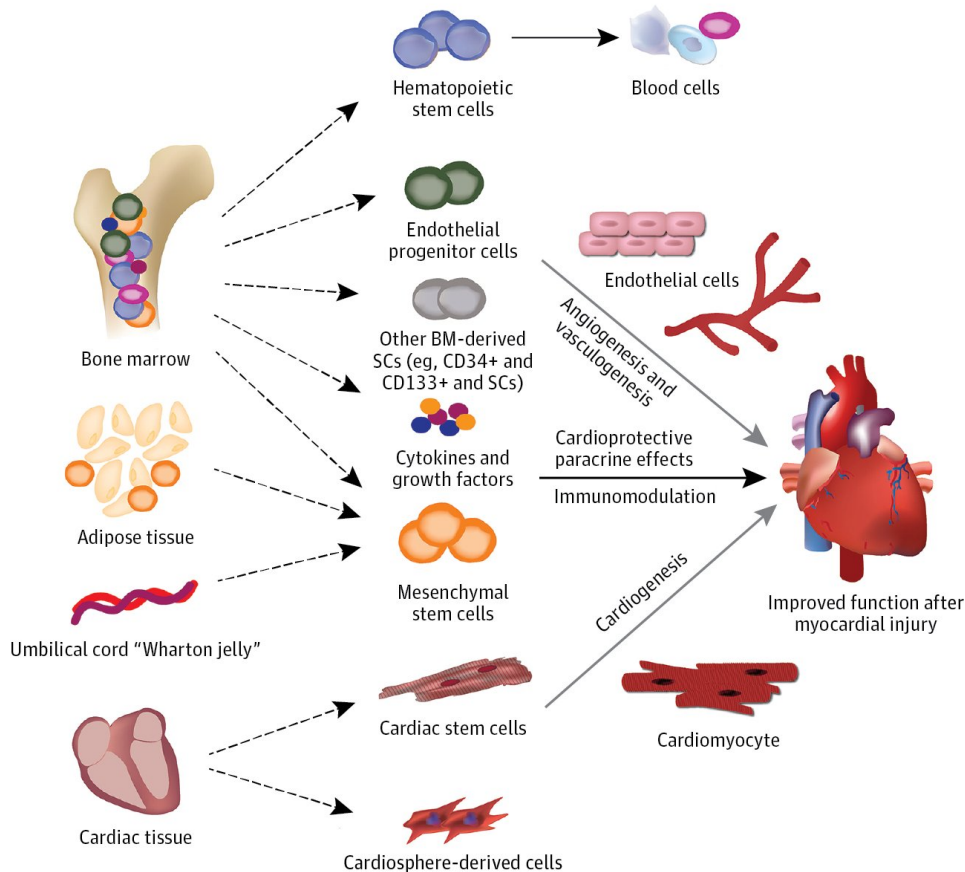


**Figure 1.4.** Adult stem cell therapy.

Source: Nguyen, P.K. et al. / *JAMA Cardiol.* 2016;1(7):831-841.

The investigated pluripotent stem cells for cardiac regeneration are:

- Human embryonic stem cells (hESCs): although their low retention rate in the injured heart, usage of ESC-derived cardiomyocytes in animal models showed beneficial effects, since they were electrically coupled to the resident cardiomyocytes. However, in non-human primates arrhythmic complications come up.<sup>17</sup> Moreover, ESCs are associated

with ethical concerns, the need of a lifelong immunosuppression and the risk of tumorigenesis.<sup>10</sup>

- Induced pluripotent stem cells (iPSCs): usage of iPSCs may overcome two important limitations of ESCs, the ethical issues and graft rejection by the patient's immune system. iPSCs are considered less immunogenic since they are derived from somatic cells, which could be autologous to the patient.<sup>18</sup> iPSCs have been tested in different animal models of MI. In pigs and mice models, showing restoration of cardiac function and improved left ventricular remodeling, despite the retention rate was low.<sup>15</sup> In immunosuppressed macaques, iPSCs improved the contractile function and their retention rate was significantly higher than the one recorded in other animal models, but ventricular tachycardias were observed, which could be due to immature cardiomyocytes.<sup>16</sup> Ongoing studies are investigating the production of more mature and pure cardiac cells from iPSCs, in order to increase the number of engrafted cells and overcome the risk of tumorigenesis and arrhythmias.<sup>16</sup>

Regardless of the type of cells used, very few transplanted cells are retained in the tissue and contribute to regenerate the myocardium via transdifferentiation, since usually 95-99% of therapeutic cells are lost within the first 24h after the delivery. Therefore, to justify the positive results observed, researchers assumed that the bioactive signalling molecules secreted by the cells are the real engine behind cardiac regeneration.<sup>18</sup> This is the so called “paracrine hypothesis”, which suggests that the secreted soluble factors eventually induce processes such as myocardial protection, activation or amplification of endogenous repair processes, neovascularization, and cardiac remodeling.<sup>15,18</sup>

### 1.1.2.2. Cell-free therapies

Taking advantage of the “paracrine hypothesis”, an opposing strategy to cell injection is based on the direct administration of bioactive signaling molecules.<sup>15,18</sup>

The three most used classes of secretory factors are:

- Growth factors (GFs): among GFs, some cardiac-regenerating inducers are insulin-like GF 1 (IGF-1), able to delay cellular aging and to promote cell survival, and vascular endothelial GF (VEGF), which reduces the infarct size post-MI in animal models but not in the clinical ones. Another GF with a regenerative potential is neuregulin 1 (NRG1), whose administration activate of the ERBB2/ERBB4 signaling pathway, which induces CM proliferation. However, although pre-clinical cases were promising, in clinical cases the results were inconsistent.<sup>18</sup> This could be explained by the low amount of therapeutic molecules at the target sites due to inefficient delivery or fast elimination of GFs. To overcome this limitation without the usage of higher amounts of GFs, proper delivery vehicles as scaffolds have been used.<sup>18</sup>
- MicroRNAs: miRNAs are highly conserved, single-strand, small non-coding RNAs that regulate gene expression post-transcriptionally by annealing with complementary sequences of mRNAs (Figure 1.5).<sup>10</sup> Numerous studies have connected miRNAs and various cardiovascular diseases, showing that miRNA expression levels are altered in MI and HF. Therefore, in the last decade miRNAs have become a therapeutic target for the treatment of MI: some of them, such as miR-199a-3p and miR-590-3p, are able to promote CMs proliferation, while others affect other target processes associated with MI, including inflammation.<sup>18</sup> For instance, a “miRNA combo” (constituted by miR-1, miR-133, miR-208 and miR-499) was reported to convert cardiac fibroblasts into

functional cardiomyocyte-like cells, both *in vitro* and *in vivo*.<sup>19</sup> Even though miRNAs are normally detected outside the cell in body fluids, circulating miRNAs are at risk to be cleaved by specific enzymes. Hence, a proper vehicles to deliver and protect miRNAs is needed, such as a hydrogel scaffold.<sup>18</sup>

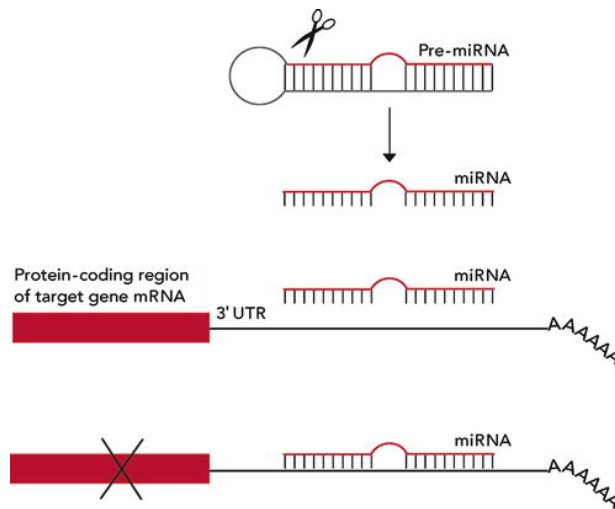


**Figure 1.5.** miRNA silencing mechanism.

Source: Dubitzky, W. et al. / *Encyclopedia of Systems Biology*. 2013.

- Exosomes: exosomes are small extracellular vesicles (30–100 nm diameter) that are secreted by many cell types, including stem cells, and contain various cargos such as RNAs, lipids, or proteins. Exosomes have a role in cell-cell communication among cardiac cells, hence their usage could promote cell survival, reduce inflammation and decrease oxidative stress *in vitro* and *in vivo*. In addition to these cardioprotective properties, the possibility to load exosomes with therapeutic factors supports their use as biological vehicle for clinical application.<sup>10,18</sup>

Taking advantage from transcriptomic analysis, a novel approach to replace lost CMs is to use cell-free therapies with the aim of inducing endogenous CMs proliferation or performing direct reprogramming of fibroblasts into CMs.<sup>10</sup>

#### *1.1.2.2.1. Endogenous cardiomyocyte proliferation*

Another way to restore heart functionality is the activation of endogenous regeneration potentials. Mammalian cardiomyocytes are terminally differentiated cells, which have already exited the cell-cycle: self-renewal occurs at a rate of 1% per year for adults aged 25 years, which decreases to 0.45% by 75 years. Therefore, the possibility of stimulating cardiac proliferation represents a promising tool to repair mammalian postnatal hearts.

A first approach is to control the expression of specific cell-cycle regulators. In fetal cardiomyocytes cell division is promoted by several cyclin-dependent kinases (CDKs), whose expression is inhibited postnatally by the upregulation of the transcription factor MEIS1. Therefore, the inhibition of MEIS1 and, accordingly, the overexpression of CDKs are capable of reactivating the cell cycle in adults.<sup>16,20</sup>

A second approach is the modulation of the oxidative stress. After birth, the heart undergoes a dramatic change in oxygenation state and a subsequent switch from glycolytic to oxidative metabolism occurs. As a consequence, reactive oxygen species (ROS) production in mitochondria increases and increased ROS level induces the activation of the DNA damage response (DDR) pathway, which is responsible for cell-cycle arrest of postnatal cardiomyocytes. Therefore, ROS scavenging triggers the inhibition of the DDR pathways, thus inducing cardiomyocyte proliferation and cardiac repair. To decrease ROS level, a stepwise exposure to systemic hypoxia can be performed.<sup>16</sup>

Thus, stimulation of endogenous regenerative capacity of resident cardiomyocytes may be a promising method to improve cardiac function after MI.<sup>16,20</sup>

#### 1.1.2.2.2. Conversion of endogenous fibroblasts into induced cardiomyocytes

In the last decade, researchers started to investigate the possibility to convert resident cardiac fibroblasts to cardiomyocytes by direct reprogramming, which may be a game changer for heart regeneration.

Cardiac fibroblasts (CFs) account for up to 50% of all cardiac cells and are completely differentiated somatic cells, without cardiogenic potential. Indeed, CFs provide structural support, secrete biochemical signals and contribute to scar formation upon cardiac damage. After MI, CFs expand and constitute the majority of the cells in the injured zone, and they are the main players in fibrosis. Therefore, reprogramming CFs into cardiomyocytes would greatly contribute to the overall contractility of the heart.<sup>21</sup>

In addition, CFs offer other therapeutical advantages. Firstly, skipping the pluripotent intermediate stage would lower the risk of tumor formation. Secondly, patient-derived fibroblasts can be collected via biopsy, grown *in vitro* and delivered successively to damaged heart. Lastly, the direct reprogramming of the scar tissue by means of defined factors can contribute to the overall contractility of the cardiac muscle.<sup>21</sup>

The first step towards this new approach was the direct reprogramming of mouse fibroblasts *in vitro* in 2010. This result was achieved forcing the expression of a combination of three genes encoding developmental transcription factors: Gata4, Mef2c and Tbx5, a cocktail referred to as GMT. Thereafter, GMT was also demonstrated *in vivo* and the results were improved when Hand2 was added, obtaining a cocktail defined as GHMT.<sup>19</sup> To translate the reprogramming approaches to the clinic, GMT or GHMT were tested *in vitro* on human cells. Srivastava *et al.* discovered that direct cardiac reprogramming in human fibroblasts is more challenging than in murine ones, because a longer time is needed to obtain cardiomyocytes and most of the induced cardiomyocytes are not completely mature, but in a

partially reprogrammed state. Therefore, these cocktails are not enough to obtain reprogramming, and additional factors are required to successfully induce a shift towards a cardiac phenotype, such as *Esrrg*, *Mesp1*, *Myocd* and *Zfp192*.<sup>19</sup> Human reprogrammed cardiomyocyte-like cells showed a similar gene expression profile to cardiomyocytes and exhibited sarcomere structure and spontaneous calcium fluxes, which is associated with the contractile activity.<sup>10</sup>

The second documented method for converting CFs into CMs both *in vitro* and *in vivo* is the delivery of “miRNA combo”, also known as “miR combo” (described in paragraph 1.2.2.).<sup>22</sup>

Currently, both GMT/GHMT and “miR combo” are delivered *in vivo* through either lenti- or retro-viruses and each virus brings an individual reprogramming factor. However, this approach presents several drawbacks such as the different expression ratios between each reprogramming factor in every transduced fibroblast and the inability to control cellular targeting, since they infect any dividing and proliferating cell. Moreover, there is a potential for immunogenicity. For this reason, there is the need of a relatively safe gene delivery method. In that regard, adeno-associated viruses (AAV) have recently emerged as alternative and promising vectors for gene therapy, since they possess low immunogenicity and non-pathogenicity.<sup>22</sup> but an alternative virus-free method was found to be effective on the transdifferentiation to cardiomyocyte-like cells: a combination of nine small molecules, known as 9C (9C: CHIR99021, A83-01, BIX01294, AS8351, SC1, Y27632, OAC2, SU16F, and JNJ10198409), with up to 97% of the reprogrammed cells spontaneously beating.<sup>19</sup>

On the other hand, Ding and his groups found an alternative virus-free method to successfully transdifferentiate human somatic cells into cardiomyocyte-like cells- This virus-free method consists of a combination of nine small molecules, known as 9C (9C: CHIR99021, A83-01, BIX01294, AS8351, SC1, Y27632, OAC2, SU16F, and JNJ10198409),

with up to 97% of the reprogrammed cells spontaneously beating.<sup>10,19</sup> Compared to transcription factors and miRNAs, small molecules presents several advantages *in vitro*, such as better temporal control and more efficient cell delivery. Moreover, they are non-immune, safer, and cheaper. However, once they enter inside the body, they can spread to other organs with ambiguous influence. Therefore, biomaterials should be combined to help and control local delivery of multiple drugs.<sup>10</sup>

Currently, direct reprogramming *in vivo* has been performed only on mice delivering the reprogramming cocktails through a retrovirus.<sup>10</sup> Interestingly, *in vivo*-generated cardiomyocyte-like cells seem to mimic endogenous cardiomyocytes better than their cultured counterparts. This result was probably due to the exposition to a physiological microenvironment, including electromechanical stimulation and interactions with neighboring cells.<sup>10</sup>

Additionally, Qian *et al.* demonstrated that a co-injection of the protein thymosin  $\beta$ 4 and GMT can increase the migration ability of fibroblasts to the site of injection, resulting in an improved ejection fraction and a reduced scar formation.<sup>23</sup>

Although direct reprogramming *in vivo* improves cardiac function after MI in mice, several challenges still remain to be addressed before clinical application, such as the low reprogramming efficiency, the immaturity and heterogeneity of induced cardiomyocyte-like cells, and the lack of a delivery method without side-effects. AAV vectors and small molecules present some limitations. AAV vectors have a limited capacity that restricts their application for multiple genes, while small molecules can enter the blood and spread to other organs with unclear impact. It is therefore necessary to develop novel biomaterials to enable local delivery of multiple drugs in a controllable way.<sup>16,19</sup>

### *1.1.3. Cardiac tissue engineering (CTE): a biomaterial-based approach*

Both cell-based therapies and cardiac regenerating agent delivery have shown promising results, but their delivery presents several challenges. Therefore, efforts have been made to optimize their delivery to a specific site, for the whole duration of the therapy, in a suitable environment.

The use of biomaterials as a three-dimensional scaffold have been the basis of tissue engineering (TE) and this set a new scenario in the field of regenerative medicine. For this reason, recently cardiac tissue engineering (CTE) has emerged as a prospective option for MI treatment.

CTE is a strategy that combines a cell source, a biomaterial as the matrix or scaffold, and bioactive molecules, with the possibility to induce a mechanical or a chemical stimulation to regenerate or model human tissue.<sup>24</sup>

Biomaterials play a pivotal role in CTE. Together with supporting mechanically the damaged myocardial wall and avoiding the post-MI negative remodeling, these materials improve cell retention and cell survival, promoting integration into the host tissue and decreasing the immediate cell loss due to mechanical washout, as usually 95-99% of therapeutic cells are lost within the first 24h after the delivery. Likewise, for bioactive molecules, the use of a biomaterial represents an alternative solution to systemic administration and avoids the need for repeated injections and the high costs associated with the treatment.<sup>11</sup> Bioactive molecules can be encapsulated or entrapped by polymeric materials, capable of forming 2D or 3D matrices which enable their delivery to the target site, increasing their stability and extending drug shelf life. The release can be triggered by various mechanisms, depending on the degradation rate of such matrices, the presence of exogenous triggers, and environmental conditions. Consequently, the mechanical properties of drug delivery platforms can be designed and tailored to the final application. Moreover, proteins and protein-binding features can be incorporated into biomaterials to resemble more accurately the ECM and to influence cellular responses.<sup>18</sup>

The most widely implemented strategies for CTE are cardiac patches or scaffolds and *in situ* gelling systems, but also nano-carriers can be fabricated from biomaterials (Figure 1.6).

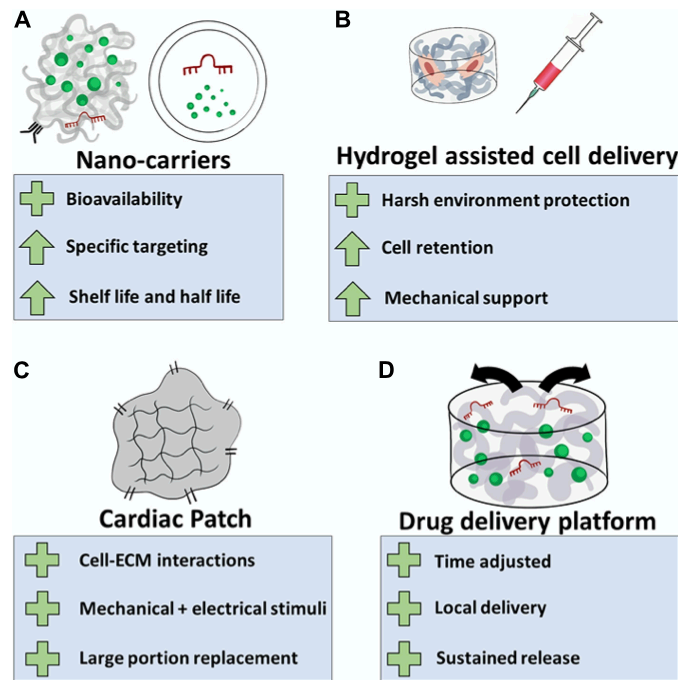


**Figure 1.6.** Biomaterial-based approaches for CTE.  
 Source: Bar, A. et al. / *Front. Bioeng. Biotechnol.* 2020; 8:126.

#### 1.1.3.4. Bioactive nanocarriers

Nano-carriers include agents such as natural or bio-inspired biomolecule carriers and nanoparticles (NPs). Bio-inspired carriers are mainly liposomes, which are closed bilayer phospholipid systems able to encapsulate drugs, proteins/peptides, and DNA. Since liposomes cannot target specifically the heart, they reach the infarcted zone through an intracardiac injection or by conjugation of specific ligands on their surface. They are extremely interesting for their cost-effectiveness and scalable synthesis.<sup>18</sup>

However, the use of cationic lipids is commonly associated with cell toxicity, in addition the presence of a positive charge can result in the

interaction with serum proteins, thus inducing aggregate formation. Therefore, cationic liposomes with minimal toxicity and high transfection efficiency are highly demanded. To overcome cationic lipid-associated toxicity and poor physiological stability, polymeric NPs can be exploited as alternative loaded with drugs and nucleic acids (e.g. small RNA species, mRNA, and plasmid DNA) to promote their efficient delivery to the cells. Specifically, nucleic acids could be a valid alternative to standard drugs since it offers higher specificity, greater activity, and less toxicity. In this regard, NPs display the ability to enhance the circulation time, biodistribution, and bioavailability of oligonucleotides, as well as protecting them from enzyme degradation. Regarding the treatment of acute myocardial infarction, miRNAs are emerging tool among nucleic acids to induce cardiac regeneration. However, the direct administration of miRNA is limited by fast elimination and degradation in blood circulation. Therefore, polymeric NPs can be exploited as miRNA carriers.<sup>18,25</sup>

Despite the potentials of polymeric materials as main constituent of miRNA-loaded NPs, the encapsulation of oligonucleotides is often impaired by the negative charge and the hydrophobic properties of the polymer. Recently, several tailored hybrid systems have been proposed to preserve the positive aspects of the polymer while enhancing the entrapment of miRNA into the NPs due to the cationic lipid properties. Typically, hybrid systems involve the combination of a synthetic, hydrophobic, and anionic polymer such as poly-(lactic-co-glycolic acid)(PLGA), with a cationic complex encapsulating miRNA. The complexing agent can be a polymer (e.g. PEI, chitosan), one of the specific agents usually leveraged for nucleic acids condensation, or a cationic lipid.<sup>26,27</sup>

When a cationic lipid is used, it is generally combined with a neutral co-lipid such as dioleoyl-phosphatidyl-ethanolamine (DOPE) and cholesterol. The role of the cationic lipid is to interact with its positive charge with negatively charged miRNA. The use of a neutral co-lipid in the DNA/RNA-cationic lipid complex enhances the efficiency of gene transfer, although its

influence depends on the type of cationic lipid used, molar ratio between the two, and the target cells. Specifically, neutral co-lipids may help DNA to escape from endosome into the cytoplasm and increase DNA ability to dissociate from the plasmid/lipid complex.<sup>28,29</sup>

Innovative bioartificial NPs for miRNA delivery were recently developed at Politecnico of Turin by Nicoletti *et al.*<sup>30,31</sup>. These hybrid NPs were obtained by the combination of cationic liposome, composed of cationic lipid [2-(2,3-didodecyloxypropyl)-hydroxyethyl] ammonium bromide (DE) and helper lipid 1- $\alpha$ -dioleoylphosphatidyl ethanolamine (DOPE), and the synthetic carboxyl groups-terminated co-polymer poly-(lactic-co-glycolic acid) (PLGA-COOH) (Figure 1.7). PLGA is a synthetic polymer used for preparing miRNA delivery systems. PLGA is a biocompatible co-polymer approved by US FDA (Food & Drugs Administration), widely used in biomedical applications. PLGA NPs are able to encapsulate and deliver bioactive molecules with several advantages such as sustained-release efficacy ranging from days to weeks in physiological conditions, long-term stability of loaded biomolecules, numerous functionalization options, high *in vivo* cellular uptake and rapid escape from endo-lysosomal compartment. PLGA NPs have generally shown low encapsulation efficiency (<50%) of hydrophilic molecules due to their high hydrophobic nature. For this reason, cationic lipids thanks to their positive charge are widely used to allow high encapsulation of miRNA.<sup>32,33</sup>

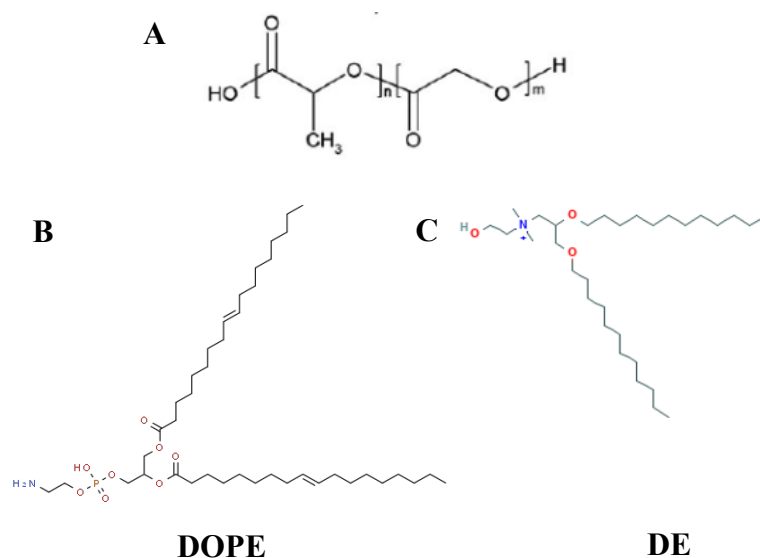


**Figure 1.7.** Chemical structures of (A) Poly (D,L-lactide-co-glycolide) (PLGA), (B) dioleoylphosphatidylethanolamine (DOPE), and (C) [2-(2-3didodecyloxypropyl)hydroxyethyl] ammonium bromide (DE).

#### 1.1.3.1. Cardiac patches

The primary goal of CTE is the fabrication of a completely mature, three-dimensional (3D) functioning heart tissue, developed *ex vivo* and then transplanted *in vivo*. To address this aim, biomaterials are used to fabricate engineered scaffolds in the form of patches that can be used to replace injured areas of the heart. These porous matrices act as ECM replacement and may be loaded with cells and/or bioactive molecules. Their design is optimized to provide a proper microenvironment to the cells, leading to tissue development and maturation.<sup>11</sup> Since both cardiac muscle and blood vessels are direction-oriented tissue constructs, anisotropic features are needed to induce a better tissue organization. Electrospinning is the most investigated technique in literature to obtain this feature, thanks to the possibility to obtain matrices with aligned fibers.<sup>18</sup>

Besides the 3D architecture, ECM-cell interactions are needed to recreate functional heart tissue. To achieve this, biochemical cues have been investigated. If a decellularized ECM of porcine origin is used, these molecules

are naturally embedded in the material, while they need to be added if synthetic polymers are used.<sup>18</sup>

Additionally, patches can acquire contractile functions by electrical or mechanical stimulation.<sup>18</sup>

However, the use of cardiac patches has some limitations. Firstly, the need of an open-chest surgery and the associated patient's risk of death during surgery, especially if when they present comorbidities. Secondly, although the fabrication materials are biocompatible and biodegradable, chronic immune rejection is still under study because long-term safety studies are missing. Finally, in small animal models cardiac patches do not electrically integrate with the host, due to the presence of a fibrotic scar barrier. Thus, future designs need to focus not only on the improvement of the patch functionality but also on its synchronization with the resident cardiomyocytes.<sup>27</sup>

#### *1.1.3.2. Hydrogels*

Hydrogels are tridimensional cross-linked networks of hydrophilic polymers, that have the unique ability to swell in water or biological fluids, retaining a large amount of them.<sup>34</sup> Hydrogels can absorb from 10-20% up to thousands of times their dry weight in water, increasing in dimensions while maintaining their shape. Their swelling behavior, which is determined by the presence of hydrophilic groups attached to the polymeric backbone (e.g. -OH, CONH-, -CONH<sub>2</sub>, and -SO<sub>3</sub>H) and by the chemical composition, the network structure, the crosslinking density, and the synthesis methods.<sup>35</sup>

Hydrogels can be classified in many different ways on the basis of several parameters such as the preparation method, the physical properties, the materials used to synthesize them, the overall charge, the biodegradability, and the type of crosslinking, as shown in Figure 1.7.<sup>34</sup>

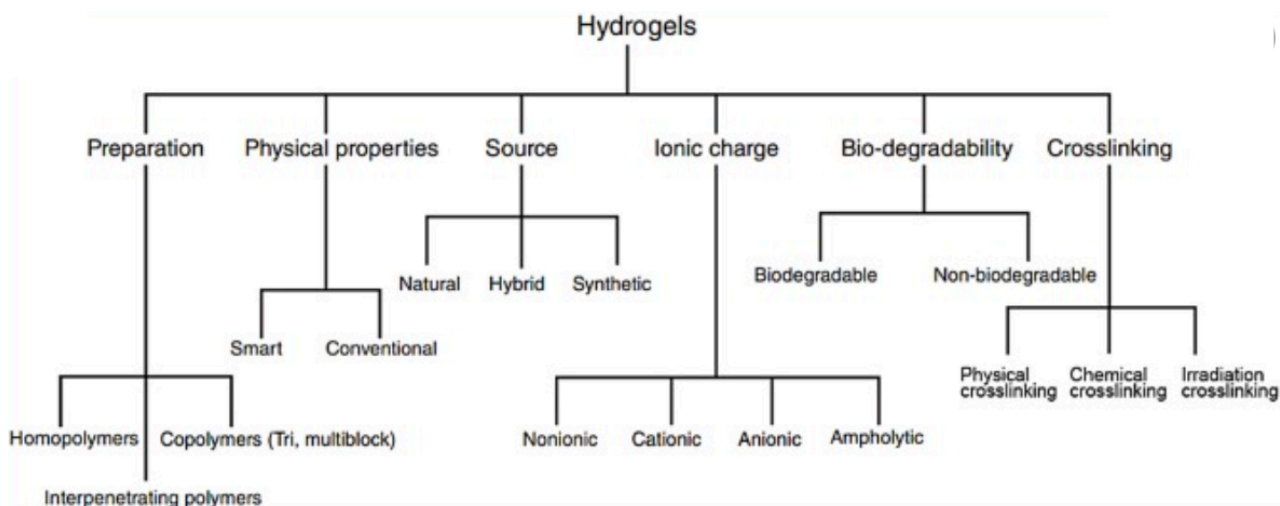


**Figure 1.7.** Classification of hydrogels.

An important classification depends on the nature of the cross-link junctions between the polymeric chains. Chemically cross-linked hydrogels have permanent junctions, such as covalent bonds, while physically cross-linked ones are also called reversible gels because the network is formed mainly by molecular entanglements and secondary forces such as ionic interactions, hydrogen bonding, or hydrophobic forces. These latter are interactions that can be disrupted by changes in physical conditions or by the application of external stresses.<sup>36,37</sup>

Hydrogels are particularly suitable for tissue engineering applications and their chemical and physical properties can be manipulated to obtain a gel tailored to the required application.<sup>34</sup> The manufacturing process used is crucial to control the porosity, which permits free diffusion of metabolites, oxygen, and water. Other characteristics typical of the microscale are also affected, including surface topography and chemical environment.<sup>38,39</sup>

#### *1.2.1.2. Cell-laden hydrogels*

Several studies clearly demonstrated how encapsulating cells in hydrogels increase their therapeutic efficacy in terms of positive LV

remodeling, which was revealed via echocardiography. The better integration with host tissue is mainly due to enhanced retention since hydrogels provide the cells with a mechanically stable environment, preventing them from being washed away by the body's defense barriers.<sup>40</sup> Attention should be paid to the gelation process of the hydrogel, because it should pass from sol to gel without harming the cells.<sup>39</sup>

#### *1.2.1.3. Injectable hydrogel-based gene delivery systems*

Recently, progress has been made in understanding how cells utilize nucleic acids (NA), allowing researchers to use them as a treatment for a broad spectrum of diseases. Plasmid DNA (pDNA) and messenger RNA (mRNA) or small interfering RNA (siRNA) and miRNA can be used to trigger or suppress the expression of specific genes and transcription factors, respectively. The safest way of transfection is the delivery of naked NA molecules directly into the cells. However, the success rate of this method is quite low because, at physiological pH, the negative charges of NA molecules and plasma membrane electrostatically repel each other. Hydrogel systems based on natural polymers could be used to achieve a more efficient delivery.<sup>41</sup>

To induce a cardiovascular tissue repair, is essential to support new blood vessel formation; to this regard, the combination of gene therapy and tissue engineering offers the unique opportunity to induce a therapeutic vascular growth. Among the growth factors used to this end, the most promising are the ones belonging to vascular endothelial growth factor (VEGF), fibroblast growth factor (FGF), and hepatocyte growth factor (HGF) families. They are usually combined with pDNA and pDNA polyplexes are loaded into the hydrogel.<sup>41</sup>

Apart from sustaining neovessel growth, replacing the dead cardiomyocytes is also crucial to heal the damaged myocardium. This can be addressed through miRNA-based therapies. However, systemic delivery of

naked miRNA mimics presents significant drawbacks, such as the need for serial daily administration and the potential accumulation in off-target organs.<sup>42</sup> Therefore, hydrogels represent a powerful tool to better elicit cellular response.

## 1.2. Hydrogels

### 1.2.1. Hydrogels for cardiac tissue repair

For cardiac applications, biomaterials have been prepared and delivered in three main configurations: injectable hydrogels, cardiac patches, and cell sheets, which consist of plates with cell monolayers cultured on them and the materials they are made of are temperature sensitive to allow cell detachment at room temperature (Figure 1.8).

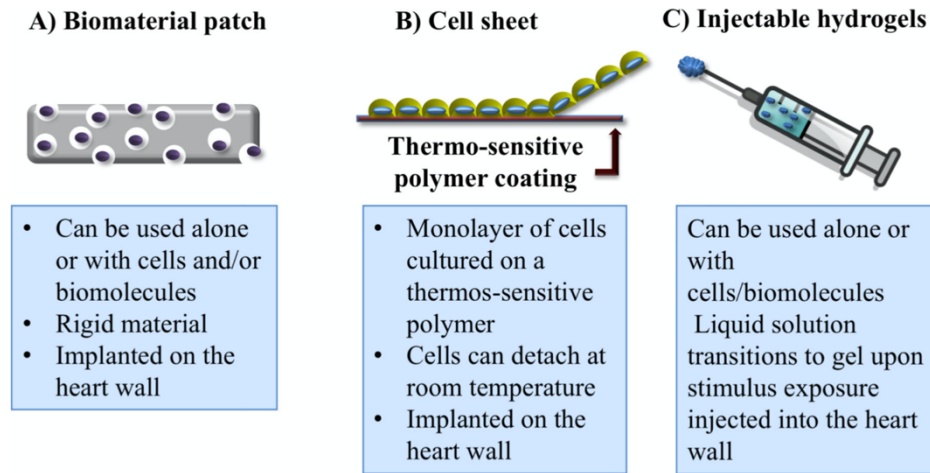


**Figure 1.8.** CTE applications.

Source: Peña, B. et. al. / *Macromol. Biosci.* 2018, 18, 1800079.

Among these approaches, injectable hydrogels represent the optimal one for cardiac regeneration. The first advantage is their injectability, allowing the direct delivery of material into the myocardium through minimally invasive approaches. A less invasive approach allows shorter hospitalization times and an easier translation into clinical applications.<sup>40</sup> Hydrogels can be injected as a liquid or in a partially crosslinked gel form and swap to gel state depending on external stimuli or initiators. For instance, thermo-sensitive hydrogels initiate in situ gelation at body temperature, while other methods of crosslinking can be photo-crosslinking, pH-dependent crosslinking, or ionic crosslinking.<sup>38</sup>

Thanks to the high percentage of water and their viscoelastic nature, hydrogels are optimal to be seeded with cells. Hydrogels possess a low interfacial tension, leading to a low deposition of ECM proteins, important for cell attachment. However, natural polymers present a high protein affinity and

are largely employed to develop an analogue of the native ECM.<sup>43</sup> Furthermore, they prevent the lack of cell retention at the injection site.<sup>18</sup>

Hydrogels provide an optimal release also for other biomolecules and drugs since they allow to control release kinetics.<sup>39</sup> Hydrogels can respond to different types of stimuli, thus therapeutic agents will be released depending on their properties and the physical and chemical cues exerted by the external environment, as shown in Figure 1.9.<sup>43</sup>

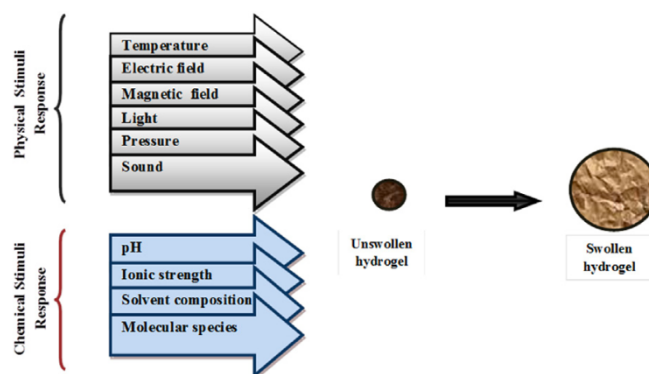


**Figure 1.9.** Stimuli-responsive hydrogels.

Source: Bar, A. et al. / *Front. Bioeng. Biotechnol.* 2020; 8:126.

Finally, injectable hydrogels act as a bulking agent after MI.<sup>11</sup>

Injectable hydrogels represent an optimal approach for cardiac regeneration and have been extensively investigated as acellular matrices, as carriers of cells, or for the delivery of biomolecules.

#### *1.2.1.1. Acellular hydrogels*

Acellular hydrogels have shown positive results in cardiac repair as bulking agents to support mechanically the impaired myocardium and prevent left ventricular (LV) remodeling. Several researchers have focused on this type of hydrogel in order to find

materials that mimic better the native environment by providing biological and chemical cues.<sup>40</sup>

Biomaterials alone are able to trigger thickening of the heart wall, which reduces wall stresses by the Laplace law. This law states the direct proportionality of wall stress with pressure and radius and its inverse proportionality to the wall thickness. To achieve this goal, biomaterials must be scrupulously chosen to give the hydrogel optimum mechanical properties in terms of adequate conductivity, elastomeric and stress relaxation characteristics, indentation and Young's modulus properties.<sup>39</sup>

Two different acellular alginate hydrogels are listed with the few biomaterial-based scaffolds that are being evaluated in clinical trials, which are IK-5001 (Bellerophon BCM LLC, previously referred to as BL-1040 from BioLineRx) and Algisyl-LVR<sup>TM</sup> (LoneStar Heart Inc., Laguna Hills, CA, United States).

#### *1.2.1.2. Cell-laden hydrogels*

Several studies clearly demonstrated how encapsulating cells in hydrogels increase their therapeutic efficacy in terms of positive LV remodeling, which was revealed via echocardiography. The better integration with host tissue is mainly due to enhanced retention since hydrogels provide the cells with a mechanically stable environment, preventing them from being washed away by the body's defense barriers.<sup>40</sup> Attention should be paid to the gelation process of the hydrogel, because it should pass from sol to gel without harming the cells.<sup>39</sup>

### *1.2.1.3. Injectable hydrogel-based gene delivery systems*

Recently, progress has been made in understanding how cells utilize nucleic acids (NA), allowing researchers to use them as a treatment for a broad spectrum of diseases. Plasmid DNA (pDNA) and messenger RNA (mRNA) or small interfering RNA (siRNA) and miRNA can be used to trigger or suppress the expression of specific genes and transcription factors, respectively. The safest way of transfection is the delivery of naked NA molecules directly into the cells. However, the success rate of this method is quite low because, at physiological pH, the negative charges of NA molecules and plasma membrane electrostatically repel each other. Hydrogel systems based on natural polymers could be used to achieve a more efficient delivery.<sup>41</sup>

To induce a cardiovascular tissue repair, is essential to support new blood vessel formation; to this regard, the combination of gene therapy and tissue engineering offers the unique opportunity to induce a therapeutic vascular growth. Among the growth factors used to this end, the most promising are the ones belonging to vascular endothelial growth factor (VEGF), fibroblast growth factor (FGF), and hepatocyte growth factor (HGF) families. They are usually combined with pDNA and pDNA polyplexes are loaded into the hydrogel.<sup>41</sup>

Apart from sustaining neovessel growth, replacing the dead cardiomyocytes is also crucial to heal the damaged myocardium. This can be addressed through miRNA-based therapies. However, systemic delivery of naked miRNA mimics presents significant drawbacks, such as the need for serial daily administration and the potential accumulation in off-target organs.<sup>42</sup> Therefore, hydrogels represent a powerful tool to better elicit cellular response.

### 1.2.2. Composition of injectable hydrogels

Injectable hydrogels for cardiac tissue engineering can be prepared from natural, synthetic, or hybrid materials, which are a combination of the two. Among these, the best biomaterial has not yet been identified, given that both the natural and the synthetic ones present strengths and weaknesses.

Synthetic materials have gained particular interest thanks to their strong mechanical properties and easily controllable features, that allow mimicking those of the specific application. During the synthesis process, mechanical, chemical and physical properties can be tuned, such as tensile strength, porosity, degradation and gelation rate.<sup>38</sup> Furthermore, synthetic polymers possess more stability and less variability, therefore their production can be scaled up without compromising the quality. However, synthetic polymers present some drawbacks, among which the most important are the poor biocompatibility and the lack of cell adhesion sites. Although the risk of immune rejection upon implantation is minimized, the low cell attachment makes them less bioactive.<sup>44</sup>

In contrast, natural polymers possess good biocompatibility and biodegradability, thanks to their derivation from native ECM or ECM-like components. Naturally derived hydrogels can be made of protein-based materials, polysaccharide-based materials and those derived from decellularized tissues. All of them allow water absorption, swelling, and therefore the diffusion of nutrients and waste products, improving cell survival and motility into the surrounding area. Furthermore, they are renewable and have little toxicity. Nevertheless, their use is hindered by poor mechanical properties, insufficient electrical conductivity, long gelation time and rapid degradation.<sup>44</sup> Additionally, these polymers are related to immune response complications and are subjected to batch-to-batch variability because materials extracted from different natural sources are not identical.<sup>34</sup>

In order to combine the advantages of both natural and synthetic polymers, design of hybrid and composite hydrogels have been investigated.<sup>44</sup>

The choice of the type of polymer is based on the final application and the desired cellular interactions. Among the natural polymers, the most used for cardiac hydrogels are chitosan, fibrin, decellularized ECM, collagen, gelatin and alginate.

#### *1.2.2.1. Chitosan*

Chitosan is a linear polysaccharide obtained by partially deacetylating chitin and its physical and mechanical properties are strictly related to the molecular weight and the degree of deacetylation. This material is extensively employed in hydrogel preparation because it presents several advantages such as antibacterial properties, bioactivity, biocompatibility, and low cost. Chitosan is a material with many application possibilities, including wound healing and drug delivery systems, owing its controllable degradability. In the orthopedic field it enhances bone formation, even though it has to be combined with other materials to increase the mechanical strength.<sup>34</sup>

Lastly, chitosan-based hydrogels improve cardiac function because they can be conjugated with several bioactive molecules, allowing the protection of the transplanted cells, angiogenesis promotion, and infarct size reduction.<sup>40</sup>

#### *1.2.2.2 Fibrin*

Fibrin is another natural polymer that has been widely used for cardiac tissue engineering. Fibrin is formed by rapid polymerization of fibrinogen monomers, using the enzyme thrombin as cross-linking agent. The physicochemical properties of fibrin hydrogels, such as the length of the fibers and the pore size, the stability of the gel, and the mechanical properties are determined by the modulation of the

fibrinogen and thrombin ratio.<sup>45,46</sup> These hydrogels are able to mimic the native extracellular matrix environment thanks to fibrin ligands able to interact with cells and cell mediators. Moreover, the degradation products are nontoxic. These features enable the survival of the transplanted cells after the injection of the hydrogel into the heart, consequently increasing angiogenesis and reducing the infarct size.<sup>46</sup> Nevertheless, fibrin does not represent the best candidate for CTE owing to the poor mechanical properties and shrinkage of the gel, and the risk of disease transmission.<sup>45</sup> To overcome these obstacles, hybrid composites can be synthesized by combining fibrin with synthetic biodegradable polymers, such as polyglycolic acid. An alternative are genipin-crosslinked fibrin hydrogels, that also demonstrate improved mechanical properties.<sup>47</sup>

#### *1.2.2.3. Decellularized ECM*

Decellularized tissues are natural scaffolds derived from tissues or organs, in which the cellular and nuclear contents are removed, but the tridimensional structure and biophysical and topographical properties of the native ECM are preserved.<sup>48</sup> ECM scaffolds have drawn attention for cardiac engineering applications. The decellularization method should be chosen carefully for each type of tissue to preserve the micro and nano-structure and the biological properties.<sup>34</sup> Once the ECM is decellularized, to obtain an injectable hydrogel it is lyophilized, ground into a powder and the powder digested in acid media. After that, this ECM solution is diluted with water to achieve a specific concentration and exposed to physiological conditions (i.e 37°C and pH 7) to obtain a hydrogel.<sup>44</sup>

ECM-derived hydrogels are optimal to induce cell attachment, proliferation, migration and differentiation. However, they have slow gelation times and a fast degradation rate, thus reducing cell and biomolecules retention in the infarct area. One method to reduce the degradation is to use cross-linking agents such as genipin.<sup>44</sup>

#### *1.2.2.4. Collagen*

Collagen is one of the most popular biomaterials thanks to its excellent biocompatibility, as it is an important protein component of the ECM. There are many different types of collagen in various human tissues, among which type I is the most frequently employed for cardiac application. Collagen-based hydrogels possess high biodegradability, low toxicity and the ability to promote cardiomyocytes attachment and survival.<sup>44</sup> Injection of collagen into injured cardiac tissue has been shown to reduce fibrosis and improves left ventricular stroke volume and ejection fraction.<sup>49</sup>

On the other hand, collagen-based hydrogels possess weak mechanical and electrical properties which are important features for cardiac tissue repair. To address this shortcoming, collagen can be crosslinked via chemical or physical methods or can be blended with other materials, such as carbon nanotubes (CNTs).<sup>44</sup> Moreover, collagen hydrogels have other limitations, such as the thrombogenic potential of the degradation products, high cost of isolation and purification, and easy denaturation of its structure when exposed to high temperature or different kinds of irradiation.<sup>34</sup>

#### *1.2.2.5. Gelatin*

Gelatin is a natural polymer resulted from collagen denaturation through partial hydrolysis which can be carried out using acid or alkaline solutions, obtaining type A or type B gelatin respectively.<sup>50</sup> Although the two types of gelatins differ in amino acids composition, both of them present the typical sequence (Gly-X-Y)<sub>n</sub>, made of glycine, proline and hydroxyproline, respectively. Typical chemical structure of gelatin is shown in Figure 1.10. However, type A gelatin presents a composition of arginine, glycine, and aspartic acid of the RGD sequence which is more similar to the one of type I collagen. Since type

I collagen is the major constituent of native ECM, type A gelatin is to prefer in tissue engineering applications.<sup>51</sup> For instance, type A gelatin is the most suitable for scaffold production because it presents more carboxylic groups.<sup>50</sup>

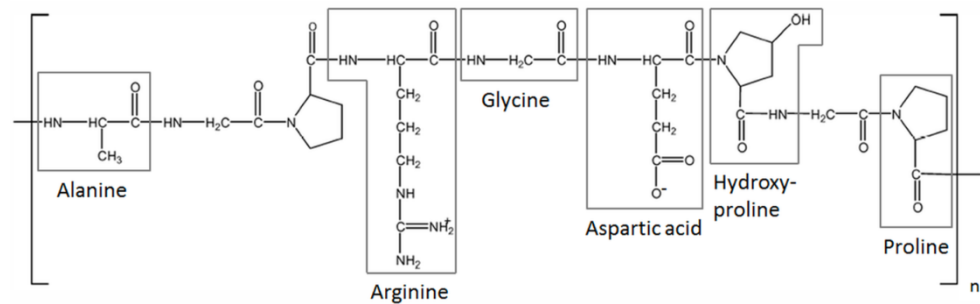


**Figure 1.10.** Gelatin chemical structure composed of different amino acids including the components of the adhesion peptide RGD.

This material has been extensively used in CTE due to its biocompatibility, biodegradability, nontoxicity, and limited immunogenicity.<sup>45</sup> It can serve as a structural element or coating agent to induce cell attachment.<sup>34</sup>

However, gelatin hydrogels present poor mechanical stability and durability, because gelatin is in the sol state at physiological temperature. Hence, a cross-linking agent is usually added to form hydrogels, such as chemical agents like glutaraldehyde (GTA), carbodiimides, and genipin (GP), or enzymes like transglutaminase, tyrosinases, and horseradish peroxidases.<sup>19</sup>

In cardiovascular tissue applications, the synthesis of gelatin nanofibrous matrices through electrospinning is another way to further increase gelatin strength and to obtain optimal mechanical properties for contracting CMs.<sup>34</sup>

#### *1.2.2.6. Alginate*

Another widely investigated biomaterial for cardiac tissue engineering is alginate, a negatively charged polysaccharide derived from brown algae cell walls and several bacteria strains. However, only algal alginate is used for commercial purposes because the bacterial one possesses a higher molecular weight.<sup>52</sup> Alginate is a biocompatible, biodegradable, non-immunogenic, non-thrombogenic and low-cost polymer. Alginate hydrogels have been used as bulking agent to support the weakened myocardium or in cell delivery systems.<sup>38,45</sup>

### 1.3 Alginate in cardiac regeneration

#### *1.3.1. Promising properties of alginate*

Alginate is a linear copolymer composed of two acidic monomers, 1→4 linked  $\alpha$ -L-guluronic acid (G) and  $\beta$ -D-mannuronic acid (M). These acidic monomers are distributed as blocks forming regions of M-blocks and G-blocks, as well as heteropolymeric sequences (GMGMGM). Alginates extracted from different seaweeds present a variable arrangement of these blocks, with a composition ranging

from 10% G to 75% G. This structural variability affects the molecular weight (MW) and consequently physical properties such as viscosity, sol/gel transition, and water-uptake ability.<sup>53-55</sup>

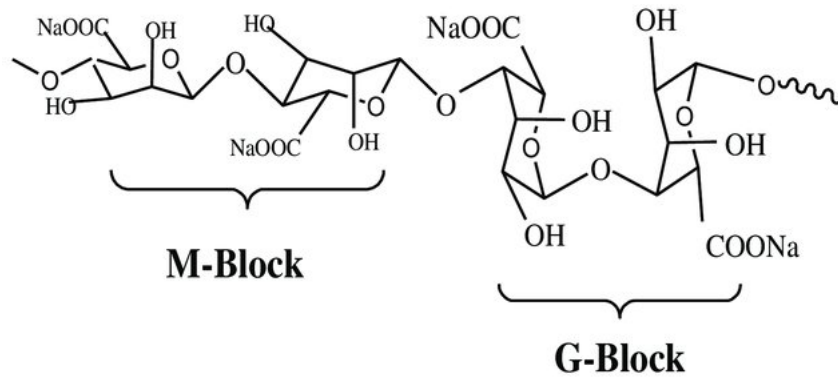


**Figure 1.11.** Chemical structure of sodium-alginate.

*Source: Salisu, A. et al. / Desalination and water treatment. 2015; 57(33):1-9.*

Alginate is usually commercialized as sodium salt. Sodium alginates MW is expressed as an average of all the molecules present in the sample and varies between 33,000 and 400,000 g/mol. Specifically, a MW increase is related to higher G-block content.<sup>55</sup> Using alginate with higher G-block content can improve the mechanical properties of the hydrogels by increasing their strength and brittleness, although also an increased viscosity is observed.<sup>55,56</sup>

Sodium alginate is produced in various grades, generally described as low (up to about 50 mPa·s), medium (up to about 400 mPa·s), and high viscosity alginates (up to about 1000 mPa·s). The viscosity grade is determined by the viscosity of 1% sodium alginate aqueous solution. Medium viscosity grade alginate is widely used for different applications.<sup>57</sup>

Alginate possesses great affinity for divalent cations, such as  $\text{Ca}^{2+}$ ,  $\text{Ba}^{2+}$ , and  $\text{Zn}^{2+}$ , which bind together G monomers of the different alginate chains. The resultant pattern is known as “egg box” model and results in a physical hydrogel formation through a mechanism of ionotropic gelation.<sup>54,56</sup>

Specifically, gelation in presence of  $\text{Ca}^{2+}$  leads to the formation of inter- and intra-chain bridges. Firstly, G residues of adjacent chains are linked together by

calcium ions, resulting in dimers. Then, tightly linked dimers with higher  $\text{Ca}^{2+}$  concentration interact electrostatically forming interdimer associations. Therefore, high G-block contents determine stiffer and more stable hydrogels.<sup>58</sup>

Calcium chloride ( $\text{CaCl}_2$ ) is the most frequently used source of  $\text{Ca}^{2+}$  ions to induce an external gelation. A  $\text{CaCl}_2$  solution is added slowly to a viscous sodium alginate solution and localized instantaneous gelation occurs at the surface of the alginate, making extremely difficult to control the homogeneity and the strength of the hydrogel. To overcome these limitations, approaches to reduce the gelation rate have been investigated. Draget *et al.* developed an internal gelation mechanism delivering calcium in an insoluble form, such as calcium carbonate ( $\text{CaCO}_3$ ). After mixing  $\text{CaCO}_3$  with an alginate solution, Glucono- $\delta$ -lactone (GDL) is added to lower the pH and dissociate  $\text{Ca}^{2+}$  ions, which initiate the gelation of alginate solution in a more gradual manner.<sup>53,54</sup>

Alginate can be crosslinked also through chemical strategies. However, physical cross-linking is more often used because it can be easily performed using biocompatible calcium salts, while chemical one requires the use of cross-linking agents, solvents, and other chemicals. Moreover, chemical cross-linking is time-consuming since the lack of chemical traces and end-product biocompatibility should be ensured.<sup>56</sup>

Alginate is widely used in biomedical applications thank to its biocompatibility, non-toxicity, non-immunogenicity, bio-adhesivity, and antibacterial/-viral activity.<sup>58</sup> In addition, alginate possesses non-thrombogenic properties, which make it an attractive polymer for cardiac applications.<sup>40</sup>

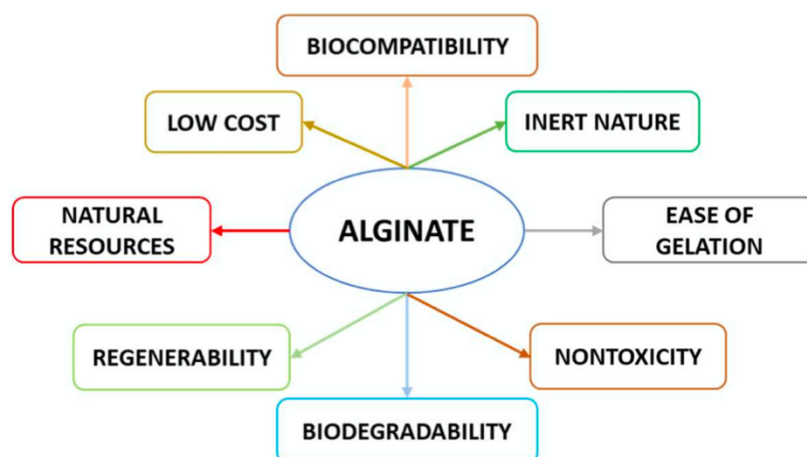


**Figure 1.12.** Advantages of alginate.  
 Source: Puculescu, R. G.. et al. *Polymers*. 2020; 12(2417).

Alginate hydrogels emerged as a promising approach in cardiac regeneration since they support heart vascularization, re-cellularization, and restoration of the electrical conductivity. These hydrogels can be modified to enhance their positive effects, and possible implementations are the inclusion of different cell types, bioactive molecules, functional oligomers and conductive materials. Alginate can be used as support material or as delivery system choosing an *in-situ* or non *in-situ* administration, respectively.<sup>58</sup>

To date, two different alginate hydrogels are currently being evaluated in clinical trials: Algisyl-LVR™ (LoneStar Heart Inc., Laguna Hills, CA, United States) and IK-5001 (Bellerophon BCM LLC, previously referred to as BL-1040 from BioLineRx, Jerusalem, Israel).

### 1.3.2. Algisyl LVR

Algisyl LVR™ is the most used and commercially available hydrogel implied in preventing left ventricle dilatation exacerbation in patients subjected to MI and HF. In this system, a “self-gelling alginate” mechanism is implemented, using alginate as soluble component and an insoluble component made of gelling ion particles in a solvent. Specifically, an aqueous solution of

sodium alginate with 4.6% mannitol and water insoluble calcium alginate particles suspended in 4.6% mannitol solution are used.<sup>59</sup> Hydrogel formation begins when the two components are mixed in the presence of a solvent and continues during its delivery, until the hydrogel sets *in situ*.<sup>60</sup> Algisyl LVR™ is delivered through 9-15 intramyocardial injections of 0.25-0.35 ml of the self-gelling alginate, during an open-heart procedure.<sup>59</sup>

Until now, Algisyl LVR™ has been tested in two clinical trials with positive outcomes.

The first clinical trial (NCT00847964), also known as SYM-08-001, was published in 2015, in which the treatment was administered to 11 patients with dilated cardiomyopathy, among which only 9 were able to complete the follow-up after 24 months. At the last time point of the follow-up, no deaths occurred and a reduction in the LV end-systolic and LV end-diastolic dimension (LVESD-LVEDD) was observed. Furthermore, an improvement of 28% in the LV ejection fraction (LVEF) was recorded, thus improving the overall patients' quality of life.(alginate) However, the small number of patients enrolled in the study was a big limitation. Nevertheless, encouraging results declared Algisyl LVR™ as safe and feasible for further clinical trials.<sup>56</sup>

AUGMENT-HF (N: NCT01311791) was the second trial carried out using Algisyl LVR™. The trial was conducted on 78 subjects with dilated cardiomyopathy from five different countries, among which only 40 received the treatment. Results at the follow-up showed an increase of the mean peak VO<sub>2</sub>, which represents the maximum O<sub>2</sub> amount in the blood provided by the heart during physical activity, and in the six-minute walk test (6MWT). In addition, an increase in LVEF and a decrease in LVEDD and left ventricle mass were observed after one year.<sup>58</sup>

All these results demonstrated that Algisyl LVR™ is able to reduce cardiac tension ameliorating the general mechanical support, thus enabling the natural healing of the heart. Moreover, no immune reactions or rejections occurred.<sup>58</sup>

To date, a third clinical trials is currently ongoing to assess the efficacy and the safety of Algisyl LVR™ in patients with moderate to severe HF.<sup>58</sup>

### 1.3.3 IK-5001

IK-5001 is an injectable bioabsorbable cardiac matrix device and comprises a solution of 1% sodium alginate plus 0.3% calcium gluconate. The implant of this hydrogel is performed *via* percutaneous radial artery access under local anesthesia, avoiding the need for open-heart surgery and general anesthesia. IK-5001 enters both in the myocardial tissue and in the extracellular space, where it undergoes gelation thanks to the high concentration of calcium ions in the infarcted myocardium. Thus, IK-5001 acts as a temporary artificial extracellular matrix and once the myocardial extracellular calcium declined, it is eliminated by kidneys, generally in 3-6 months after the injection.<sup>58,61</sup>

Once positive outcomes were recorded in a MI swine model treated with IK-5001, Frey *et al.* tested the hydrogel in the pivotal study NCT01226563 to verify its feasibility in patients recovering from a moderate-to-large MI.<sup>58</sup> Hence, 2 ml of IK-5001 was injected into the free-flowing infarct-related artery (IRA) of 27 patients.<sup>61</sup> LV remodeling and function were monitored by echocardiography, before deployment and at defined time points after deployment. Namely, patients were controlled at day 30, 90, and 180. The deployment was well tolerated by all patients and did not induce additional myocardial damages or re-elevation of cardiac biomarkers.<sup>56</sup> No adverse events were correlated with the treatment, except for a single episode of syncope occurred at day 172.<sup>58,61</sup> Furthermore, no arrhythmias were recorded during continuous 24-hour ECG monitoring, performed at different time points. IK-5001 showed positive effects on LV remodeling, preserving LV end-diastolic volume index (LVEDVI), LV end-systolic volume index (LVESVI), and LVEF parameters.<sup>58</sup>

Although the feasibility of this device was demonstrated, this pilot study had several limitations. Firstly, a randomized control group was not included. Secondly, the study was not blinded, therefore patients may have been influenced by the placebo effect. Moreover, the patients included in the study presented LVEF > 45%, thus creating a bias toward a low-risk population. Specifically, European Society of Cardiology and American Society of Echocardiography guidelines report normal LVEF as >50% and >55%, respectively and clinical HF trials have shown that LV systolic dysfunction is indicated by LVEF < 40-45%.<sup>62</sup> Third, magnetic resonance imaging (MRI) was not carried out, although it is considered the gold standard to evaluate cardiac remodeling and functionality. Fourth, the effect of the device on coronary flow and microvascular resistance was not investigated. Finally, the study population was small, and this may be determined the limited number of adverse events.<sup>61</sup>

Researchers tried to overcome these limitations performing a placebo-controlled, multicenter, randomized, double-blinded trial, called PRESERVATION-1 (nr: NCT01226563).<sup>58</sup> The trial was conducted to determine the safety and the effectiveness of IK-5001 for the prevention of LV remodeling and congestive HF, when injected in subjects who had successful percutaneous coronary intervention with stent placement after MI.<sup>56</sup> In this case, 201 patients were treated with 4 ml of BCM, whereas 102 healthy subjects, used as control group, were treated with saline solution.<sup>63</sup>

The results of this trial were unsatisfying, since no significant difference in LVEDVI at 6 months was observed between the treated and the untreated group. Researchers chose to monitor only LVEDVI because post-infarction dilation is more directly quantified by diastolic rather than systolic volume.

Regarding secondary effectiveness endpoints, although a positive trend in change in 6MWT was recorded, it was not statistically significant.

Moreover, the occurrence of severe adverse events that were assumed related to the hydrogel was about 5% and 2.9% for BCM and saline control group, respectively.<sup>63</sup>

Therefore, IK-5001 did not determine impressive anatomical changes, nor an improved quality of life.<sup>58</sup> However, the slight increase in functionality observed in 6MWT supports further investigations on alginate potentiality to promote cardiac repair.<sup>63</sup>

#### 1.3.4. Commercial alternatives: VentriGel

A commercial and promising alternative to alginate-based hydrogels is an injectable hydrogel derived from porcine decellularized myocardial ECM, named as VentriGel (Ventrix, Inc., San Diego, California). In vitro analysis and rat MI models showed the potential of this material to promote neovascularization, cardiac differentiation of stem cells and fibrosis reduction.<sup>64</sup> Likewise, in pig models VentriGel increased myocardial tissue and decreased fibrosis in the infarct zone.<sup>65</sup> According to these positive outcomes, a first-in-man, single-arm, multicenter trial was carried out to evaluate the safety, feasibility and preliminary efficacy of VentriGel delivery in early and late MI patients.

VentriGel stiffness is about 2 orders of magnitude lower than the one of the healthy myocardium, therefore it would not be expected to support mechanically the infarct zone as the alginate counterparts do. However, thanks to its weakness, VentriGel can be delivered via a percutaneous catheter with a minimally invasive approach. After the injection, it gels into a porous and fibrous scaffold, with the aim to allow endogenous cell infiltration and matrix remodeling. Furthermore, stem cells infiltration and differentiation are favored by biochemical cues provided by this ECM-based hydrogel.<sup>64</sup>

Immediately before the procedure, lyophilized VentriGel was suspended in sterile water and loaded into a syringe. The hydrogel was

delivered *via* 1-18 sequential transendocardial injections into an infarct area with a wall thickness >8mm, identified through echocardiography. 15 patients received the injection, among which one-half were treated <12 months after MI (referred to as early MI subset) and the one-half >12 months after MI (referred to as late MI subset). VentriGel was well tolerated, and no deaths or adverse events related to the device occurred. Furthermore, Holter monitoring did not show significant ventricular arrhythmias.<sup>64</sup>

Several parameters were considered to assess VentriGel efficacy, including evaluation of 6MWT, LV volume, EF, scar size by cardiac magnetic resonance, serum B-type natriuretic peptide (BNP) level, quality of life and an assessment of the extent of HF. The treatment led to an improvement of 6MWT results, BNP levels, and LV volume at 3 and 6 months. Specifically, a decrease in LV end-systolic volume and LV end-diastolic volume occurred preferentially in late MI group. No significant changes were recorded in EF or scar size. Overall, VentriGel improved patients' functional status and quality of life.<sup>64</sup>

The main limitation of this trial is the small number of patients and the lack of a control group. Therefore, further evaluations will be conducted in larger randomized clinical trials.<sup>64</sup>

### 1.3.3. Oxidized alginate (OA)

Besides its promising properties, alginate possesses important drawbacks such as low *in vivo* degradability. Alginate hydrogels degradation occurs through dissociation of the ionic crosslinking and release of alginate strands, but only strands with MW lower than 50,000 g/mol can be removed from the body by the kidneys. Alginate degradation is hindered also by the lack of specific degrading enzymes in mammals. Finally, alginate exhibits poor cell adhesion because of the lack of specific ligands for mammalian cells.<sup>66</sup>

Partial oxidation of alginate chains can overcome these limitations. Oxidized alginate, also known as alginate dialdehyde (ADA), possess a faster degradation rate and reactive aldehyde groups.<sup>66</sup> Alginate is usually oxidized using sodium periodate, which oxidizes the hydroxyl group at the second and third positions (C-2 and C-3) of the uronate residues in the alginate chain. Subsequently, the cleavage of the carbon-carbon bond occurs, forming two aldehyde functional groups at the oxidized carbon of the monomeric unit. The resulting functional groups can react simultaneously with hydroxyl groups of the adjacent unoxidized uronic residues in the polymer chain, forming cyclic hemiacetals, or they can remain available for further functionalization. The form with aldehyde groups is in equilibrium with the one that presents hemiacetals.<sup>56,66</sup> A slight decrease in the MW is observed in ADA.<sup>56</sup>

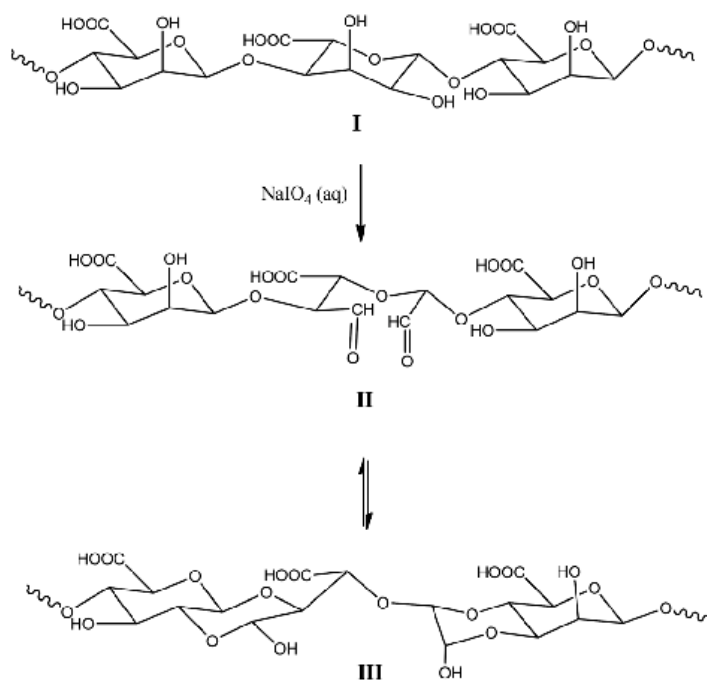


**Figure 1.13.** Reaction scheme for the periodate oxidation reaction of alginate (I) forming ADA (II) followed by formation of intermolecular cyclic hemiacetal moieties (III).

Source: Jejurikar, A. *et al.* / *Journal of Materials Chemistry*. 2012; 22(19):9751-58.

Alginate oxidation in aqueous solution can be performed only at low concentration of alginate (<4%) because alginate forms a very viscous solution that is difficult to handle.<sup>66</sup> To address this issue, Balakrishnan *et al.* designed

an alternative ADA synthesis method carried out in 1:1 ethanol-water mixture. A larger quantity of oxidized product was obtained performing periodate oxidation of alginate in ethanol-water solution. ADA from aqueous and ethanol-water media were compared in terms of yield of product and degree of oxidation. The former was higher in ethanol-water medium, whereas the effect of the periodate concentration on the degree of oxidation was similar.<sup>67</sup>

The mainly used techniques to investigate the presence of aldehyde groups are Fourier-transform infrared spectroscopy (FTIR) and Nuclear Magnetic Resonance (NMR), in which spectra new peaks are usually observed in the range of 1725-1751  $\text{cm}^{-1}$  and at 92.2 ppm, respectively.<sup>66</sup>

Although prepared under the same gelling conditions and in presence of divalent cations, ADA hydrogels are usually weaker than alginate ones. The degradation rate of the hydrogels is strongly related to the degree of oxidation, as well as to the pH and temperature of the media.<sup>56</sup>

ADA reactivity is higher than the alginate one, since it contains functional groups that can form covalent bonds with bioactive molecules containing amino groups, such as gelatin (GEL). ADA/GEL hydrogels are the most investigated ones for tissue engineering application.<sup>66</sup> Crosslinking between the two polymers occurs through Schiff-base reaction between the amino groups of lysine or hydroxylysine GEL side groups and the aldehyde groups of ADA.<sup>67</sup> ADA degree of oxidation strictly determines mechanical properties, degradation profile and swelling behavior of ADA/GEL hydrogels, as well as ADA/polymer hydrogels.<sup>66</sup>

As mentioned before, periodate oxidation improves *in vivo* biodegradability. This is due to the lower MW of ADA and the susceptibility of aldehyde groups to hydrolysis. Specifically, the cleavage of the carbon-carbon bond in the uronate residue alters the chair conformation to an open-chain adduct. This conformational change allows a free rotation on the glycosidic linkage of alginate, which could behave as an acetal group susceptible to hydrolysis.<sup>56,68</sup>

To date, ADA-based hydrogels have been tested in both bone and soft tissue engineering applications. Specifically, Boccaccini *et al.* largely investigated ADA-based hydrogels for cardiac applications.

In most of his works Boccaccini and colleagues performed ADA partial oxidation in water-ethanol mixture, starting from a 20% (w/v) sodium alginate in ethanol solution and a 7.75 mmol periodate solution. To prepare ADA/GEL hydrogels they generally dissolve ADA and GEL in PBS and in DI water, respectively, to obtain 5% (w/v) stock solutions. Then GEL solution is slowly added to the one of ADA under continuous stirring and a hydrogel precursor is obtained. Finally, hydrogels are crosslinked adding a calcium chloride solution and keeping it for several minutes to allow ionic gelation. Following this protocol, Boccaccini et al. obtained hydrogel films or microcapsules, injectable hydrogels or an ADA/GEL bioink to use for scaffold fabrication through 3D printing.

## 1.4 Thymosin $\beta_4$

### 1.4.1. Thymosin $\beta_4$ for cardiac applications

A deeper knowledge about the regulatory pathways involved in cardiac development may help in enhancing current therapies for cardiac repair and regeneration. In this regard, biochemical cues determining cardiogenesis, cardiac cell-fate decisions, and cardiac differentiation have been clarified.<sup>69</sup> Specifically, while studying gene expression during cardiac morphogenesis, Srivastava *et al.* found that thymosin  $\beta_4$  ( $T\beta_4$ ) is abundantly expressed in the developing heart from mesenchymal stem cells (MSCs) and embryonic endothelial progenitor cells (eEPCs).<sup>70,71</sup> This peptide interacts with G-actin monomers and acts as an actin-sequestering protein in most cell types with a subsequent effect on actin-cytoskeletal organization, necessary for cell motility, organogenesis, and other cell biological events. Although  $T\beta_4$  lacks a secretion signal, its presence was confirmed in injured tissues such as skin and cornea, where it promoted wound healing thanks its beneficial effects on cell migration and survival and angiogenesis.<sup>70</sup> Concerning myocardium,  $T\beta_4$  can protect it from death after an ischemic damage through different mechanisms.

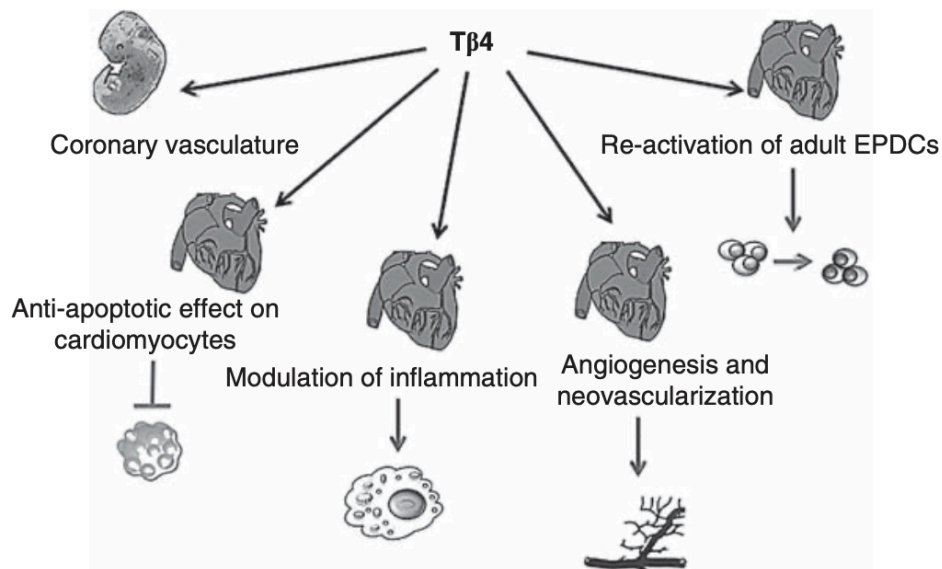


**Figure 1.14.** Multiple functions of Thymosin  $\beta_4$ .

Source: Bollini, S. *et al.* / *Expert Opin. Biol. Ther.* . 2015; 15(Suppl. 1):S163-S174.

Firstly,  $T\beta_4$  provides cardioprotection by supporting resident CMs survival and repair since it can activate kinases Akt (protein kinase B), a serine/threonine kinase able to enhance CMs differentiation, proliferation and hypertrophy, resistance to apoptosis after hypoxia, and enhancing coronary angiogenesis.<sup>71</sup>

Secondly,  $T\beta_4$  modulates the inflammatory process after MI. Inflammatory mediators such as interleukins and tumor necrosis factors (TNF- $\alpha$ ) have a key role in adverse cardiac remodeling. Sosne *et al.* have demonstrated that exogenous  $T\beta_4$  can strongly reduce the effects due to TNF- $\alpha$  stimulation, leading to a reduction of the infarct zone. In addition,  $T\beta_4$  showed the ability to react with  $H_2O_2$  produced at the site of injury, forming a strong anti-inflammatory derivative which increased macrophage infiltration during the early inflammatory phase in mouse MI models.<sup>71</sup>

Thirdly,  $T\beta_4$  may reduce fibrosis.  $T\beta_4$  is a precursor of acetylated SDKP (Ac-SDKP), a tetrapeptide which successfully reduced fibrosis when administered in rat MI models. Therefore, studies on the ability of  $T\beta_4$  to release the tetrapeptide are currently ongoing. Additionally,  $T\beta_4$  possesses the ability to reduce profibrotic gene expression in mouse MI model, such as collagen type I and type III.<sup>72</sup> (gupta)

Fourth,  $T\beta_4$  induces angiogenesis and vascularization of ischemic myocardium. Although the mechanisms are still unclear,  $T\beta_4$  can activate quiescent adult EPDCs, their directional migration, and their differentiation in vascular smooth muscle cells (VSMCs) and possibly endothelial cells (ECs). The effect of this treatment was demonstrated on murine cardiac explants, where EPDCs differentiated *in vitro* into fibroblasts, VSMCs and ECs.<sup>71,72</sup>

As mentioned before, a combination of different transcriptional factors has shown the ability to reprogram resident CFs into newly born CMs. Srivastava *et al.* proposed to deliver  $T\beta_4$  alongside GMT to enhance the degree of cardiac repair. Besides the positive effects listed above,  $T\beta_4$  is able to increase the number of fibroblasts that become activated and proliferative, allowing GMT to induce direct reprogramming in more cells. In rodent and pig models, generally fibroblasts take three weeks to migrate from adult heart explants, whereas only two weeks were needed

when  $T\beta_4$  is delivered. Moreover, co-injection of  $T\beta_4$  and GMY lead to an improved EF and a reduced scar size.<sup>70</sup> Although the mechanisms of cardiac repair triggered by GMT and/or  $T\beta_4$  is not fully understood, the two may act synergistically to promote cardiac repair and regeneration.

Currently, a formulation to obtain an optimized and sustained release in the long term of  $T\beta_4$  is under investigation. Intra-cardiac and/or periodic intra-peritoneal administrations are the most common to deliver  $T\beta_4$  shortly after MI. Although a protective effect on resident CMs was observed, optimal delivery and dosing of  $T\beta_4$  during both the acute and chronic phase are not achieved yet.<sup>71</sup>

Gene therapy strategies are also used to induce an exogenous  $T\beta_4$  stimulation. Specifically,  $T\beta_4$  delivery *via* recombinant adeno-associated viral vectors was shown to reduce acute rejection in pigs after a cardiac allograft transplantation.<sup>71</sup>

To date, composite hydrogels have been the most efficient methods to obtain a controlled, robust and durable delivery.  $T\beta_4$  encapsulation allows to localize and prolong the bioactivity, because it inhibits washout of the peptide from the injection site. Different research team have tested collagen-chitosan hydrogels and demonstrated successfully that  $T\beta_4$  released from these systems was more efficient than  $T\beta_4$  in the soluble form, both *in vitro* and *in vivo*. Furthermore, this system requires only one injection.<sup>49,71</sup>

A hydrogel-based strategy was also used to deliver  $T\beta_4$  together with cells and test its ability to improve cells transplantation potency. For instance,  $T\beta_4$  was encapsulated in gelatin microspheres, which were loaded into a fibrin patch together with swine MSCs (sMSCs). Then, the patch was tested in a rat model of MI. This system enhanced the engraftment, survival and vasculogenic effect of sMSCs, thus improving infarct size and cardiac functionality after MI.<sup>71,73</sup>

Ultimately, the potent anti-inflammatory, pro-survival and pro-angiogenic effects make  $T\beta_4$  an attractive candidate for the treatment of MI and HF. Results of

extensive preclinical trials support the benefits related to a controlled spatial release and long-term delivery of the peptide, highlighting the value of pursuing clinical trials.

## II. AIM OF THE WORK

---

Myocardial infarction is one of the leading causes of death worldwide. Heart injury is followed by loss of cardiomyocytes, which are replaced by fibrous scar tissue. As a result, cardiac contraction and pump function decrease resulting in mechanical dysfunction and pathological cardiac dilatation, eventually leading to fatal heart failure. Traditional treatments of ischemic heart disease are focused on targeting the remodeling process in the failing heart, but they do not effectively renew the impaired myocardium. Therefore, scientific research has recently focused on regenerative approaches to enhance the poor regenerative capacity of adult cardiomyocytes and to ultimately promote heart regeneration. An emerging approach is the direct reprogramming of endogenous cardiac fibroblasts into cardiomyocyte-like by forcing the expression of defined transcription factors. To address this aim, microRNAs represent a promising strategy. Specifically, transfection of four microRNA mimic (termed “miRcombo”) have shown to achieve direct reprogramming.<sup>74</sup>

This innovative regenerative strategy is currently under investigation in BIORECAR ERC consolidator project ([www.biorecar.polito.it](http://www.biorecar.polito.it)). This thesis project has been performed within BIORECAR ERC project, with the aim of developing a biomaterial-based platform to provide the infarcted myocardium with biochemical cues able to induce direct reprogramming of human cardiac fibroblasts. Recently, innovative efficient nanoparticles for targeted cell reprogramming were developed within this project.<sup>28</sup> These nanoparticles may represent an effective strategy to *in situ* deliver the therapeutic agents. Therefore, the aim of this project was to develop a novel injectable hydrogel able to induce a local and controlled release of microRNA-loaded nanoparticles capable of inducing direct reprogramming of cardiac fibroblasts into induced cardiomyocytes.

Alginate was selected as the material as it is widely used in cardiac tissue engineering since it is a biocompatible, biodegradable, non-immunogenic, non-thrombogenic and low-cost polymer. Moreover, alginate-based hydrogels have been already approved for cardiac applications for restoration of normal left ventricle volume (Algisyl LVR™). However, alginate exhibits low *in vivo* degradability and poor cell adhesion. For this reason, the first goal of this thesis project was the preparation of an alginate derivative able to overcome these limitations. Specifically, a partial oxidation of alginate chains was performed, and oxidized alginate also known as alginate dialdehyde (ADA)-derivative was obtained. Modified alginate was characterized by evaluating its physicochemical properties. The oxidation process was expected to determine a lower molecular weight of the polymer and to provide functional groups for covalent binding with molecules containing amino groups, such as gelatin (GEL).

ADA/GEL is the most popular ADA-based hydrogel which has been investigated for tissue engineering applications. GEL was introduced to further enhance the biological performance of ADA. Firstly, GEL exhibits RGD sequences which act as cell adhesion sites. Specifically, fibroblasts agglomeration was observed on ALG or ADA hydrogels due to a poor cell-material interaction, whereas an increasing amount of GEL promoted cell adhesion, spreading, and proliferation.<sup>75</sup> In addition, upon degradation of the hydrogel matrix, cell migration and proliferation would be facilitated. Moreover, when GEL is added to the hydrogel composition it exhibits slightly higher mechanical strength, higher swelling ratio, shorter gelation time and lower degradation rate, compared to ADA hydrogels.

Therefore, the development of covalently and ionically crosslinked ADA/GEL hydrogel has been investigated. Their degradation and swelling behavior were investigated and compared. Furthermore, rheological measurements were performed to evaluate mechanical properties of the injectable hydrogel.

The final aim is to identify the most suitable composition which allows the temporary physical support to the damaged myocardium by replacing some of the lost functions of the ECM, while preventing adverse cardiac remodeling and dysfunction. To address this aim, the mechanical stiffness of the clinically approved Algisyl-LVR™

device is taken as reference (0.2-3 kPa).<sup>60</sup> With time, ADA/GEL hydrogel gradually disappears. Thus, as NPs can be entrapped in the polymer matrix, it can act as drug delivery platform releasing the therapeutic agent while degrading. Therefore, the composition should also ensure a controlled and prolonged release over time.

### III. MATERIALS AND METHODS

---

#### 3.1. Materials

Sodium alginate (sodium salt of alginic acid, medium viscosity grade, 600 - 900 cps) was obtained from MP Biomedicals. Sodium metaperiodate ( $\text{NaIO}_4$ , MW = 213,98), calcium chloride di-hydrate ( $\text{CaCl}_2 \cdot 2\text{H}_2\text{O}$ ) and gelatin (Bloom X, Type A, porcine skin, suitable for cell culture) were purchased from Sigma-Aldrich. Dialysis membranes tubing were supplied from Spectrum Lab (Spectrum<sup>TM</sup> Spectra/Por<sup>TM</sup>), based on regenerated cellulose with a molecular weight cut off of 6000 to 8000 Dalton. Silver nitrate ( $\text{AgNO}_3$ ), potassium iodide (KI) and soluble starch solution were purchased from Alfa Aesar.

#### 3.2. Methods

##### *3.2.1. Alginate dialdehyde formulation protocol*

ADA was synthesized by controlled oxidation of sodium alginate in an equal volume of ethanol-water mixture. Specifically, 5 g of sodium alginate was dispersed in 25 ml ethanol, giving a 20% (w/v) dispersion, and sodium metaperiodate (1.605 g) was dissolved in 25 ml deionized (DI) water, giving a 7.5 mmol periodate solution. Relative molar ratio between sodium metaperiodate and alginate monomer units was 0.297, corresponding to 29.7 mol.% of maximum (theoretical) oxidation degree in case of complete reaction without formation of secondary products.

Then, the periodate solution was slowly added to the sodium alginate dispersion under magnetic stirring in dark conditions at room temperature. After 6

hours, the reaction was quenched by adding 5 ml of ethylene glycol under continuous stirring at 500 rpm for 30 minutes. The resulting solution was placed in 8 dialysis membrane (MWCO: 6000-8000 Da) and dialysis was performed against DI water for 3 days changing water twice a day, to remove any traces of unreacted sodium metaperiodate.

Thereafter, a test with silver nitrate ( $\text{AgNO}_3$ ) was conducted to verify the absence of periodate in the dialysate. Specifically, a 0.5 ml aliquot of the dialysate was added to 0.5 ml of 1% (w/v) solution of silver nitrate, checking the absence of any precipitate.

Finally, ADA solution was frozen at  $-20^\circ\text{C}$  for 2 days and lyophilized for 3 days, obtaining the final product.

The synthesis was repeated in triplicate.

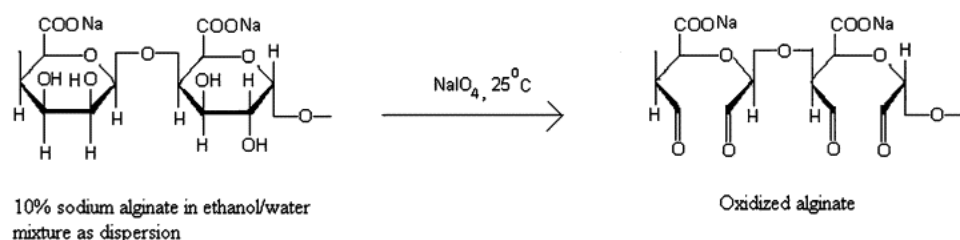


**Figure 3.1.** Periodate oxidation of sodium alginate.

Source: Balakrishnan, B. et al. / *Carbohydrate RESEARCH*. 2005; 340(7):1425-29.

### 3.2.2. Characterization of oxidized alginate

#### 3.2.2.1. Yield of production

The yield of production was determined by measuring the dried weight ratio between the product obtained after the reaction and the starting sodium alginate. The yield of oxidized product was calculated by the following equation:

$$\text{Yield of production (\%)} = \frac{\text{weight of ADA obtained from the oxidation reaction (g)}}{\text{weight of initial Na}^+\text{Alg (g)}} \cdot 100$$

### 3.2.2.2. Determination of the molecular weight

Molecular weight of sodium alginate was determined using the viscosity method.

The experiment was carried out at 25°C with Ubbelodhe viscosimeter placed in a constant temperature aqueous bath (Figure 3.2). An alginate solution of known concentration was put inside the viscosimeter, and the efflux time was repeatedly measured until consistent readings were obtained. To record the efflux time, a polymer solution of known concentration is put in the reservoir and aspirated to the upper bulb, creating vacuum in that chamber. Once the solution has reached the upper bulb, air is admitted again and the solution flows down the capillary by gravity. The time needed for the solution to flow between the two marks is recorded and is known as efflux time.

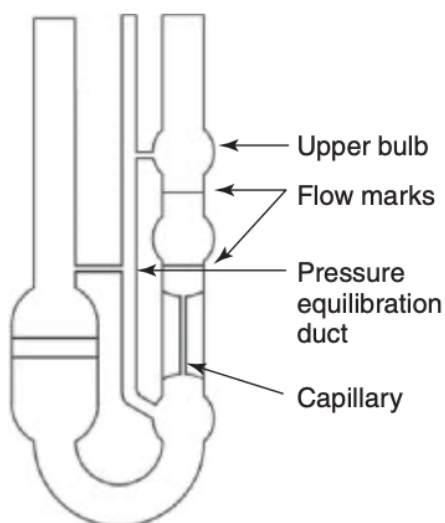


**Figure 3.2.**  
viscosimeter.  
*Velázquez, M. et al. /  
Synth., charact., and*

2013; 340(7):355-66.

Ubbelodhe  
*Source: Neira-  
Handbook of Pol.  
processing.*

Efflux times were measured for solutions of sodium alginate, which was dissolved in 0.1 M NaCl solution to get the final concentrations 0.0125%,

0.025%, 0.05% and 0.1% (w/v). For all the times recorded, the efflux time of a 0.1M NaCl solution was taken as a reference.

Some terms related to the viscosity of the solutions were defined as following:

- Relative viscosity, defined as the ratio between  $t$  and  $t_0$ , which are the average efflux time of the solution at a certain concentration and of the solvent, respectively:  $\eta_{rel} = t/t_0$ .
- Specific viscosity, defined as  $\eta_{spec} = \eta_{rel} - 1$ .
- Reduced viscosity, defined as the ratio between the specific viscosity and the solute concentration:  $\eta_{rid} = \eta_{spec}/c$ .
- Inherent viscosity, defined as  $\eta_{inh} = \ln(\eta_{rel})/c$ .

By plotting  $\eta_{rid}$  and  $\eta_{inh}$  and identifying their intercept, an estimation of the intrinsic viscosity ( $\eta$ ) was obtained.

Afterward, the viscosity average molar mass ( $M_\eta$ ) of sodium alginate was calculated from the measured ( $\eta$ ) following the Mark-Houwink equation:

$$[\eta] = K \times M_\eta^\alpha$$

By adapting  $\alpha$  and K values for ALG, the equation becomes:

$$[\eta] = 2.0 \cdot 10^{-5} \times M_\eta^{1.076}$$

### 3.2.2.3. Determination of the degree of oxidation

The degree of oxidation was investigated by determining Uv-Vis absorption using a microplate spectrophotometer (Synergy HTX Multi-Mode Reader, Figure 3.3). The determination of the oxidation degree was made by an indirect method, measuring the unconsumed sodium metaperiodate before quenching the reaction with ethylene glycol, using an indicator solution. The

indicator solution (IS) was prepared by mixing equal volumes of 20% (w/v) KI and 1% (w/v) soluble starch solution, using phosphate buffer (pH=7) as solvent.



**Figure 3.3.** Synergy HTX Multi-Mode Reader.

A calibration curve of sodium metaperiodate solutions was prepared from a 0.32 mg/ml stock solution (SS) of  $\text{NaIO}_4$  in DI water, diluting SS in DI water with final concentrations ranging from 0.0016 mg/ml to 0,02 mg/ml. The resulting  $\text{NaIO}_4$  solutions were placed in a 12-well plate, where IS was added to reach a total volume of 1 ml. The absorbance of the triiodine-starch complexes was measured at a specific wavelength of 486 nm in triplicate.

N° of dilution	Dilution factor (DF)	$\text{NaIO}_4$ (mg/ml)	$\text{NaIO}_4$ ( $\mu\text{g/ml}$ )
1	16	0.02	0.467
2	32	0.02	0.234
3	50	0.0064	0.1495
4	100	0.0032	0.0748
5	299	0.0016	0.0374

**Table 3.1.** Dilutions and concentration of  $\text{NaIO}_4$  used for the calibration curve to calculate ADA degree of oxidation.

To determine the oxidation degree of ADA, 1 ml aliquot of the reaction mixture was collected before quenching the reaction and diluted to 250 ml with DI water. Then, 3 ml of the diluted solution were mixed with 1.5 ml of IS and

further DI water was added to obtain a final volume of 5 ml. The absorbance of the mixture was measured right after with plate reader (Synergy HTX Multi-Mode Reader) at 486 nm. The amount of unconsumed periodate was calculated from the absorbance using the calibration curve described above.

After determining the unconsumed  $\mu\text{mol}$  of  $\text{NaIO}_4$  from the calibration curve, the degree of oxidation was calculated using the following equation:

$$\text{Degree of oxidation (\%)} = \frac{\text{initial NaIO}_4 - \text{final NaIO}_4(\mu\text{mol})}{\text{initial NaIO}_4 (\mu\text{mol})} \cdot 100$$

Initial  $\text{NaIO}_4$  corresponds to the initial moles of sodium metaperiodate used to oxidized alginate, while final  $\text{NaIO}_4$  refers to the moles after the reaction calculated using the calibration curve.

#### 3.2.2.4. FTIR Analysis

FTIR spectroscopy with attenuated total reflectance (ATR), ATR-FTIR Frontier FT-IR Perkin Elmer instrument (Figure 3.4) was used to investigate the formation of aldehyde groups in the alginate chains. Lyophilized samples of ADA and alginate powder were analyzed using a spectral range of 4000-600  $\text{cm}^{-1}$ , at a resolution of 4  $\text{cm}^{-1}$  using 32 scans.

ATR-FTIR spectra were recorded in triplicate to evaluate the results of all the syntheses performed.



**Figure 3.4.** ATR-FTIR Frontier FT-IR Perkin Elmer.

#### 3.2.2.5. *NMR Analysis*

Solid state-NMR experiments of alginate powder and ADA lyophilized samples were performed for  $^{13}\text{C}$  using a Bruker AVANCE III HD NMR spectrometer with a magnetic field frequency and strength of 500 MHz and 11 T, respectively.

$^{13}\text{C}$  CPMAS NMR (crosslinking polarization under magic angle spinning NMR) spectra were recorded for ADA samples of all the synthesis and for ADA/GEL samples (described in paragraph 3.2.3.2.4.). In ADA/GEL samples, a Schiff's base formation between ADA and GEL was investigated.

For all the spectra, tetramethylsilane (TMS) using tyrosine hydrochloride (carboxylic carbon 172.48 ppm for TMS) was assumed as the secondary reference for  $^{13}\text{C}$ .

### 3.2.3. ADA/GEL hydrogel formulation

#### 3.2.3.1. Chemical crosslinking

ADA and gelatin (GEL) crosslinking through Schiff-base reaction (Figure 3.5) was investigated.

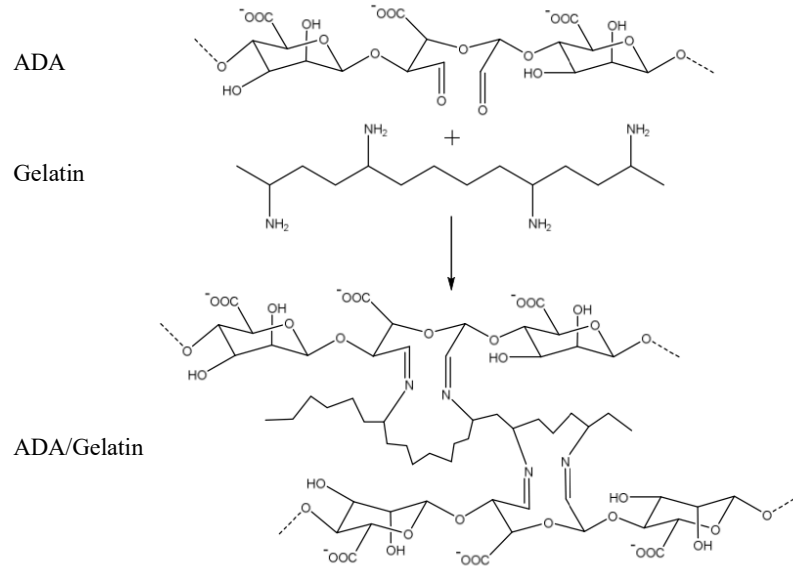


**Figure 3.5.** Crosslinking of ADA and GEL *via* Schiff base reaction.

To prepare ADA-GEL solutions, gelatin and ADA were dissolved separately in DI water. Then, gelatin solution was slowly added to a solution of ADA under continuous stirring at 37°C to facilitate reaction and crosslinking between them. The weight ADA/GEL ratios in the final hydrogels were 50/50, 70/30, 80/20, 90/10, and 95/5.

Starting concentration (% w/v)		Weight ratios (%)		Final concentration (% w/v)		Label for composition
ADA	GEL	ADA	GEL	ADA	GEL	
5	5	95	5	4.75	0.25	5-ADA95/GEL5
5	5	90	10	4.5	0.5	5-ADA90/GEL10
5	5	80	20	4	1	5-ADA80/GEL20
5	5	70	30	3.5	1.5	5-ADA70/GEL30
5	5	50	50	2.5	2.5	5-ADA50/GEL50
10	10	95	5	9.5	0.5	10-ADA95/GEL5
10	10	90	10	9	1	10-ADA90/GEL10
10	10	80	20	8	2	10-ADA80/GEL20
10	10	70	30	7	3	10-ADA70/GEL30
10	10	50	50	5	5	10-ADA50/GEL50

**Table 3.2.** Labels used for different samples as a function of their composition.

### 3.2.3.2. Ionic crosslinking

An internal gelation mechanism was realized delivering insoluble calcium-alginate ( $\text{Ca}^{2+}$ -Alg) particles into alginate bulk.

#### 3.2.3.2.1. $\text{Ca}^{2+}$ -Alg preparation

Insoluble calcium alginate particles were prepared by precipitation of alginate solutions with calcium salts solution. Specifically, alginate was dissolved in DI water under magnetic stirring at room temperature.  $\text{CaCl}_2$  was also dissolved in water, obtaining solutions with a calcium molarity value ranging from 3M to 6M. Then, 3M  $\text{CaCl}_2$  solution was slowly added to alginate solution with alginate concentrations ranging from 1.5% to 0.025% (w/v), whereas 4M, 5M, and 6M  $\text{CaCl}_2$

solutions were slowly added to 0.1% and 0.05% (w/v) alginate solutions. Particle formation was observed for each composition listed in Table 3.3.

Sample	Alginate (%w/v)	CaCl <sub>2</sub> (M)
Ca <sup>2+</sup> -Alg <sub>1.5</sub> /3M	1.5	3 M
Ca <sup>2+</sup> -Alg <sub>0.8</sub> /3M	0.8	3 M
Ca <sup>2+</sup> -Alg <sub>0.4</sub> /3M	0.4	3 M
Ca <sup>2+</sup> -Alg <sub>0.20</sub> /3M	0.20	3 M
Ca <sup>2+</sup> -Alg <sub>0.1</sub> /3M	0.1	3 M
Ca <sup>2+</sup> -Alg <sub>0.05</sub> /3M	0.05	3 M
Ca <sup>2+</sup> -Alg <sub>0.025</sub> /3M	0.025	3 M

Sample	Alginate (%w/v)	CaCl <sub>2</sub> (M)
Ca <sup>2+</sup> -Alg <sub>0.1</sub> /4M	0.1	4 M
Ca <sup>2+</sup> -Alg <sub>0.1</sub> /5M	0.1	5 M
Ca <sup>2+</sup> -Alg <sub>0.1</sub> /6M	0.1	6 M
Ca <sup>2+</sup> -Alg <sub>0.05</sub> /4M	0.05	4 M
Ca <sup>2+</sup> -Alg <sub>0.05</sub> /5M	0.05	5 M
Ca <sup>2+</sup> -Alg <sub>0.05</sub> /6M	0.05	6 M

**Table 3.3.** Ca<sup>2+</sup>-Alg formulations tested.

The fabricated particles were centrifugated for 10 minutes at 3600 rpm and washed in DI water, to remove the calcium chloride solution from their surface. The centrifugation and the washing procedure were repeated 4 times, followed by freeze-drying and milling.

### 3.2.3.2.2. Alginate/ADA and Ca<sup>+</sup>-Alg formulation

An 8% (wt) alginate stock solution (SS) was prepared in DI water. Starting from this, samples named **0NaAlg-0CaAlg<sub>00</sub>** were produced. DI water was added to the SS under continuous stirring to obtain diluted solutions of 1% (w/v) alginate. Dispersion of Ca<sup>2+</sup>-Alg were prepared by mixing DI water and freeze-dried Ca<sup>2+</sup>-Alg microparticles. For alginate hydrogels, Ca<sup>2+</sup>-Alg microparticles obtained from a starting alginate solution of 0.1% or 0.05% (w/v) and with 3M Ca<sup>2+</sup> were used. The dispersion was obtained by using two syringes connected with a Luer lock connection (Figure 3.6), until a macroscopically homogeneous mixture was obtained. Thereafter, alginate solution was added to the Ca<sup>2+</sup>-Alg dispersion testing different ratios. Using the same syringes mechanism, the alginate solution was first ejected into the syringe containing Ca<sup>2+</sup>-Alg dispersion and the resulting mixture was displaced back and forth between the syringes five times. The final suspension (Alginate, Ca<sup>2+</sup>-Alg) was poured into an appropriate container to form a gel. The mixing time was around 7 seconds.

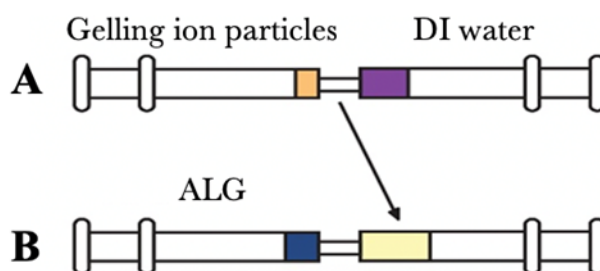


**Figure 3.6.** Schematic illustration of the two-component alginate system. (A) Insoluble gelling ion particles dispersed in DI water. (B) Mixing of aqueous ALG solution and particles dispersion.

The same procedure was performed using ADA solutions as soluble component of the gelling system, obtaining **0ADA-0CaAlg<sub>00</sub>** samples. DI water was added to an 8% (wt) ADA stock solution in order to obtain diluted solutions of 1% or 2% (w/v) ADA. For ADA hydrogels, Ca<sup>2+</sup>-Alg microparticles obtained from a starting alginate solution of 0.1% or 0.05% (w/v) with 4M, 5M, and 6M Ca<sup>2+</sup> were used. ADA solution and Ca<sup>2+</sup>-Alg dispersion were mixed at different ratios.

Starting polymers concentrations, their ratio, and final polymer concentration are listed in Table 3.4.

Sample	ALG or ADA (% w/v)	Ca <sup>2+</sup> -Alg particles		Final polymer concentration (% w/v)
		Type (initial (% w/v) )	% w/v	
1NaAlg-1CaAlg <sub>0.1</sub>	1%	0.1%	2%	3%
1NaAlg-1CaAlg <sub>0.1</sub>	1%	0.1%	1%	2%
1NaAlg-0.5CaAlg <sub>0.1</sub>	1%	0.1%	0.5%	1.5%
1NaAlg-0.25CaAlg <sub>0.1</sub>	1%	0.1%	0.25%	1.25%
1ADA-1CaAlg <sub>0.1</sub>	1%	0.1%	1%	2%
2ADA-1CaAlg <sub>0.1</sub>	2%	0.1%	1%	3%
2ADA-2CaAlg <sub>0.1</sub>	2%	0.1%	2%	4%
2ADA-2CaAlg <sub>0.05</sub>	2%	0.05%	2%	4%
2ADA-4CaAlg <sub>0.05</sub>	2%	0.05%	4%	6%

**Table 3.4.** ALG/ Ca<sup>2+</sup>-Alg and ADA/Ca<sup>2+</sup>-Alg hydrogels formulation.

Based on rheological characterization, the 2ADA-4CaAlg<sub>0.05</sub> sample was selected for further experiments and for NPs-loaded hydrogel formation.

### 3.2.3.2.3. ADA/GEL

ADA/GEL hydrogels were obtained also by ionically crosslinking. ADA and GEL were dissolved in DI water separately, then placed into two syringes and mixed using a Luer lock connector. The two polymers were mixed at five different weight ratios 70/30, 80/20, 90/10, 95/5, and 100/0 (% w/w).  $\text{Ca}^{2+}$ -Alg particles with 3 M  $\text{Ca}^{2+}$  were dispersed in DI water and then mixed with ADA/GEL solution. The soluble and the insoluble component of the gelling system were blended in a 2 to 4 ratio. The content of the syringes was displaced back and forth 5 times. The mixture was poured into an appropriate container to form a gel. The overall mixing time was around 7 seconds. Samples named **0ADA<sub>00</sub>G<sub>0</sub>-4CaAlg<sub>00</sub>** were obtained with a final polymer concentration of 6% (w/v). All the mixing steps are schematically represented in Figure 3.7.

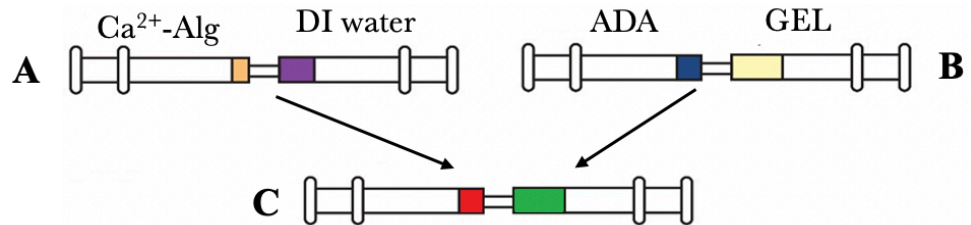


**Figure 3.7.** Schematic illustration of the gelling system. (A) Insoluble  $\text{Ca}^{2+}$ -Alg particles dispersed in DI water. (B) Aqueous ADA and GEL solution. (C) Mixing of the two gelling components.

ADA and GEL concentration, polymers ratios, and final polymer concentration are listed in Table 3.6.

Sample	ADA		GEL		Ca <sup>2+</sup> Alg particles		Final polymer concentration (% w/v)
	wt%	Final %w/v	wt%	Final %w/v	Type (initial (%w/v))	%w/v	
2ADA <sub>100</sub> G <sub>0</sub> -4CaAlg <sub>0.05</sub>	100	2%	0	0%	0.1%	4%	6%
2ADA <sub>95</sub> G <sub>5</sub> -4CaAlg <sub>0.05</sub>	95	1.9%	5	0.1%	0.1%	4%	6%
2ADA <sub>90</sub> G <sub>10</sub> -4CaAlg <sub>0.05</sub>	90	1.8%	10	0.2%	0.1%	4%	6%
2ADA <sub>80</sub> G <sub>20</sub> -4CaAlg <sub>0.05</sub>	80	1.6%	20	0.4%	0.1%	4%	6%
2ADA <sub>70</sub> G <sub>30</sub> -4CaAlg <sub>0.05</sub>	70	1.4%	30	0.6%	0.1%	4%	6%

**Table 3.6.** Crosslinking of ADA and GEL *via* Schiff base reaction.

#### 3.2.4. NPs-loaded hydrogel formation

PLGA/DE-DOPE/miRNA NPs were obtained by nanoprecipitation method as describe before<sup>30</sup>. Firstly, DE-DOPE/miRNA lipoplexes were prepared by electrostatic interactions between positively charged DE-DOPE and negatively charged miRNA. Briefly, 6  $\mu$ L of DE-DOPE suspension (1 mg/mL) and 10  $\mu$ L of miRNA (5  $\mu$ M) were incubated for 20 min, followed by vortexing vortex (2000-2500 rpm). Complexes formation was allow to proceed for other 20 min. Finally, DE-DOPE/miRNA lipoplexes were diluted in Milli-Q water to a final volume of 1 mL. Then, DE-DOPE/miRNA PLGA NPs were obtained by nanoprecipitation of PLGA-COOH into DE-DOPE/miRNA lipoplexes suspension. adapted from a previous work<sup>113</sup>. Firstly, 1 mg/mL PLGA solution was obtained by dissolving the polymer in acetone, 1 mL of DE-DOPE/miRNA lipoplexes was poured into a glass test tube and stirred (ca. 870-900 rpm), paying attention to vortex formation inside the suspension. Then, the PLGA solution (127  $\mu$ g/mL) was dropped into the lipoplexes suspension under magnetic stirring and the reaction was allow to proceed for 30 min. Afterwards, the mixture was poured in a beaker under agitation until complete acetone evaporation. Finally, 1 mL of PLGA/DE-DOPE/miRNA NPs was obtained.

Once miRNA-loaded NPs were obtained, they were suspended in DI water and mixed with a 2% (w/v) ADA solution using two syringes connected with a Luer lock connection. Simultaneously Ca<sup>2+</sup>-Alg particles with calcium molarity of 3 M were dispersed in DI water. Thereafter, NPs-loaded ADA solution and Ca<sup>2+</sup>-Alg dispersion were mixed using the previous syringes mechanism, by ejecting first ADA/NPs solution in the syringe containing the dispersion and then displacing the mixture back and forth 5 times. Afterward, the mixture was put into an opportune container. All the mixing steps are schematically represented in Figure 3.7.

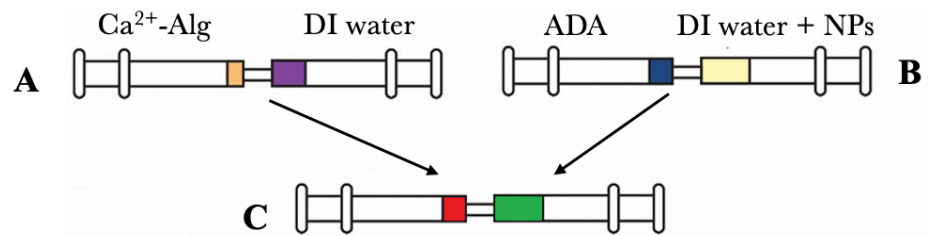


**Figure 3.7.** Schematic illustration of the gelling system. (A) Insoluble Ca<sup>2+</sup>-Alg particles dispersed in DI water. (B) Aqueous ADA solution and NPs embedding. (C) Mixing of the two gelling components.

ADA concentration, final polymer concentration, and NPs concentration are listed in Table 3.5.

Sample	ADA (% w/v)	Ca <sup>2+</sup> -Alg particles		Final polymer concentration (% w/v)	NPs concentration (µg/mL)
		Type (initial (% w/v))	% w/v		
2ADA-4CaAlg <sub>0.05</sub>	2%	0.1%	2%	4%	-(blank)
2ADA-4CaAlg <sub>0.05</sub> -NPs <sub>6.7</sub>	2%	0.05%	2%	4%	6.7
2ADA-4CaAlg <sub>0.05</sub> -NPs <sub>13.4</sub>	2%	0.05%	4%	6%	13.4

**Table 3.5.** ADA/Ca<sup>2+</sup>-Alg/NPs hydrogels formulation.

### 3.2.5. Hydrogel characterization

#### 3.2.4.1. Oscillatory rheological measurements

A MCR 302 rheometer (Anton Paar) was used to evaluate the *in situ* gelation of different alginate/ADA solutions. Specifically, a plate-plate geometry was chosen ( $d = 25$  mm). Hydrogels were prepared as described above and deposited directly onto the base of the instrument. The set-up of the experiment was timed to 30 seconds from the first syringe-to-syringe displacement.



**Figure 3.8.** MCR 302 rheometer, Anton Paar

Hydrogels behavior was evaluated by recording changes in storage modulus ( $G'$ ) and loss modulus ( $G''$ ) values related to variations in parameters for oscillatory tests, such as strain (strain sweep), time (time sweep), and frequency (frequency sweep).

For the oscillatory test, an amplitude strain sweep was carried out at a frequency of 5 Hz and deformation ranging from 0.01 to 100. The deflection of the measuring system causing the deformation is increased stepwise from one measuring point to the next, while keeping constant the frequency. This test was performed to identify the linear viscoelastic region (LVE Region), which indicates the strain amplitude range that provides a linear material

response, without destroying the structure of the sample. For the following oscillatory tests, the measurements were carried out at strain levels within the LVR. Time sweep analysis was performed to evaluate the material gelling time, that is the time needed for soft materials to transit from fluid flow-like behavior to solid elastic behavior. The gelling time was identified as the instant of time in which the curve of the storage modulus ( $G'$ ) and of the loss modulus ( $G''$ ) intersect (Figure 3.9).

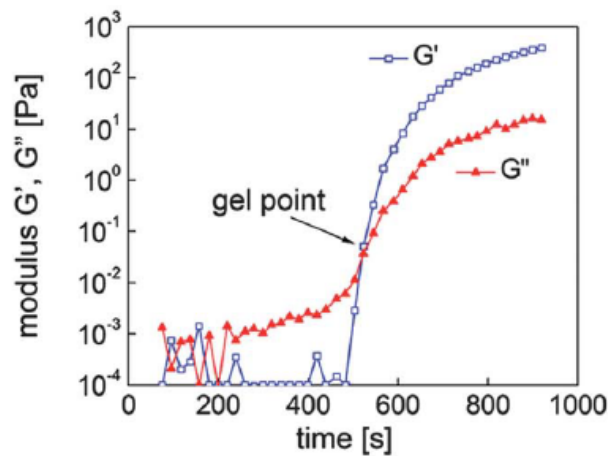


**Figure 3.9.** Gel point detection through time sweep analysis.

Source: Dawedeit, C. et al. / *Soft matter*. 2015; 8(13):3518-21.

The test was performed using a frequency of 1 Hz and a constant strain of 1.0%. The hydrogel precursor was extruded directly on the rheometer plate before gelation occurs. Frequency sweep analysis was performed to describe the time-dependent behavior of a sample in the non-destructive deformation range, since the selected shear-strain amplitude was in the LVE Region. Specifically, samples behavior was evaluated in terms of  $G'$  and  $G''$  values by applying a shear-strain, whose amplitude was in the LVR. An angular frequency range of 0.1-100 rad/s and a constant strain of 1.0% were used.

The analyses were performed at a constant temperature of 25°C for all the samples, while ADA/GEL, ADA/ $\text{Ca}^{2+}$ -Alg/NPs, and ADA/GEL/  $\text{Ca}^{2+}$ -Alg

were tested at 37°C. The temperature was kept constant during all the measurements to provide for isothermal conditions.

Each type of hydrogel was tested in triplicate.

#### *3.2.4.3. Swelling and degradation study*

For swelling and degradation tests three hydrogel samples per type were poured into test tubes (Eppendorf Tubes® 3810X) and immersed into 1 ml of DI water for each time point.. All the samples were incubated at 37°C, with a controlled atmosphere of 5% CO<sub>2</sub> and 95% relative humidity (Thermo Scientific Heraeus heating Oven). Their weight was recorded prior to the immersion ( $W_0$ ) and after each time points ( $W_i$ ), after being passed on blotting paper to remove the excess of water. After the samples were weighted, fresh DI water was added to the test tubes to carry on the test.

The swelling and degradation of the samples were calculated according to the following equation:

$$\text{Swelling (w\%)} \text{ or } \text{Degradation} = \frac{W_i}{W_0} \cdot 100$$

Positive values were considered as swelling (w%) and negative values were considered as degradation (w%).

Swelling and degradation studies were conducted until complete dissolution of the hydrogels.

#### *3.2.4.4. NPs release from NPs-loaded hydrogels*

Swelling and degradation study was performed on NPs-loaded hydrogels. Specifically, samples of 2 ml were put in test tubes and 500 µl of DI water was added on the top of the hydrogels. Release media were

collected and analyzed to evaluate NPs release at designed time points, i.e. after 1, 3, 6, 24, 48, 120, 168, and 216 hours.

Dynamic light scattering (DLS, Litesizer™ 500, Anton Paar, USA, Figure 3.10-A) was used to perform zeta potential ( $\zeta$ ) measurements of the released NPs. Samples were loaded in Anton-Paar  $\Omega$ -shaped capillary cuvettes (Figure 3.10-B), that are able to create a stable electric field exactly at the measurement position, resulting in reproducible  $\zeta$  measurements. Temperature was set at 37°C. NPs were tested as control signal.

All the measurements were made in triplicate.

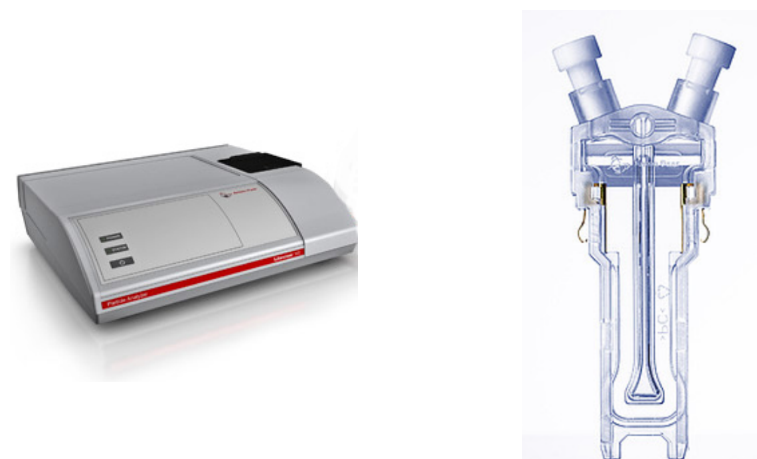


**Figure 3.10.** (A) DLS, Litesizer™ 500, Anton Paar, USA. (B)  $\Omega$ -shaped capillary cuvette, Anton Paar, USA.

#### 3.2.4.5. *miRNA release from NPs-loaded hydrogels*

miRNA release from NPs-loaded hydrogels was evaluated testing the release media collected at each time point with an Invitrogen Qubit 4 Fluorometer (Thermo Fisher Scientific, US, Figure 3.11) and its dedicated analysis kit (Qubit microRNA buffer, Thermo Fisher), prepared according to manufacturer's instructions. NPs solutions were

centrifugated at 15000 rpm and at and 4°C for 15 min to obtain a pellet. 20 µl of supernatant was withdrawn and pour in a test tube and mixed with 180 µL of Qubit™ buffer solution, rapidly vortexed and analysed with Qubit™ 4 Fluorometer. The resultant mixture was analyzed with Qubit to evaluate miRNA release. MiRNA release profile was calculated as: amount of miRNA detected at each timepoint / amount of miRNA inside the NPs.

ADA hydrogel without NPs was tested to measure blank signal.



**Figure 3.11.** Invitrogen Qubit 4 Fluorometer, Thermo Fisher Scientific, US.

## IV. RESULTS AND DISCUSSION

---

### 4.1. Oxidation of sodium alginate

#### *4.1.1. Oxidation degree and molecular weight of the modified alginate*

Alginate oxidation using sodium metaperiodate as oxidizing agent leads to the cleavage of the adjacent diols in the polysaccharide chains forming their dialdehyde derivatives<sup>47,57</sup>. Sodium alginate was oxidized in ethanol-water mixture for 6 hours, at room temperature, and dark conditions. Alginate solutions in aqueous medium are very viscous even at low concentration, making the reaction difficult to handle and leading to a small quantity of oxidized product. On the other hand, carrying out the reaction in ethanol-water mixture requires a small quantity of solvent to obtain a higher quantity of oxidized product.

The polymer synthesis was repeated three times following the same protocol and under the same conditions. Before freeze-drying, a test using  $\text{AgNO}_3$  confirmed the absence of periodate from the three different dialysates. Specifically, in  $\text{NaIO}_4$  samples silver iodide (a silver salt) is formed by the reaction between silver and iodine and a visible brown precipitate appeared. Instead, the precipitate was not present in the dialysate aliquots.

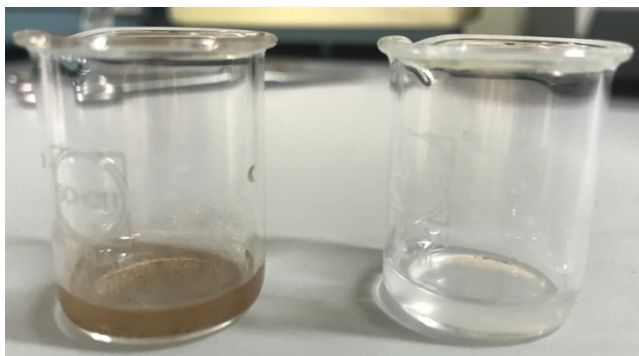


**Figure 4.1.** AgNO<sub>3</sub> test performed on NaIO<sub>4</sub> samples (left side) and on the dialysate (right side)

As shown in Figure 4.2, during the synthesis process each  $\alpha$ -glycol group consumes one molecule of periodate, and the rate of the reaction is strictly related to the stereochemistry of the  $\alpha$ -glycol group under certain conditions. Relative molar ratio between sodium metaperiodate and alginate monomer units was 0.27, corresponding to 29.7% of maximum theoretical oxidation degree in case all the hydroxyl groups are oxidized without formation of secondary products.

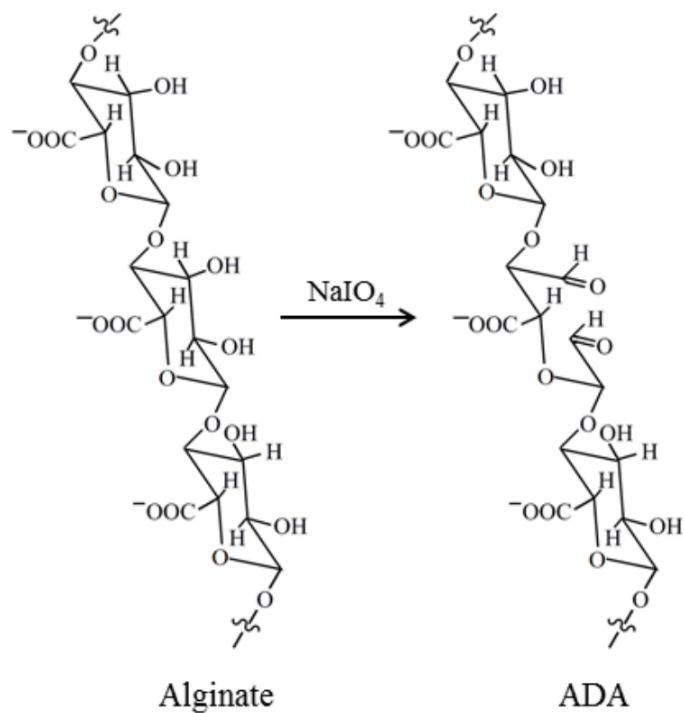


**Figure 4.2.** ADA synthesis from alginate by periodic oxidation.

ADA of different degree of oxidation can be obtained by varying the quantity of oxidizing agent and sodium alginate. The equivalent weight of  $\text{NaIO}_4$  to sodium alginate was 32.1% in the current study.

To identify the oxidation degree of ADA obtained from each synthesis, a Iodometric titration method was used to detect the residual periodate present in the reaction mixture after quenching. Iodometry is an indirect method of determination since a product of a preliminary reaction is titrated. An indicator solution containing starch and potassium iodide (KI) was added to the solution being titrated. Specifically, KI was used since it helps to solubilize the free iodine, which is quite insoluble in pure water under normal conditions. The addition of iodine ( $\text{I}^-$ ) to iodine ( $\text{I}_2$ ) solutions resulted in the formation of triiodine ( $\text{I}_3^-$ ) ions, which can be absorbed by starch and form a triiodine-starch complex. The amylose fraction of starch interacts with  $\text{I}_3^-$  ions, and this absorption caused the solution to change its color from deep blue to light yellow. The end point in iodometry corresponds to a loss of blue color due to the formation of the complex. Therefore, the darker the color, the higher the amount of unconsumed  $\text{NaIO}_4$ .

Increasing concentrations of sodium metaperiodate were tested with indicator solution, leading to darker solutions and resulting in an increasing absorbance measured by UV-Vis spectroscopy at 486 nm wavelength. A calibration curve (Figure 4.3) was obtained from these data. This curve was used to predict the concentration of the analyte in the reaction mixture and to calculate the degree of oxidation of the different ADA samples.

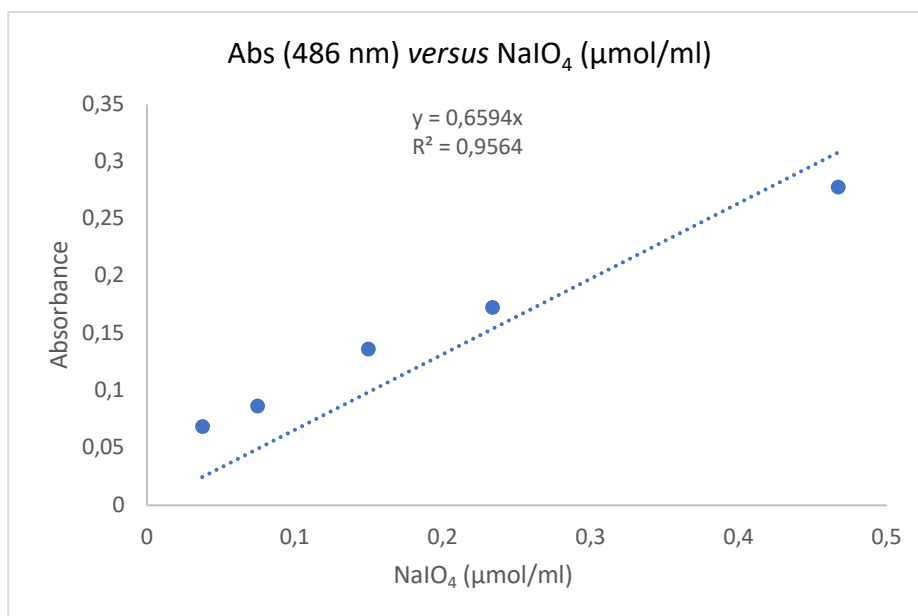


**Figure 4.3.** Calibration curve for NaIO<sub>4</sub> solutions.

The UV-Vis absorbance of the solutions containing sodium alginate and sodium metaperiodate was measured after the reaction. Subsequently, in the equation of the calibration curve the parameter “y” was replaced by the absorbance value and “x” was obtained, which corresponds to the concentration of NaIO<sub>4</sub> in the sample. The mean oxidation degree of the synthesized ADA was found to be  $23.0 \pm 0.1\%$ , presented in Table 4.1. This data revealed that sodium metaperiodate was not completely consumed during oxidation because of the hemiacetal formation between oxidized and unoxidized alginate residues.

Periodate equivalent (wt%)	Degree of oxidation of ADA (%)
32.1	$23.0 \pm 0.1$

**Table 4.1.** Degree of oxidation of ADA obtained by periodate oxidation of sodium ALG.

Hence, the molar percentage of oxidized monomer units in the polymer was quite similar to the theoretical value.

During the oxidation process, sodium periodate does not only oxidize ALG uronic acid, but also triggers the scission of polysaccharide chain leading to a lower MW of the resulting ADA.<sup>66</sup> Therefore, a slight decrease in ADA MW is expected to an extent depending on the periodate equivalent used. Molecular weight of alginate from *Macrocystis pyrifera* (MP Biomedicals) was estimated by viscosity method. Specifically, the reduced and the inherent viscosities were experimentally obtained, and then they were plotted against concentration. Afterward, the intrinsic viscosity was obtained by the extrapolation of these curves to zero concentration (intercept with the  $y$ -axis).<sup>76</sup> Once the intrinsic viscosity value was known, MW of sodium alginate was estimated using  $K$  and  $\alpha$  values reported in the literature.<sup>77</sup> Specifically, an average value of 287 kDa was obtained.

Material	$\eta_{inh}$ to zero concentration	$\eta_{rid}$ to zero concentration	Average intrinsic viscosity	$M_{\eta}$ (kDa)
ALG	767.03 dL/g	767.37 dL/g	767,2 dL/g $\pm$ 0.25	287.24 kDa

**Table 4.2.** Intrinsic viscosity and viscosimetric molecular weight of ALG.

#### 4.1.2. Yield of ADA production

The yield of oxidized alginate was evaluated as the amount of pure and dry product yielded in the process. The ratio between the quantity of product formed and alginate used revealed the process yield (%). For the first reaction the yield of product was:

$$\text{Yield of ADA production (\%)} = \frac{3,5 \text{ g of ADA}}{5 \text{ g of NaAlg}} \cdot 100 = 70\%$$

For the second reaction, the same starting quantity of alginate was used. Final weight of obtained lyophilized ADA was 3.39 g, resulting in a yield of:

$$\text{Yield of ADA production (\%)} = \frac{3,39 \text{ g of ADA}}{5 \text{ g of NaAlg}} \cdot 100 = 67.84 \cong 68\%$$

From the third reaction, 3.23 g of ADA were obtained. Therefore, the yield of production was:

$$\text{Yield of ADA production (\%)} = \frac{3,23 \text{ g of ADA}}{5 \text{ g of NaAlg}} \cdot 100 = 64.68 \cong 65\%$$

Yield variations within the triplicate experiments were not significant, determining a mean yield of  $68\% \pm 0,7$ . These results confirmed that performing the reaction in ethanol-water mixture requires a smaller amount of solvent to obtain a 60-70% yield of the oxidized product.



**Figure 4.4.** Freeze-dried ADA sample.

#### *4.1.2. Formation of aldehyde groups*

The formation of aldehyde groups was confirmed by ATR-FTIR and  $^{13}\text{C}$ -NMR spectroscopy. FTIR spectroscopy allows the analysis of functional groups within a sample based on their absorbance at different wavenumbers at  $600\text{-}4000 \text{ cm}^{-1}$ . FTIR spectra of alginate powder and samples of lyophilized ADA obtained from the three syntheses are shown in Figure 4.5.

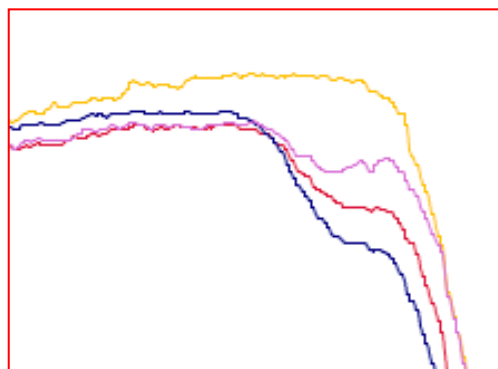
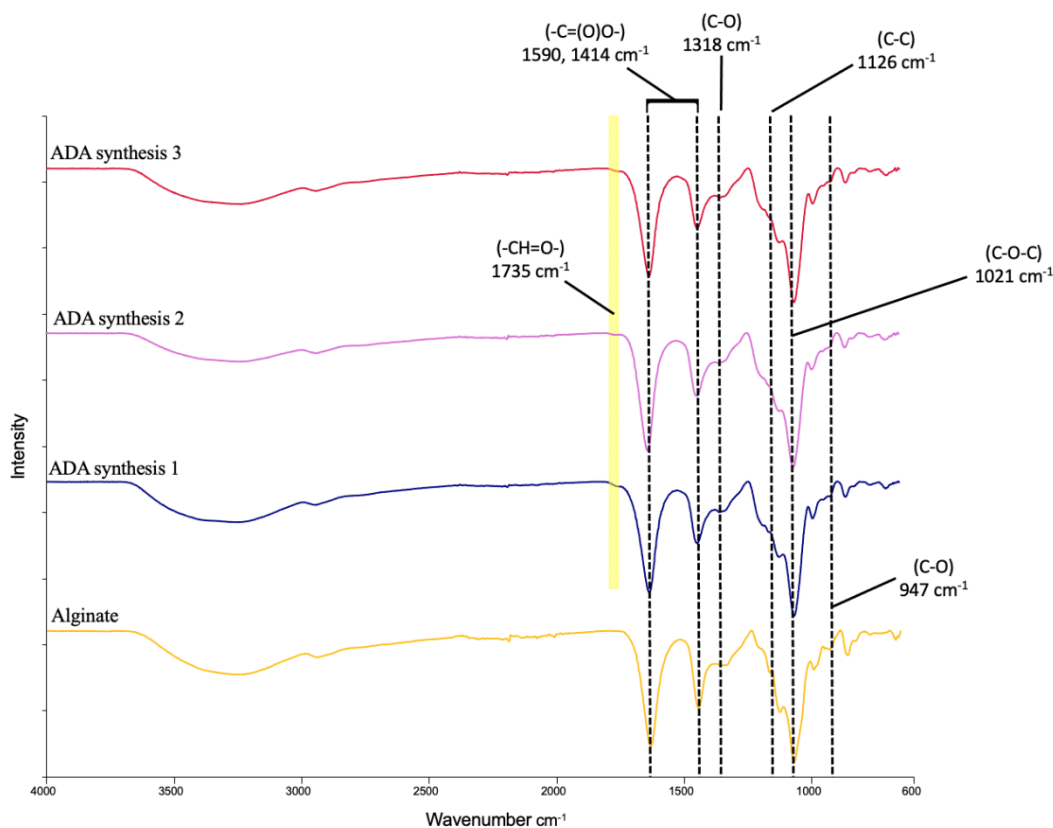


**Figure 4.5.** (A) ATR-FTIR spectra of ALG and three samples of different lyophilized ADA. (B) Zoom of the spectra at 1740-1725  $\text{cm}^{-1}$ .

Sodium alginate spectrum presented the characteristic absorption band of its polysaccharide structure at 1318  $\text{cm}^{-1}$  (C-O stretching), 1126  $\text{cm}^{-1}$  (C-C stretching), 1021  $\text{cm}^{-1}$  (C-O-C stretching), and 947  $\text{cm}^{-1}$  (C-O stretching). Absorption bands at 1590  $\text{cm}^{-1}$  and 1414  $\text{cm}^{-1}$  are related to asymmetric and

symmetric stretching peaks of carboxylate salt groups (-C(=O)O-) of alginate.<sup>78</sup> In ADA spectrum, a band with a very low intensity was detected between 1740 and 1725 cm<sup>-1</sup> highlighting the formation of aldehyde groups.<sup>78</sup> Previous literature showed that this band is difficult to detect because of hemiacetal formation of free aldehyde groups with hydroxyl groups on the adjacent uronic acid subunits.<sup>79</sup>

This was not present in the alginate spectrum, as expected. Alterations in the characteristic pattern of absorption bands clearly indicated a change in the material composition.

To further assess aldehyde groups formation, <sup>13</sup>C MAS NMR spectroscopy was carried out on alginate and ADA lyophilized samples, and the spectra are shown in Figure 4.6. The spectra of alginate showed the presence of 12 peaks corresponding to the carbon atoms of mannuronate (M) and guluronate (G) units, assigned as shown in Figure 4.6. The spectra of ADA showed the presence of an additional peak at 92.2 ppm, which can be attributed to hemiacetalic carbons corresponding to aldehyde groups.<sup>80</sup> This behavior indicated that not all the aldehyde groups remain free and only a fraction of them will be available for chemical modifications by amination.<sup>80</sup> Moreover, the signals corresponding to G1, G4, G3 and G5 of ADA became smaller compared to those of alginate, whereas the signals corresponding to M did not change significantly. This result indicated that the oxidation process affects G units of alginate preferentially.<sup>80</sup>

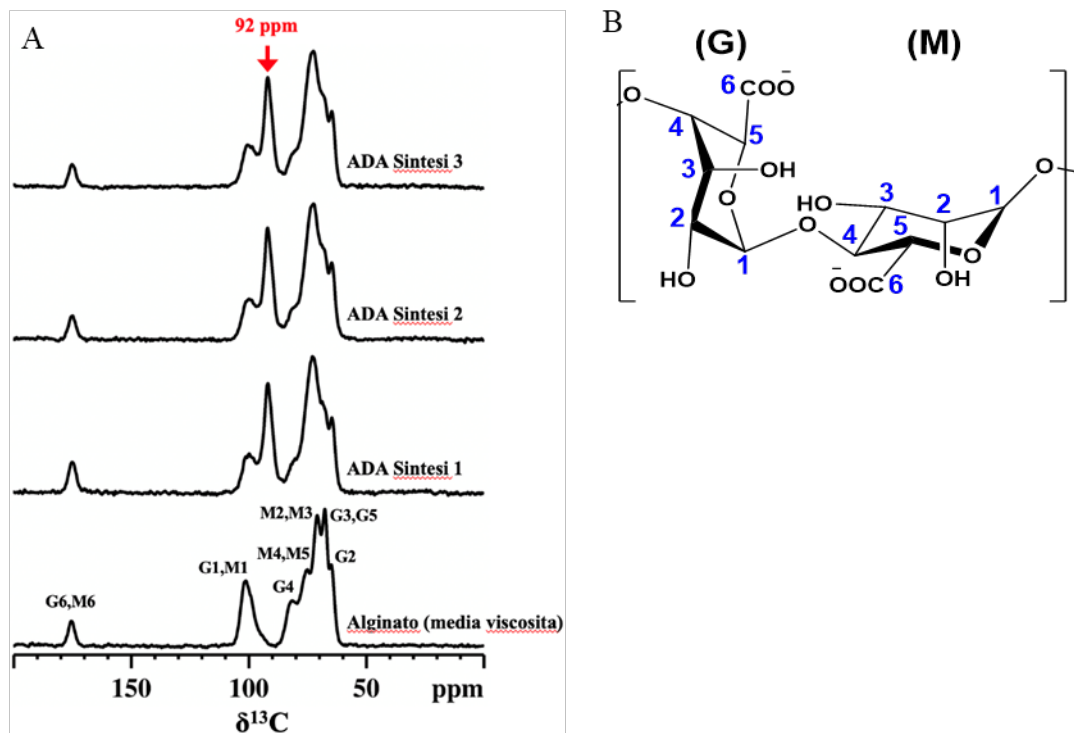


**Figure 4.6.** (A)  $^{13}\text{C}$  NMR spectra of ALG and three samples of different lyophilized ADA. (B) I: unoxidized G unit, II: oxidized G unit.

## 4.2. Chemically crosslinked hydrogels

### 4.2.1. ADA/GEL hydrogels

Although alginate-based hydrogels are widely used in biomedical applications, they exhibit low *in vivo* degradability and poor cell adhesion, since mammalian cells lack specific ligands<sup>44,45</sup>. These drawbacks can be overcome through the functionalization of ADA with a bioactive molecule, like gelatin. Gelatin is a biodegradable protein, produced by hydrolytic degradation of collagen, which possess the ability promote cell adhesion and proliferation. Gelatin incorporation into ADA gels can enhance their biological activity. The conjugation of ADA and gelatin can be obtained through Schiff base formation between the oxidized units of alginate and the amino groups of gelatin (Figure 4.7), obtaining a stable yet physiologically degradable gel network.<sup>78,81</sup>

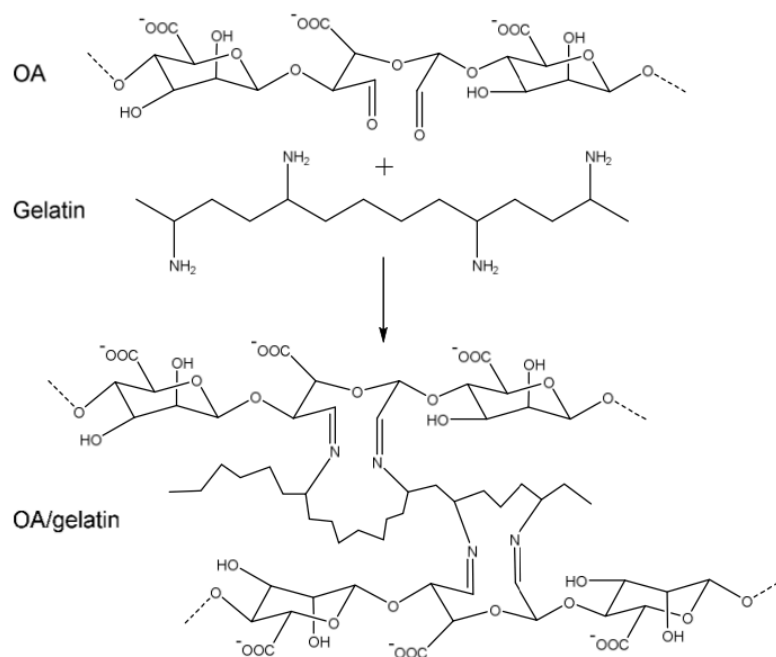


**Figure 4.7.** Crosslinking of ADA and gelatin *via* Schiff base reaction.

ADA/GEL hydrogels were produced by blending ADA/GEL in five different ratios, 50:50, 70:30, 80:20, 90:10, and 95:5, using two final polymer concentrations of 5 and 10% (w/v), as shown in Table 4.2. After 3 hours of continuous magnetic stirring, gel formation was not observed for any of the tested compositions.

Starting concentration (% w/v)		Weight ratios (%)		Final concentration (% w/v)		Label for composition	Gel formation
ADA	GEL	ADA	GEL	ADA	GEL		
5	5	95	5	4.75	0.2 5	5-ADA95/GEL5	×
5	5	90	10	4.5	0.5	5-ADA90/GEL10	×
5	5	80	20	4	1	5-ADA80/GEL20	×
5	5	70	30	3.5	1.5	5-ADA70/GEL30	×
5	5	50	50	2.5	2.5	5-ADA50/GEL50	×
10	10	95	5	9.5	0.5	10-ADA95/GEL5	×
10	10	90	10	9	1	10- ADA90/GEL10	×
10	10	80	20	8	2	10- ADA80/GEL20	×
10	10	70	30	7	3	10- ADA70/GEL30	×
10	10	50	50	5	5	10- ADA50/GEL50	×

**Table 4.2.** ADA/GEL mixture composition and gel formation.

Rheological characterization of the solution listed in Table 4.2 was also conducted. Specifically, time sweep studies were performed on 5-ADA95/GEL5, 5-ADA90/GEL10, and 5-ADA80/GEL20 samples in order to determine the rate and the extent of crosslinking. The crossover point of  $G'$  and  $G''$ , which is the point at which  $G'$  and  $G''$  are equal, is defined as the state of gel formation, indicating that the fluid has transitioned from fluid flow like behavior to solid elastic behavior. The gel point was not detected for any sample and for 5-ADA95/GEL5 and 5-ADA80/GEL20 samples was not even possible to display  $G'$  trend, since sol-to-gel phase transition occurred rapidly.

The formation of Schiff base bond was further investigated through  $^{13}\text{C}$  NMR spectroscopy. The  $^{13}\text{C}$  NMR spectra of prepared hydrogels are presented in Figure 4.8.

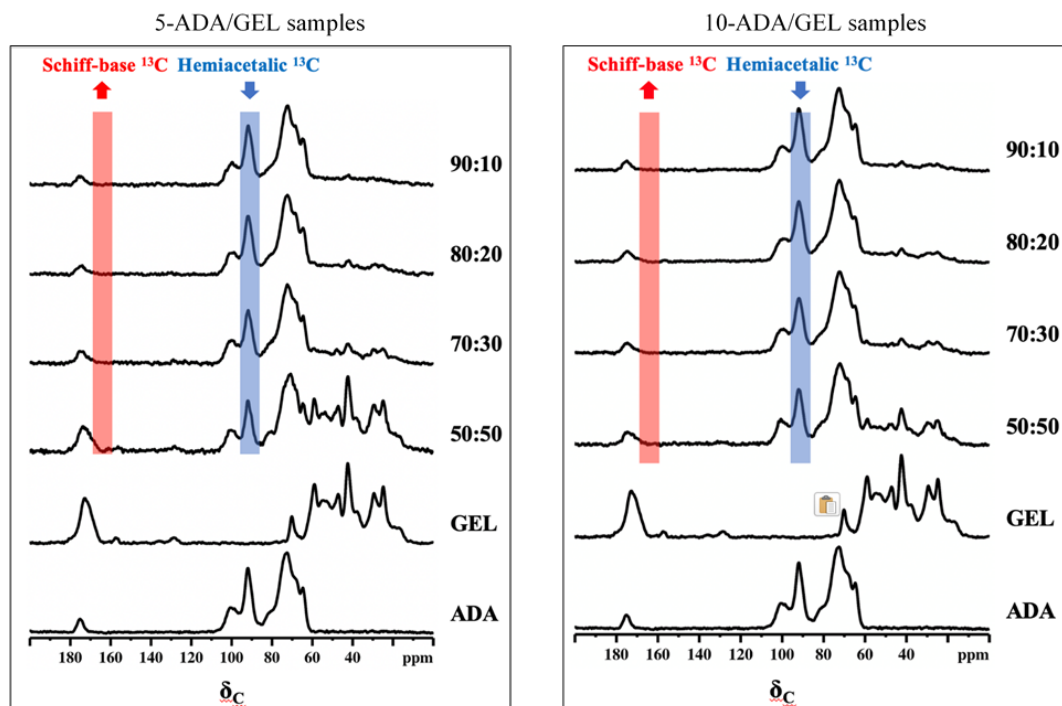


**Figure 4.8.**  $^{13}\text{C}$  NMR spectra of ADA and ADA/GEL samples.

In  $^{13}\text{C}$  NMR spectra of ADA and ADA/GEL samples, the peaks in the region of 60-80 ppm were related to the pyranose carbons of the alginate backbone and are found in all samples. Moreover, the peak at 92.2 ppm indicating the formation of aldehyde groups was present in all ADA and ADA/GEL samples. In ADA/GEL spectra, further peaks in the region of 10-60 ppm are attributed to the presence of gelatin. The intensity of the various peaks in this ppm range decreased by decreasing the gelatin content, therefore it reflected the relative concentration of gelatin in the samples. In  $^{13}\text{C}$  NMR spectra of all the ADA/GEL samples the peak at 175 ppm corresponding to Schiff base carbon (highlighted in red in figure 4.8) was not detected. This data confirmed the result of the rheological analysis, indicating the absence of Schiff base formation.

ADA/GEL crosslinking ability depends on alginate molecular weight and oxidation degree. This relationship was investigated by *Emami et al.* using several blends based on ADA and GEL with the same weight ratio (1:1 ADA:GEL, 15 wt%) but different  $M_w$  and degree of oxidation of ADA. These two parameters were used as axes of a phase diagram, in which the state of

each ADA/GEL sample was reported. In this way, it was possible to distinguish domains used to predict the sol, gel, or intermediate (weak gel) state of alginate-gelatin mixture, as shown in Figure 4.9.<sup>79</sup>

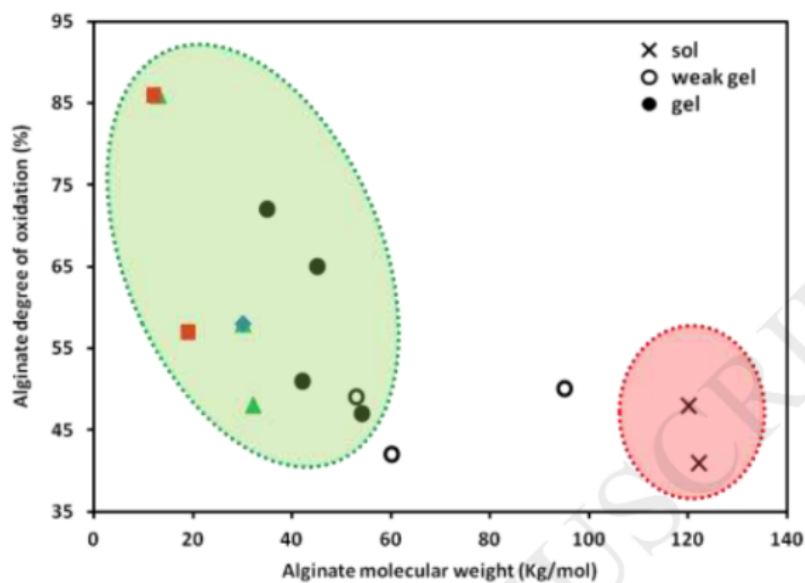


**Figure 4.9.** Phase diagram for the sol-gel state of ADA/GEL mixture.

Source: Emamin, Z. et al. / *Carbohydrate Polymers*. 2018; 198:509-517.

Although  $M_w$  of the synthesized ADA was not characterized, generally the oxidation process decreases molecular weight. Hence, ADA molecular weight was expected to be lower than 287 kDa (paragraph 4.1.1) According to this diagram, gel formation is possible using ADA with a degree of oxidation higher than 35%, while an average oxidation degree of 23% was obtained in our case. Likely, the oxidation degree obtained during ADA syntheses was too low to guarantee an effective crosslinking and the Schiff base reaction did not occur.

A gel phase could be obtained by increasing the oxidation degree. However, in the study by *Emami et al*, ADA-based hydrogels with higher degree of oxidation exhibited a maximum storage modulus of 100 Pa, one order of magnitude smaller than those of Agysil-LVR<sup>TM</sup> (1-3 kPa).<sup>44</sup> Therefore,

although chemical crosslinked ADA/GEL hydrogels could be obtained, they would not be suitable for this application due to their resultant low stiffness.

### 4.3. Ionically crosslinked hydrogels

#### 4.3.1. Gelation mechanism and $\text{Ca}^{2+}$ -Alg particles preparation

ADA/GEL hydrogels are a promising biomaterial for tissue engineering applications since they possess tunable properties such as stiffness and degradation behavior.<sup>82</sup> Hence, other research groups have also largely investigated how to crosslink the polymers. Specifically, published research findings by *Boccaccini* and his group suggested to perform concurrently a chemical and ionic crosslinking. Firstly, ADA:GEL ratio and ADA characteristics were optimized to induce Schiff base bonds formation and obtain a chemically crosslinked hydrogel precursor. Then, calcium ions were used to ensure homogeneous crosslinking throughout the polymer matrix.<sup>82</sup>

Therefore, in this work the use of crosslinking ions was investigated as an alternative to chemical crosslinking, to induce hydrogel reticulation. Ionic crosslinking of alginate- and its derivatives is commonly performed by interactions with divalent cations. Specifically, in the presence of divalent cations, G-blocks interact with them to form ionic bridges and gelation occurs.<sup>55</sup> Thanks to ionic gelation, the so-called “egg-box” model is obtained, where alginate chains are arranged in a zigzag pattern due to the ionic interaction between anionic groups of alginate and the divalent cations. Calcium ions are the most commonly used among several divalent cations. As shown in Figure 4.10, one calcium ion is located between two alginate chains, where the 10 oxygen atoms of G blocks are involved in coordination bond with  $\text{Ca}^{2+}$ .<sup>51</sup>

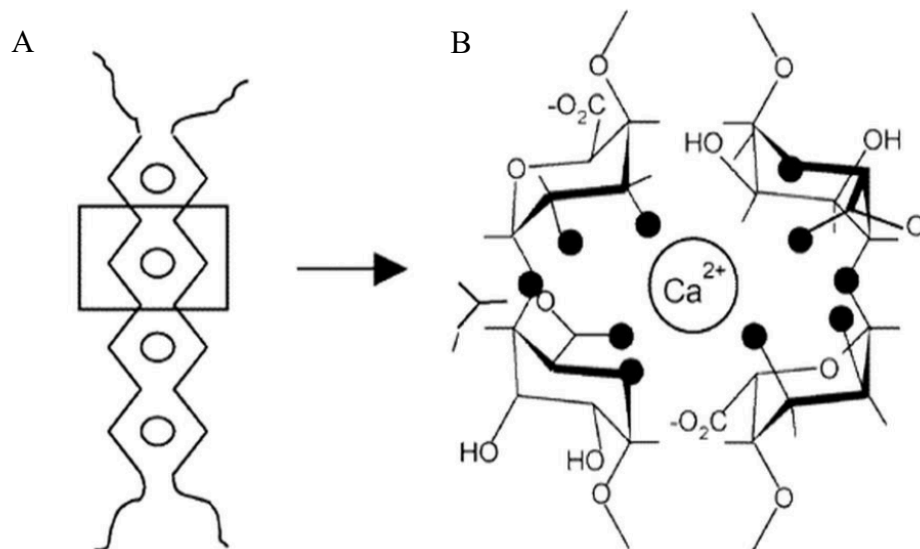


**Figure 4.10.** (A) Schematic presentation of the “egg-box model”. (B) Calcium ion coordination by the G chains in Ca<sup>2+</sup>-ALG hydrogels.

The most common gelation method is the diffusion or external gelation method, characterized by the diffusion of gelling ions from the outside into the alginate solution. However, this method is characterized by a rapid gelation, not suitable for injectable systems. Hence, alternative alginate gel systems have been formulated to obtain a delay in the gelling process, thus enabling the addition of cells or other biomaterials into the matrix prior the gel formation and the injection of the solution into the body.<sup>83</sup> An attractive alternative is Algisyl LVR<sup>TM</sup> formulation method.<sup>60</sup> Specifically, this is an internal gelling system where internally crosslinked alginate particles are released more slowly inside an alginate forming gel. The soluble alginate solution and the insoluble alginate/gelling ion particles dispersion are mixed by using a suitable mixing device, which comprises double syringe mechanism as shown in Figure 4.11. The gelation starts as the gelling ions begins crosslinking alginate molecules from the particles and the soluble alginate molecules in solution.<sup>60,83</sup>

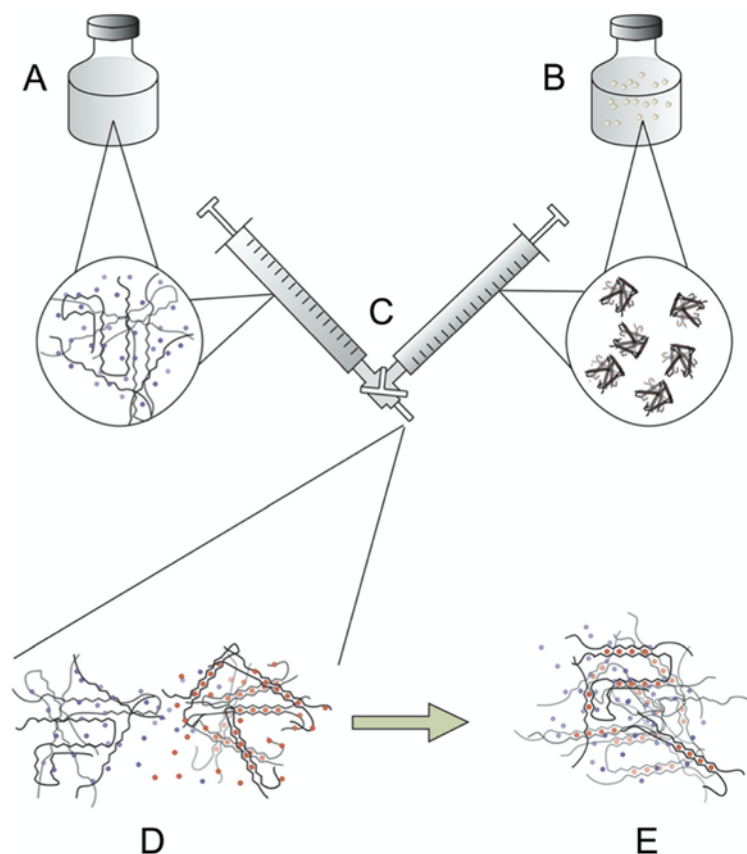


**Figure 4.11.** Schematic illustration of the two-component gelling system. (A) Aqueous sodium alginate solution. (B) Insoluble calcium alginate particles dispersion in DI water. (C) Luer-lock connector. (D) Upon mixing, gelling ions migrate from the particles. (E) Hydrogel formation.

*Source: Larsen, B. et al. / BMC Biotechnology. 2015; 15(1):1-12.*

In this study  $\text{Ca}^{2+}$  ions were used to obtain internally crosslinked alginate particles ( $\text{Ca}^{2+}$ -alg particles), implementing an internal gelation mechanism. The  $\text{Ca}^{2+}$ -alg particles were prepared by slowly drop-wise addition of a  $\text{CaCl}_2$  solution into and alginate solution, under magnetic stirring. As described in the Algysil-LVR patent (N° WO2006044342), a 3M  $\text{CaCl}_2$  solution and a 1.5% w/v alginate solution was used to produce calcium alginate  $\text{Ca}^{2+}$ -Alg particles. The same concentrations were tested, but particles precipitation was not observed. Likely, this was due to the different viscosity of alginate. Specifically, the value reported in the patent and that of alginate used in this study were 150 mPa·s and 600-900 mPa·s, respectively. Therefore, thanks to the higher viscosity, decreasing amounts of sodium alginate powder were

dissolved in DI water to identify which ones allow particles precipitation and separation.

The tested concentrations are listed in Table 4.3. Particle precipitation was successfully obtained only with 0.1%, 0.05% and 0.025% (w/v) alginate solutions. Higher concentrations resulted in higher solution viscosity that did not allow microparticles precipitation. However, only the first two concentrations (0.1%, 0.05% (w/v)) were used, since the lowest one (0.025% (w/v)) led to a low yield of microparticles production (Table 4.3).

Sample	Alginate (%w/v)	CaCl <sub>2</sub> (M)	Precipitate formation	Yield (n=9)	
				(%w/w)	g/L
Ca <sup>2+</sup> -Alg <sub>1.5</sub> /3M	1.5	3 M	X- too viscous	-	-
Ca <sup>2+</sup> -Alg <sub>0.8</sub> /3M	0.8	3 M	X- too viscous	-	-
Ca <sup>2+</sup> -Alg <sub>0.4</sub> /3M	0.4	3 M	X- too viscous	-	-
Ca <sup>2+</sup> -Alg <sub>0.20</sub> /3M	0.20	3 M	X- too viscous	-	-
Ca <sup>2+</sup> -Alg <sub>0.1</sub> /3M	0.1	3 M	✓	50 ± 10	8.5 ± 1
Ca <sup>2+</sup> -Alg <sub>0.05</sub> /3M	0.05	3 M	✓	46 ± 9	4.2 ± 0.8
Ca <sup>2+</sup> -Alg <sub>0.025</sub> /3M	0.025	3 M	✓	47 ± 14	2.1 ± 0.7

**Table 4.3.** Yield of production of Ca<sup>2+</sup>-Alg microparticles at different ALG concentrations.

The concentration of gelling ions into the insoluble microparticles affects gelling kinetics, hydrogel strength and elasticity. The higher the Ca<sup>2+</sup> concentration, the higher the gel strength. For that reason, once optimal alginate concentrations were selected, CaCl<sub>2</sub> solutions with increasing molarity were used to obtain Ca<sup>2+</sup>-Alg microparticles. For 0.1% (w/v) ALG solutions particles precipitation was observed with 4M and 5M CaCl<sub>2</sub>, while for 0.05% (w/v) ALG solutions this was observed also with 6M CaCl<sub>2</sub> (Table 4.4).

Sample	Alginate (%w/v)	CaCl <sub>2</sub> (M)	Precipitate formation	Yield (n=9)	
				(%w/w)	g/L
Ca <sup>2+</sup> -Alg <sub>0.1</sub> /4M	0.1	4 M	✓	62	1.1
Ca <sup>2+</sup> -Alg <sub>0.1</sub> /5M	0.1	5 M	✓	104	0.9
Ca <sup>2+</sup> -Alg <sub>0.1</sub> /6M	0.1	6 M	X – spheres formation	-	-
Ca <sup>2+</sup> -Alg <sub>0.05</sub> /4M	0.05	4 M	✓	41	0.76
Ca <sup>2+</sup> -Alg <sub>0.05</sub> /5M	0.05	5 M	✓	53	0.49
Ca <sup>2+</sup> -Alg <sub>0.05</sub> /6M	0.05	6 M	✓	18	0.33

**Table 4.4.** Yield of production of Ca<sup>2+</sup>-Alg microparticles at different CaCl<sub>2</sub> molarity.

#### 4.3.2. ALG/ Ca<sup>2+</sup>-Alg hydrogels

To investigate whether the produced Ca<sup>2+</sup>-Alg particles could induce ionic crosslinking, unmodified alginate hydrogels were firstly investigated. Different hydrogel formulations were prepared by varying the amount of Ca<sup>2+</sup>-Alg/3M particles to be dispersed, while keeping constant the concentration of alginate solution, as shown in Table 4.5.

Sample	Na-Alg (% w/v)	Ca <sup>2+</sup> -Alg particles		Final polymer concentration (% w/v)
		ALG initial (% w/v)	% w/v	
<i>Algisyl Patent</i>	1-2%	1.5 %	1-2 %	2-4%
1NaAlg-1CaAlg <sub>0.1</sub>	1%	0.1%	2%	3%
1NaAlg-1CaAlg <sub>0.1</sub>	1%	0.1%	1%	2%
1NaAlg-0.5CaAlg <sub>0.1</sub>	1%	0.1%	0.5%	1.5%
1NaAlg-0.25CaAlg <sub>0.1</sub>	1%	0.1%	0.25%	1.25%

**Table 4.5.** Composition of ALG/Ca<sup>2+</sup>-Alg hydrogels.

Rheological analyses were performed to determine if the tested hydrogels met the requirements for injectability and stability *in situ*. Specifically, the results of dynamic oscillation tests gave important information about the effect of  $\text{Ca}^{2+}$  and polymer concentration on the samples' structure.

For strain sweeps, the shear deformation of the measuring system was increased step wise from one measuring point to the next while keeping constant the frequency value. By measuring  $G'$  and  $G''$  as function of strain, strain sweep analysis allows the identification of the linear viscoelastic region (LVE Region) which indicates the range in which the test can be performed without destroying the structure of the sample. In LVE region  $G'$  values are independent of the applied deformation and the so-called plateau value is observed. In this study, the limiting value of the LVE Region was 10% for all the samples, as shown in Figure 4.11.  $G'$  values in the LVE Region were compared to evaluate hydrogels mechanical strength, which appeared mainly influenced by the amount of  $\text{Ca}^{2+}$  ions used as crosslinker. Hydrogels with a lower content of  $\text{Ca}^{2+}$  showed  $G'$  values of about 190 Pa, while stronger gels were obtained by increasing  $\text{Ca}^{2+}$  level, recording  $G'$  values around 715 Pa.

Furthermore, the values of  $G'$  and  $G''$  in the LVE Region were evaluated to determine the viscoelastic character of the samples. The measurements confirmed the gel-like behavior of the hydrogels, since for all the samples the value of  $G'$  was higher than the one of  $G''$ .

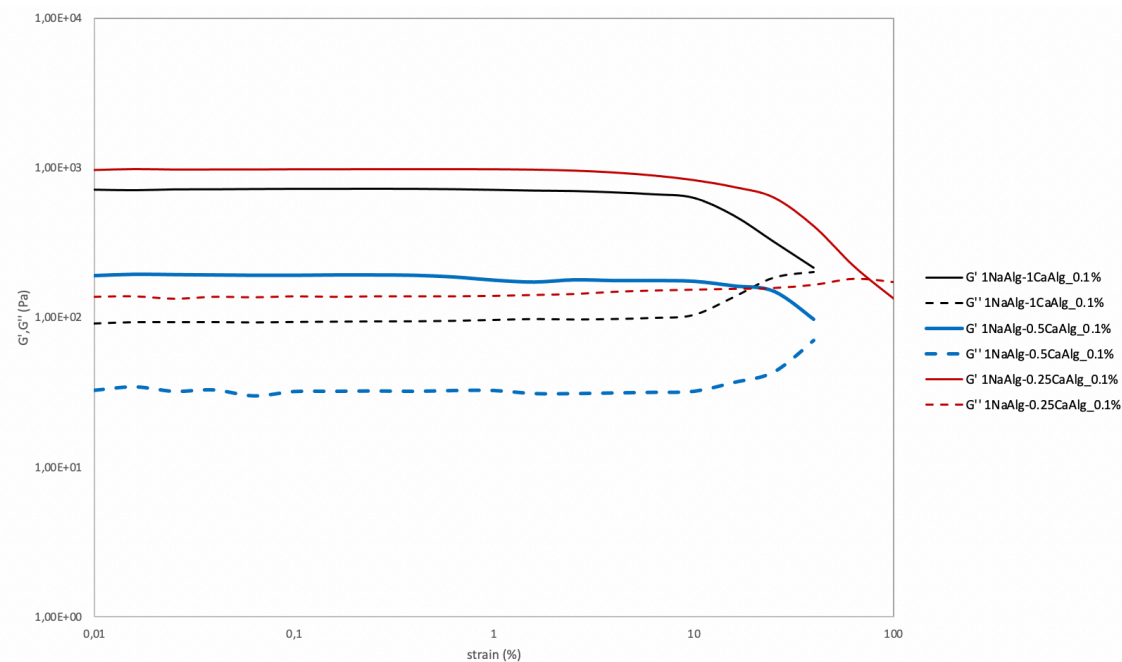


**Figure 4.12.** Results of oscillation strain test on ALG/Ca<sup>2+</sup>-Alg hydrogels.

Strain sweep test was not performed on 1NaAlg-1CaAlg<sub>0.1</sub> samples with final concentration of 3% (w/v) because hydrogel formation was not observed. Hydrogels formation and crosslinking kinetics were further confirmed by time sweep analysis, which were performed within the LVE Region of each hydrogel. Results are shown in Table 4.6.

Sample	Gel formation	Stabilization time (min)
<i>Algisyl Patent</i>	✓	<20 minutes
1NaAlg-1CaAlg <sub>0.1</sub>	X- too rapid	X
1NaAlg-1CaAlg <sub>0.1</sub>	✓	3
1NaAlg-0.5CaAlg <sub>0.1</sub>	✓	5
1NaAlg-0.25CaAlg <sub>0.1</sub>	✓	7

**Table 4.6.** Results of oscillation time test performed on ALG/Ca<sup>2+</sup>-Alg hydrogels.

For all the samples investigated the gel point was too rapid to be detected (i.e. gel point < 1 minute). The storage modulus subsequently showed a stabilizing tendency as a result of the sol-gel transition, as shown in Figure

4.13. The time for full gel formation was calculated by recording the stabilization time for  $G'$  and  $G''$  values, which is the time needed to obtain stable values of  $G'$  and  $G''$ . The stabilization times for all the compositions tested are shown in Table 4.6. The values were shorter than the one of Algisyl-LVR™, which was used as reference. Furthermore, the stabilization times increased by decreasing the  $\text{Ca}^{2+}$  content.

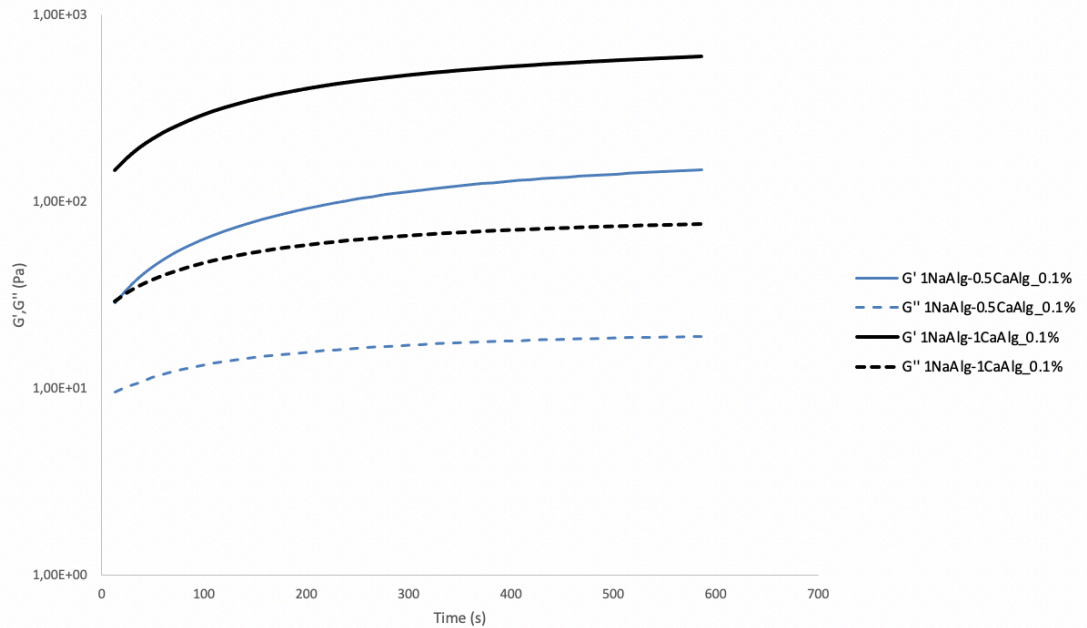


**Figure 4.13.** Results of oscillation time test on ALG/  $\text{Ca}^{2+}$ -Alg hydrogels.

Frequency sweep tests were carried out within the LVE Region of each hydrogel, thus determining the material frequency dependence, in the range of angular frequency between 0.1 and 100 rad/s. High frequencies are used to simulate rapid motion on short timescales, while low frequency zone mimics long-time behavior, simulated by slow motion. The results of the tests are reported in Figure 4.14. All the hydrogels presented  $G'$  always higher than  $G''$ , indicating a solid structure caused by a stable network of forces. Additionally,  $G' > G''$  denotes that the elastic character is dominant when a load is applied. An increase of both  $G'$  and  $G''$  values was detected with the increase in  $\text{Ca}^{2+}$  content, reaching a value of 0.7 KPa for 1 NaAlg-1CaAlg<sub>0.1</sub> sample.

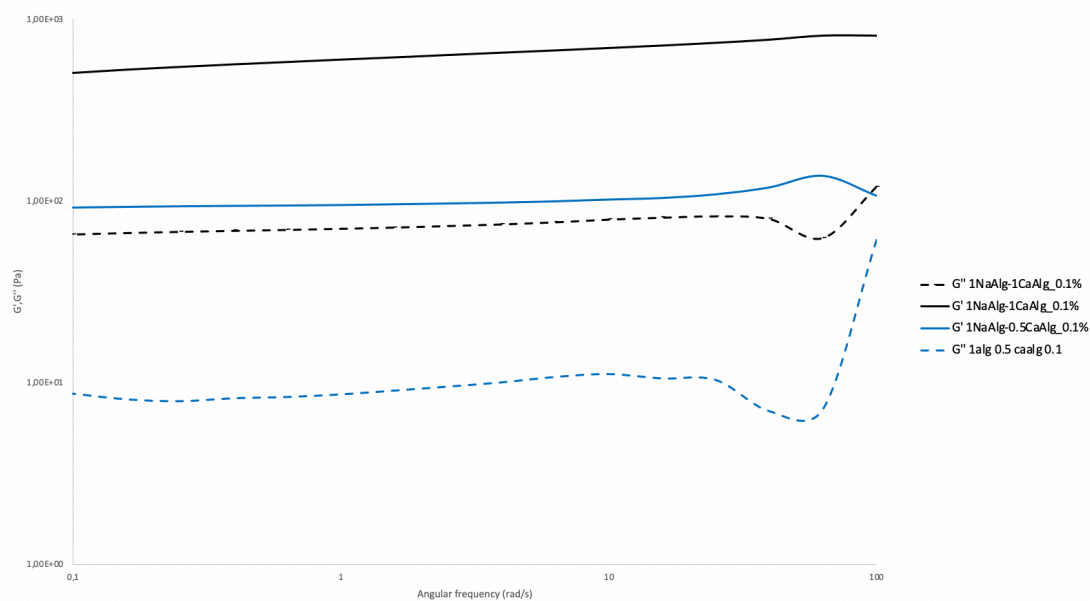


**Figure 4.14.** Results of oscillation frequency test on ALG/Ca<sup>2+</sup>-Alg hydrogels.

The results of the rheological characterizations demonstrated that Ca<sup>2+</sup>-Alg particles allow crosslinking. In addition, rheological properties of hydrogels of alginate and calcium alginate depend on microparticles concentration. G' values were recorded in the range between 0.03 and 0.4 kPa, while a value in the range of was 0.2-3 kPa is reported in Algisyl-LVR<sup>TM</sup> patent. Therefore, among the investigated ALG/Ca<sup>2+</sup>-Alg ratios, 1NaAlg/1CaAlg<sub>0.1</sub> was the one that more closely resembled Algisyl-LVR<sup>TM</sup> behavior.

#### 4.3.3. ADA/ Ca<sup>2+</sup>-Alg hydrogels

The production of ADA/Ca<sup>2+</sup>-Alg hydrogel were investigated using Ca<sup>2+</sup>-Alg/3M starting from the optimal ADA:Ca<sup>2+</sup>-Alg ratio of 1:1 identified using alginate. Both the final content of ADA and Ca<sup>2+</sup>-Alg particles were increased to 2 %w/v and 4 %w/v as shown in Table 4.7.

Rheological analyses were performed to clarify the effect of  $\text{Ca}^{2+}$  and polymer concentration on the structure of ADA/ $\text{Ca}^{2+}$ -Al hydrogels, which compositions are listed in Table 4.7. During the measurements the temperature was controlled at 37°C.

Sample	Na-ALG (% w/v)	Ca <sup>2+</sup> -Alg particles		Final polymer concentration (% w/v)
		ALG initial (% w/v)	% w/v	
1ADA-1CaAlg <sub>0.1</sub>	1%	0.1%	1%	2%
2ADA-1CaAlg <sub>0.1</sub>	2%	0.1%	1%	3%
2ADA-2CaAlg <sub>0.1</sub>	2%	0.1%	2%	4%
2ADA-2CaAlg <sub>0.05</sub>	2%	0.05%	2%	4%
2ADA-4CaAlg <sub>0.05</sub>	2%	0.05%	4%	6%

**Table 4.7.** Composition of ADA/ $\text{Ca}^{2+}$ -Alg hydrogels.

Strain sweep analysis was performed to identify the LVE Region. As shown in Figure 4.14, in this study the breakage of the structure occurred for strain higher than 10%, therefore this could be assumed as the limiting value of the LVE Region. G' values in the LVE Region were compared to evaluate hydrogels mechanical strength, and hydrogels formulated with a double amount of  $\text{Ca}^{2+}$ -Alg<sub>0.05</sub> microparticles exhibited a storage modulus significantly higher than the others, as shown in Figure 4.15. Specifically, a value of 1.6 kPa was detected, compared to 217 Pa and 185 Pa detected for 2ADA-2Ca<sup>2+</sup>-Alg<sub>0.05</sub> and for 2ADA-2Ca<sup>2+</sup>-Alg<sub>0.1</sub> hydrogel, respectively. Since improved mechanical properties are related to high crosslinking degree, this formulation resulted in an extensive and stronger interaction between divalent ions and oxygen atoms of G blocks.

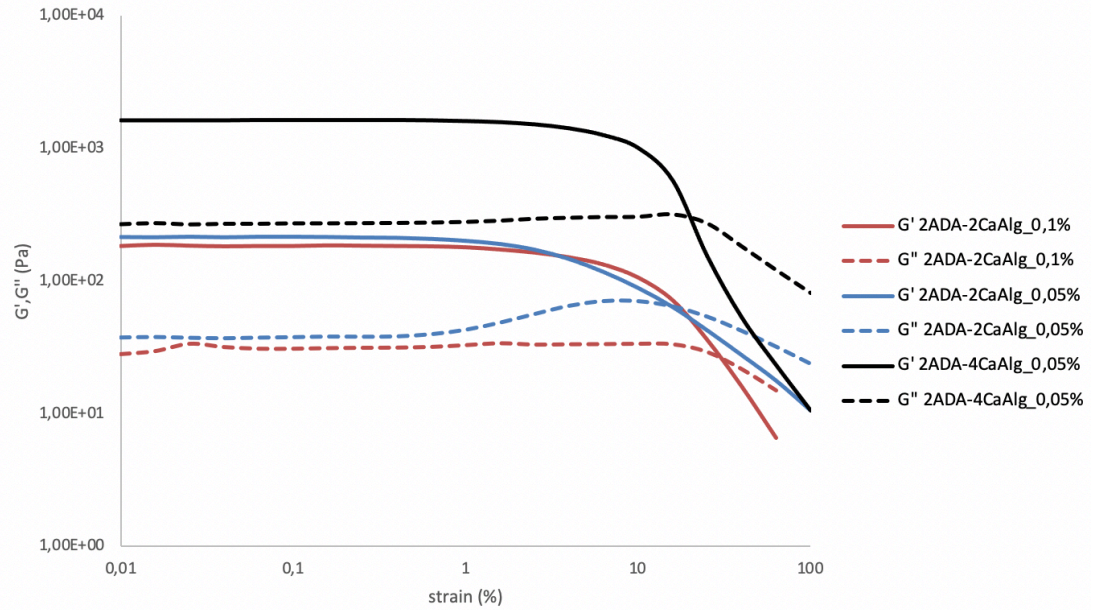


**Figure 4.15.** Results of oscillation strain test on ADA/Ca<sup>2+</sup>-Alg hydrogel

Furthermore, the values of  $G'$  and  $G''$  in the LVE Region confirmed the gel-like behavior of the hydrogels, since for all the samples the value of  $G'$  was higher than the one of  $G''$ . It is important to notice that the gel-like structure is guaranteed only for the measuring conditions applied.

Strain sweep test was not performed on 1ADA-1CaAlg<sub>0.1</sub> and 2ADA-1CaAlg<sub>0.1</sub> samples because hydrogel formation was not observed in the following 24 hours. Likely, the quantity of gelling ions was not sufficient to obtain a stable network of ionic interactions. Hydrogel formation and crosslinking kinetics were further confirmed by time sweep analysis, which were performed within the LVE Region of each hydrogel. Results are shown in Table 4.8.

Sample	Gel formation	Stabilization time (min)
1ADA-1CaAlg <sub>0.1</sub>	X- too liquid	Gel not formed after 24h
2ADA-1CaAlg <sub>0.1</sub>	X- too liquid	Gel not formed after 24h
2ADA-2CaAlg <sub>0.1</sub>	✓	7 ± 1
2ADA-2CaAlg <sub>0.05</sub>	✓	7 ± 0.5
2ADA-4CaAlg <sub>0.05</sub>	✓	7.5 ± 1

**Table 4.8.** Results of oscillation time test performed on ADA/Ca<sup>2+</sup>-Alg hydrogels.

Polymer/Ca<sup>2+</sup>-Alg ratio of 1:1 led to gel formation for alginate but not for ADA. This is mainly due to the lower molecular weight of ADA and to the increasing flexibility of the chains thanks to the breakage of the bonds between C-2 and C-3. Furthermore, less G blocks are available to interact with divalent ions because of the oxidation process.<sup>66</sup> Gel formation did not occur also by increasing the polymer amount, therefore higher levels of divalent ions were also required. Specifically, hydrogels were obtained with 2ADA-2CaAlg<sub>0.1</sub>, 2ADA-2CaAlg<sub>0.05</sub>, and 2ADA-4CaAlg<sub>0.05</sub> compositions, although the gel point was too rapid to be detected.

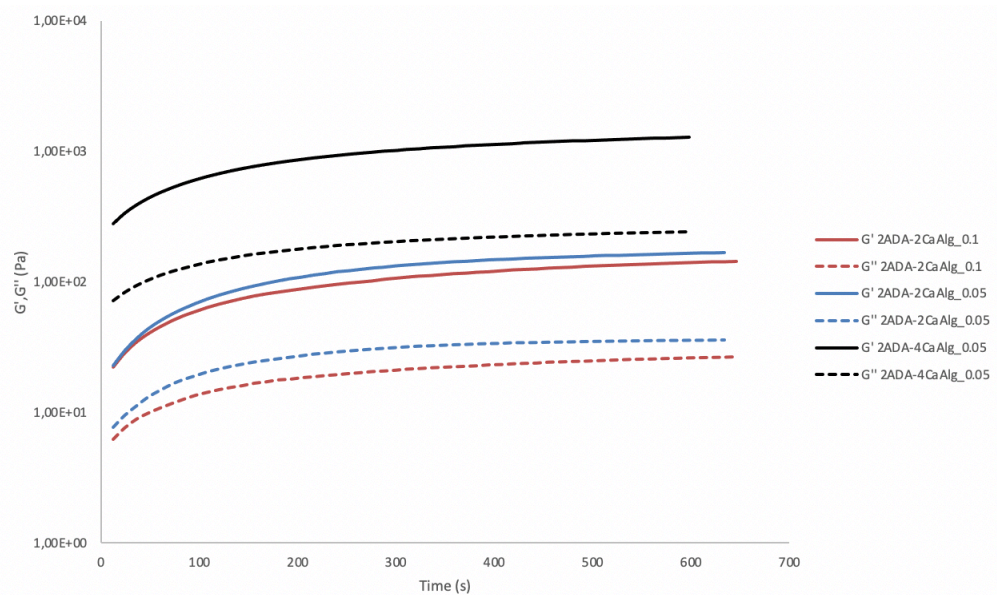


**Figure 4.15.** Results of oscillation time test on ADA/Ca<sup>2+</sup>-Alg hydrogels.

As can be observed in Figure 4.15, the gelling rate followed a similar pattern. In addition, stabilization times did not present significant differences, hence similar crosslinking kinetics were assumed.

Frequency sweep tests were carried out within the LVE Region of each hydrogel, thus determining the material frequency dependence, in the range of angular frequency between 0.1 and 100 rad/s. The results of the tests are reported in Figure 4.16. with 2ADA-2CaAlg<sub>0.1</sub>, 2ADA-2CaAlg<sub>0.05</sub>, and 2ADA-4CaAlg<sub>0.05</sub> Hydrogels presented G' always higher than G'', denoting a solid structure with a predominant elastic behavior. Furthermore, G' was poorly dependent on the applied frequency for all the hydrogel, while G'' showed a moderate dependance in hydrogels having low Ca<sup>2+</sup> content and a lower final ADA content. This aspect indicates that for these samples the viscous component started to influence the response of the material.

For hydrogels formulated with Ca<sup>2+</sup>-Alg<sub>0.05</sub> microparticles an increase of both G' and G'' values occurred by increasing Ca<sup>2+</sup> content, and the lower the microparticles concentration, the weaker the gel.

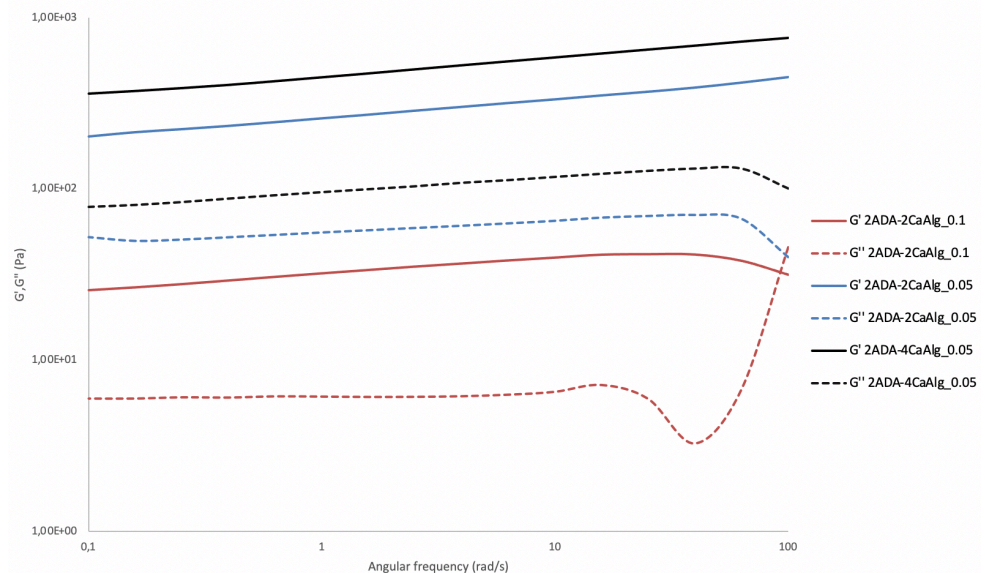


**Figure 4.16.** Results of oscillation frequency test on ADA/Ca<sup>2+</sup>-Alg hydrogel

## 4.4. NPs-loaded hydrogels

### 4.4.1. NPs formation

The final aim of this work is to develop an injectable hydrogel to deliver miRNA-loaded nanoparticles (NPs) to favor cardiac regeneration through direct reprogramming of cardiac fibroblasts into induced cardiomyocytes. The miRNA loaded NPs have been previously optimized by Nicoletti *et al.*<sup>30,31</sup> Among the natural or synthetic polymers used for NPs formulation, PLGA was chosen for making NPs with high production efficiency and stable mechanical property, thanks to its ability to sustain therapeutic drug levels for prolonged periods of time and its capability to protect miRNA from degradation.<sup>32</sup> To avoid the electrostatic repulsion between the negative charges of the polymer and the phosphate groups of nucleic acids, a condensing agent was used. In this study, DE-DOPE liposomes interacted with the selected miRNA. Specifically, [2-(2,3-didodecyloxypropyl)-hydroxyethyl] ammonium bromide (DE) and DOPE were used as cationic lipid and neutral co-lipid, respectively. (citazione articolo Letizia) DOPE was chosen since in previous studies it has been shown to be more effective than several other neutral co-lipids when used in combination with cationic lipids with the aim of cationic lipid-mediated transfection.<sup>29</sup>

DE-DOPE/miRNA PLGA-NPs were loaded into ADA-based hydrogel that showed the best mechanical properties and the highest storage modulus, which was 2ADA-4CaAlg<sub>0.05</sub> hydrogels with 3M of Ca<sup>2+</sup>. An aqueous suspension of NPs was mixed with the other components of the hydrogel, allowing their entrapment during the gelation process. Two NPs (i.e. 6.7 ad 13.4 µg/mL) concentrations were tested, and NPs-free hydrogel was included as a control.

#### 4.4.2. *In vitro* stability studies

NPs-loaded hydrogels samples were incubated at 37°C in distilled for 9 days. The results of the stability studies are shown in Figure 4.17.

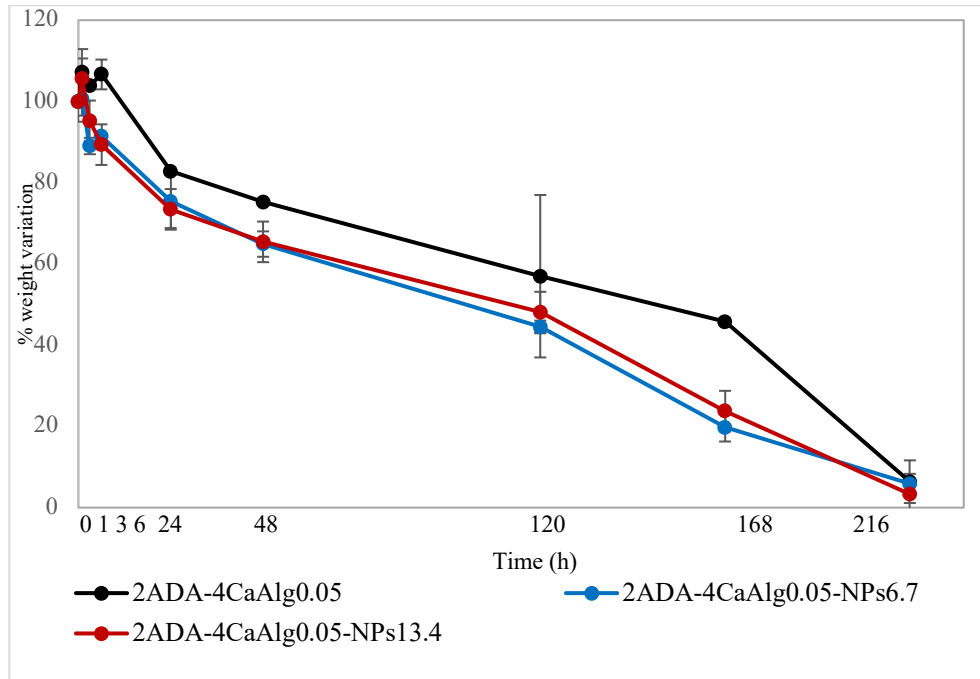


**Figure 4.17.** Swelling and degradation characteristics as a function of the incubation time of NPs-loaded ADA hydrogels. The values are given as the mean  $\pm$  SD.

*In vitro* swelling and degradation of the hydrogel samples were investigated by evaluating the % weight variation during the incubation process. At the beginning of incubation, a moderate swelling of all the hydrogels was observed (i.e. 110%). However, within 3-6 hours, a loss of weight was detected for NPs-loaded hydrogels started, while NPs-free hydrogels began to degrade after 24 hours. A similar trend was detected for the hydrogels loaded with the two NPs concentrations. NPs-free hydrogels exhibited a slower degradation profile as compared to other two and a slowed down weight loss. All the hydrogels showed complete dissolution after 9 days.

#### 4.4.3. *In vitro* NPs release

Alongside the evaluation of hydrogel degradation, the release of nanoparticles from the hydrogels was monitored. To address this aim, release media were collected at each time point and zeta potential ( $\zeta$ ) measurements were performed on them. Zeta potential is the measurement of the electrostatic potential at the electrical double layer that surrounds nanoparticles in a solution.<sup>84</sup> Hence, their escape outside the hydrogel was investigated by measuring zeta potential of NPs and release medium, and by comparing them.

Values between -10 and +10 mV are related to neutral nanoparticles, while values greater than +30 mV or less than -30 mV reveal a cationic or anionic behavior, respectively.<sup>84</sup> In this study, DE-DOPE/miRNA PLGA-NPs presented a negative zeta potential of -24 mV, which was indicative of the PLGA negative charge, proving an efficient encapsulation of lipoplexes inside the polymer.<sup>26</sup> The analysis showed a negative zeta potential also for ADA and Ca<sup>2+</sup>-Alg particles, -40 and -24 mV, respectively. For each hydrogel, the zeta potential value was an average value across all charged species.<sup>84</sup>

As shown in Figure 4.18, the zeta potential of the eluates within the first 6 hours was between -30 and -40 mV for all the samples. This value is similar to the zeta potential of alginate, possibly indicating a rapid release of uncrosslinked alginate chains from the system. Then, controlled steady increase of zeta potential was observed up to 5 days for all the samples, likely due to Ca<sup>2+</sup>-Alg release for NPs-free hydrogels and NPs release for NPs-loaded gels. A sustained rise in zeta potential was detected for samples containing higher NPs amounts (i.e. 13.4  $\mu\text{g/mL}$ ), indicating that the degradation of the polymer matrix into the media led to the release of cargo by diffusion. However, the zeta potential of hydrogels containing 6.7  $\mu\text{g}$  of nanoparticles did not show the same trend, although NPs-loaded hydrogels showed the same degradation behavior. Therefore, zeta potential increase was strictly related to the higher amount of NPs.

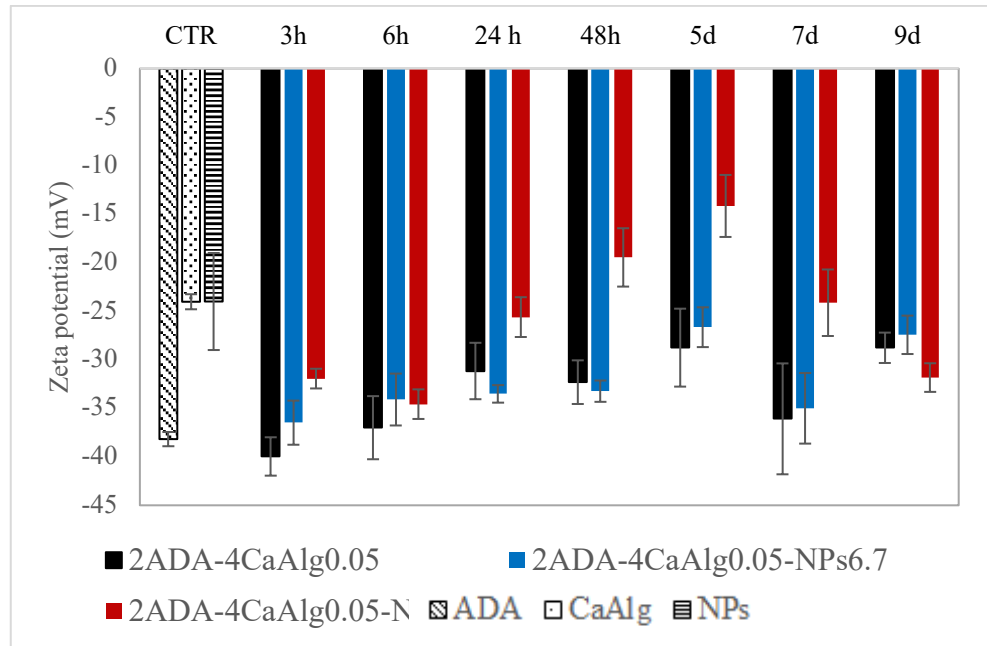


**Figure 4.18.** Zeta potential measurements of NPs-loaded ADA hydrogels. The values are given as the mean  $\pm$  SD.

#### 4.4.4. *In vitro* miRNA release

*In vitro* miRNA release from DE-DOPE/miRNA PLGA-NPs was quantified by Qubit assay. According to NPs release kinetic, the analysis was performed starting from day 1. Media collected from test tubes were centrifugated to separate miRNA from NPs. Then, supernatant was withdrawn and mixed with a buffer solution to allow nucleic acids detection. Results of the fluorometric quantification are showed in Figure 4.19.

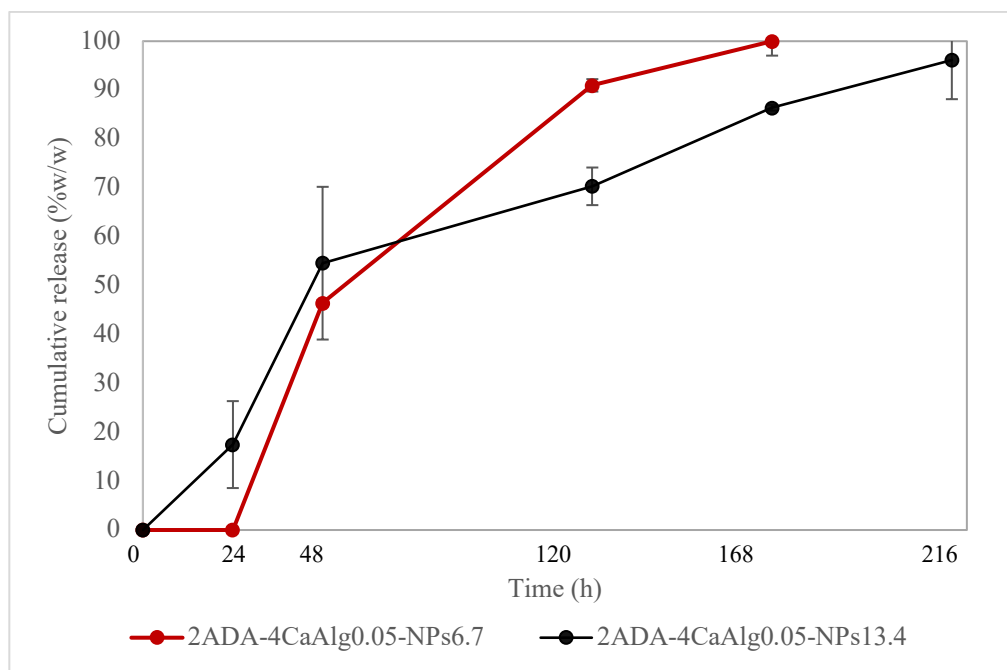


**Figure 4.19.** miRNA cumulative release from NPs.

The values are given as the mean  $\pm$  SD.

After 24 hours, NPs<sub>13.4</sub>-loaded hydrogels showed an initial miRNA release (< 20%) whereas NPs<sub>6.7</sub>-loaded hydrogels did not. However, from day 2 miRNA escape was detected in both the NPs payload. Specifically, fluorometric signals remarkably increased between day 2 and 5. This result is in agreement with the previous data obtained from ELS analysis (Figure 4.18, Figure 4.19), that revealed a significant NPs release at the same time points.

Overall, a progressive release of cargo was observed from NPs<sub>13.4</sub>-loaded and NPs<sub>6.7</sub>-loaded hydrogels, reaching 100% release after 7 and 9 days, respectively. Hence, a controlled and prolonged release of miRNA was confirmed. Since miRNA levels are related to transfection efficacy, a controlled and prolonged release is essential induce direct reprogramming of cardiac fibroblasts into cardiomyocyte-like cells.<sup>26</sup>

#### 4.5. Optimization of ionically crosslinked ADA/Ca<sup>2+</sup>-Alg hydrogels

As mentioned above, among all the tested compositions hydrogels obtained with 2ADA-4CaAlg<sub>0.05</sub> and Ca<sup>2+</sup>-Alg<sub>0.05</sub>/3M of Ca<sup>2+</sup> showed the best mechanical properties and the highest storage modulus. The maximum value obtained from the linear regime of strain sweep was assumed as storage modulus. However, the storage modulus of such hydrogels was still far from the shear modulus of the infarcted myocardium. Specifically, Rump *et al.* in normal patients shear elastic modulus is between 5 and 27 kPa during diastole and systole and increase two to eight times after MI.<sup>85</sup> Moreover, 2ADA-4CaAlg<sub>0.05</sub>/3M showed a rapid degradation in stability studies, reaching complete dissolution after 9 days.

By changing ADA:Ca<sup>2+</sup>-Alg ratio and Ca<sup>2+</sup> concentration, the degradation of the hydrogel matrix can be tailored to match the final aim, such as to control the release of the NPs. As the Ca<sup>2+</sup> concentration inside the matrix determines the degree of crosslinking and therefore the shear properties and the degradation rate, the effect of increasing concentration of Ca<sup>2+</sup> on ADA hydrogel was investigated. Specifically, hydrogels were synthesized by using 2ADA:4Ca<sup>2+</sup>-Alg ratio and Ca<sup>2+</sup>-Alg<sub>0.05</sub> particles containing increasing amount of calcium ions (Table 4.9).

Sample	ADA (% w/v)	Ca <sup>2+</sup> -Alg particles		Final polymer concentration (% w/v)
		ALG initial (% w/v)	% w/v	
2ADA-4CaAlg <sub>0.05</sub> 3M	2% w/v	0.05%	4%	6%
2ADA-4CaAlg <sub>0.05</sub> 4M	2% w/v	0.05%	4%	6%
2ADA-4CaAlg <sub>0.05</sub> 5M	2% w/v	0.05%	4%	6%
2ADA-4CaAlg <sub>0.05</sub> 6M	2% w/v	0.05%	4%	6%

**Table 4.9.** Composition of 2ADA:4Ca<sup>2+</sup>-Alg hydrogels.

#### 4.5.1. Rheological characterization

2ADA:4Ca<sup>2+</sup>-Alg<sub>0.05</sub> hydrogels underwent rheological characterization to understand the effect of the calcium bridges on their mechanical properties. During the measurements the temperature was controlled at 25°C.

Strain sweep analysis was performed to identify the LVE Region of each hydrogel, where G' values are independent of the applied deformation and the so-called plateau value is observed. As shown in Figure 4.20, the higher concentration of Ca<sup>2+</sup> the narrower the LVE Region. G' values within the different LVE Regions were compared to also evaluate the influence on the mechanical strength of the polymer matrix, and a positive correlation between the concentration of Ca<sup>2+</sup> and storage modulus was evidenced. Specifically, 2ADA-4Ca<sup>2+</sup>-Alg<sub>0.05</sub>/6M hydrogels exhibited a G' value of 3,6 kPa, which was the highest one. Therefore, an increase of calcium ions effectively led to a higher crosslinking degree. The narrowing of LVE Region occurred because stiffer hydrogels are regarded also as more brittle. For instance, the limiting value of LVE Region was about 6% and 25% for hydrogels formulated with Ca<sup>2+</sup>-Alg<sub>0.05</sub>/6M and Ca<sup>2+</sup>-Alg<sub>0.05</sub>/3M, respectively.

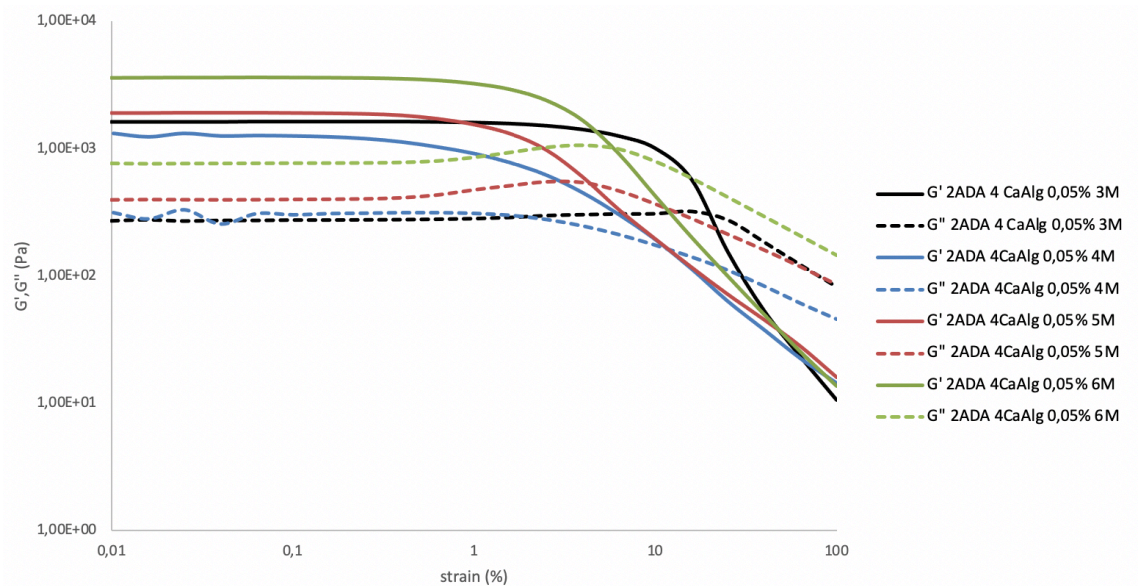


**Figure 4.20.** Results of oscillation strain test on ADA/Ca<sup>2+</sup>-Alg hydrogels.

Furthermore, for each hydrogel the value of  $G'$  was higher than the one of  $G''$  in the relative LVE Region, confirming their gel-like behavior.

Time sweep analysis was carried out to further investigate the network formation and to evaluate the crosslinking kinetics, tailoring the magnitude of the applied strain for each hydrogel. Results are shown in Table 4.11 and Figure 4.21.

Sample	Gel formation	Stabilization time (min)
2ADA-4CaAlg <sub>0.05</sub> 3M	✓	7,6
2ADA-4CaAlg <sub>0.05</sub> 4M	✓	5
2ADA-4CaAlg <sub>0.05</sub> 5M	✓	6,8
2ADA-4CaAlg <sub>0.05</sub> 6M	✓	5,8

**Table 4.11.** Results of oscillation time test performed on ADA/Ca<sup>2+</sup>-Alg hydrogels.

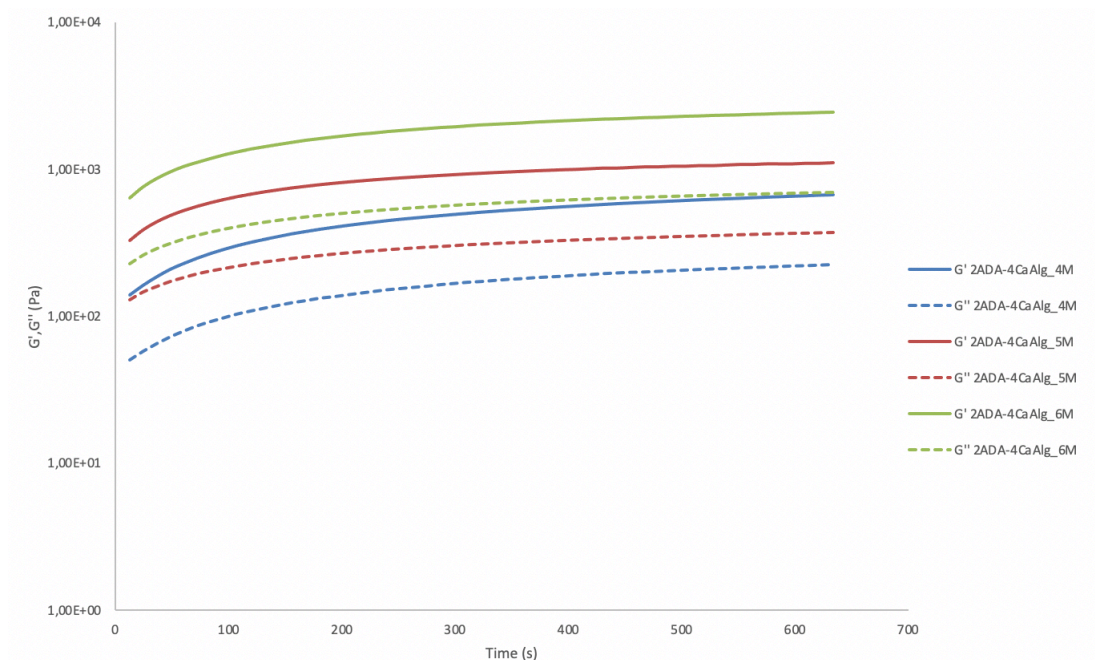


**Figure 4.21.** Results of oscillation time test on ADA/Ca<sup>2+</sup>-Alg hydrogels.

Hydrogel formation for each composition and the time to fully form the gel decreased by increasing the calcium ions amount. However, the fastest stabilization time was observed for 2ADA-4Ca<sup>2+</sup>-Alg<sub>0.05</sub>/4M. This unexpected outcome could be due to matrix inhomogeneities inside the sample and/or to experimental errors during Ca<sup>2+</sup>-Alg particles preparation, since the protocol has been optimized during the work. In addition, 2ADA-4Ca<sup>2+</sup>-Alg<sub>0.05</sub>/3M hydrogel showed the same stabilization time recorded in previous experiment (paragraph 4.3.3). The gelling rate followed a similar pattern, hence similar crosslinking kinetics were assumed.

Frequency sweep tests were carried out within the LVE Region of each hydrogel, thus determining the material frequency dependence, in the range of angular frequency between 0.1 and 100 rad/s. As shown in Figure 4.22, G' was poorly dependent on the applied frequency for each hydrogel, since the values did not undergo significant variations. In addition, G' always higher than G'' denoting a solid structure with a predominant elastic behavior. An increase in both G' and G'' values was observed by increasing the starting molarity of Ca<sup>2+</sup>-Alg particles.

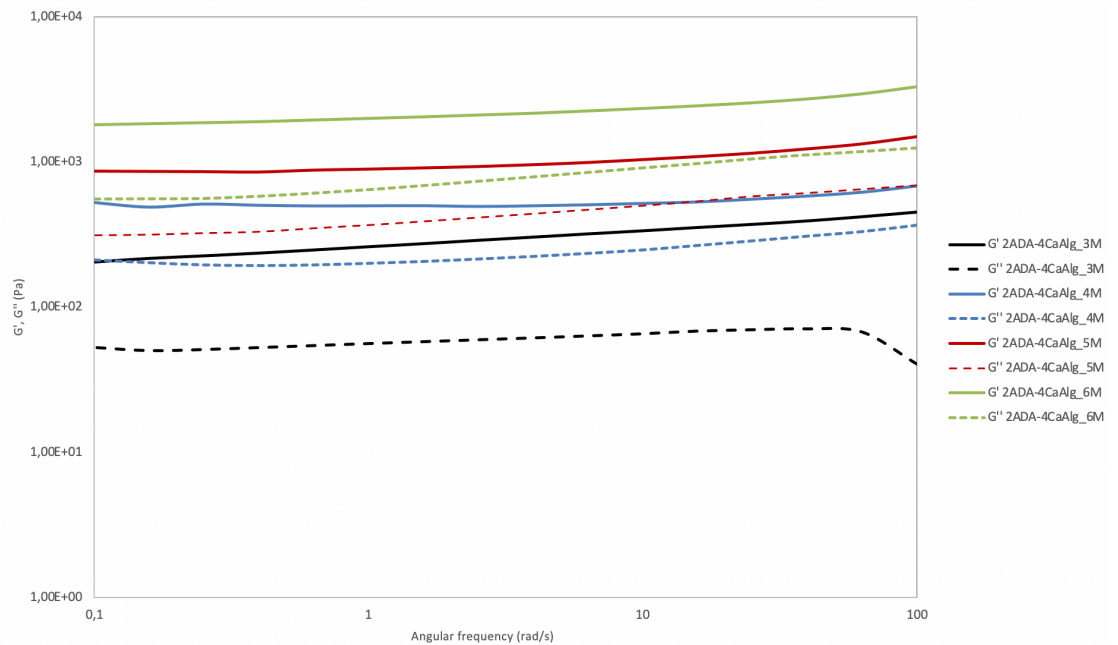


**Figure 4.22.** Results of oscillation frequency test on ADA/Ca<sup>2+</sup>-Alg hydrogels.

These rheological results clearly support that a higher number of calcium bridges allows the formation of hydrogels with mechanical properties closer to the cardiac tissue ones. Specifically, the shear modulus of 2ADA-4Ca<sup>2+</sup>-Alg<sub>0.05</sub>/6M was the closest to the one of health and damaged myocardium, which are 6 kPa and 18 kPa, respectively.<sup>44</sup> Additionally, thanks to its shear properties this hydrogel resemble the commercial device Algisyl-LVR<sup>TM</sup>, which G' value in the range between 0.2 and 3 kPa, as described in WO2006044342 patent.<sup>60</sup>

#### 4.5.2. *In vitro* swelling and degradation study

*In vitro* swelling and degradation of the different hydrogels were investigated to identify the degree of crosslinking of the formed network. Hydrogels were poured into Falcon® polystyrene test tubes, and weight gain and weight loss of the samples were evaluated during different incubation times in DI water, at 37°C, with a controlled atmosphere of 5% CO<sub>2</sub> and 95% relative humidity. The study was carried out until complete dissolution of the hydrogels.

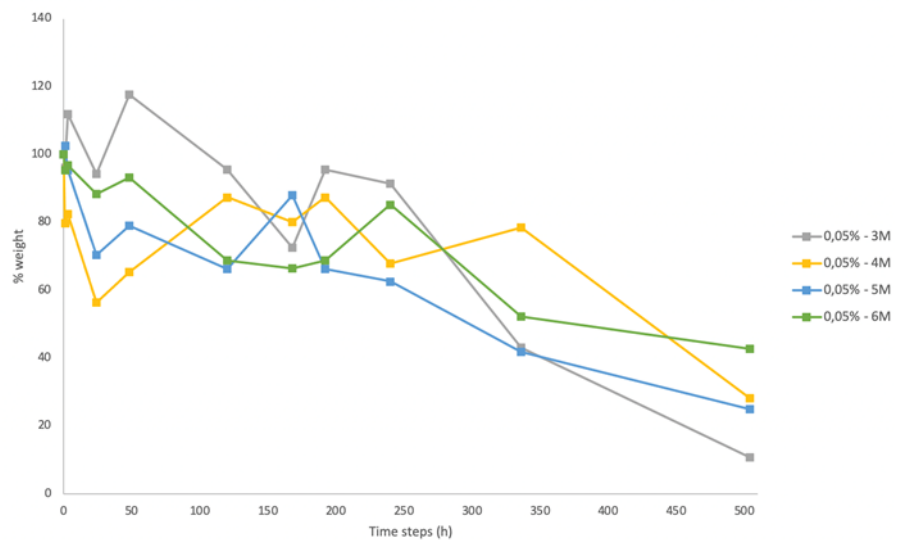


**Figure 4.23.** Swelling and degradation characteristics of (A) 2ADA:2Ca<sup>2+</sup>-Alg<sub>0.01</sub> hydrogels and (B) 2ADA:4Ca<sup>2+</sup>-Alg<sub>0.05</sub>. The values are given as the mean.

As shown in Figure 4.23, within the first 2 weeks of incubation 2ADA:4Ca<sup>2+</sup>-Alg<sub>0.05</sub> showed both weight gain and weight loss. Over longer incubation times, the weight gain of all the hydrogels was slowed down remarkably, reaching the complete dissolution after 21 days.

Overall, an increase in crosslinking degree resulted in a decrease in the weight loss. As the sample swelled and degraded concurrently when exposed to the aqueous environment and as ADA content was constant, this result was completely related to the amount of calcium ions included in the polymer matrix. As a result, high amount of uncrosslinked ADA leached out rapidly from low calcium ions-containing ADA hydrogels, which determined the high rate of weight loss observed within the first 24 hours. These results showed that biodegradability of ADA-based hydrogel is controllable by changing its composition.

This feature is of critical importance for the application in cardiac tissue engineering. For this specific application, the degradation kinetic of biomaterials should be matched to NPs and miRNA release. Specifically, during *in vitro* release study the complete leakage of nanoparticles from the hydrogel matrix occurred within about 9 days. Therefore, a composition of 2ADA:4Ca<sup>2+</sup>-Alg<sub>0.05</sub> appeared much more reliable because a prolonged lifetime was observed.

#### 4.4. Ionically crosslinked ADA/GEL hydrogel

After the optimization of ADA/Ca<sup>2+</sup>-Alg hydrogel formulation, the possibility of incorporating gelatin in the system in the presence of gelling ions such as Ca<sup>2+</sup> was investigated. ADA/GEL hydrogels were prepared by varying the ratio between the two but keeping constant the ratio between the final soluble polymeric component (i.e. 2 %w/v) and the insoluble one made of gelling ion particles (i.e. 4% w/v). These hydrogels have been easily fabricated by employing the double-syringe mixing system wherein one syringe was filled with an ADA/GEL solution, previously obtained by means of the same mechanism, and the other with the Ca<sup>2+</sup>-Alg<sub>0.05</sub> microparticles suspension. Specifically, microparticles were obtained using a 3M CaCl<sub>2</sub> starting solution.

The composition of all the samples performed is listed in Table 4.12.

Sample	ADA (% w/v)		GEL		Ca <sup>2+</sup> -Alg particles		Final polymer concentration (% w/v)
	wt%	Final %w/v	wt%	Final %w/v	Type (initial (% w/v) )	% w/v	
2ADA <sub>100</sub> G <sub>0</sub> -4CaAlg <sub>0.05</sub>	100	2%	0	0%	0.1%	4%	6%
2ADA <sub>90</sub> G <sub>10</sub> -4CaAlg <sub>0.05</sub>	90	1.8%	10	0.2%	0.1%	4%	6%
2ADA <sub>80</sub> G <sub>20</sub> -4CaAlg <sub>0.05</sub>	80	1.6%	20	0.4%	0.1%	4%	6%

**Table 4.12.** Crosslinking of ADA and GEL *via* Schiff base reaction.

Rheological measurements have been performed to investigate the crosslinking degree and the injectability of ADA/GEL hydrogels. Thermosensitive components such as gelatin can undergo reversible phase transition based on temperature, therefore the analyses were performed at 37°C to evaluate the chains interconnection in physiological-like conditions.

Strain sweep analysis was performed to identify the LVE Region of each hydrogel, where G' values are independent of the applied deformation and the so-called plateau value is observed. As shown in Figure 4.24, the limiting value of the LVE Region increased when higher amounts of GEL are used, thus obtaining more brittle hydrogels. G' values within the different LVE Regions were compared

investigate the mechanical strength of the polymer matrix, and a positive correlation between the concentration of GEL and storage modulus was found. The shear properties of ADA/GEL hydrogels have been evaluated taking 2ADA-4Ca<sup>2+</sup>-Alg<sub>0.05</sub>/3M as a reference. The latter showed a storage modulus significantly lower than the one recorded for hydrogel with 80ADA:20GEL ratio. Specifically, a shear modulus of 13,2 kPa was obtained. This result was the closest one to the expected outcome. Since improved mechanical properties are related to high crosslinking degree, 2ADA<sub>80</sub>-G<sub>20</sub>-4Ca<sup>2+</sup>-Alg<sub>0.05</sub> formulation resulted in an extensive and stronger chemical and ionic interaction between the hydrogel components.

Formation of the Schiff base as well as the ability of Ca<sup>2+</sup> to complex with hydroxyl groups of ADA.

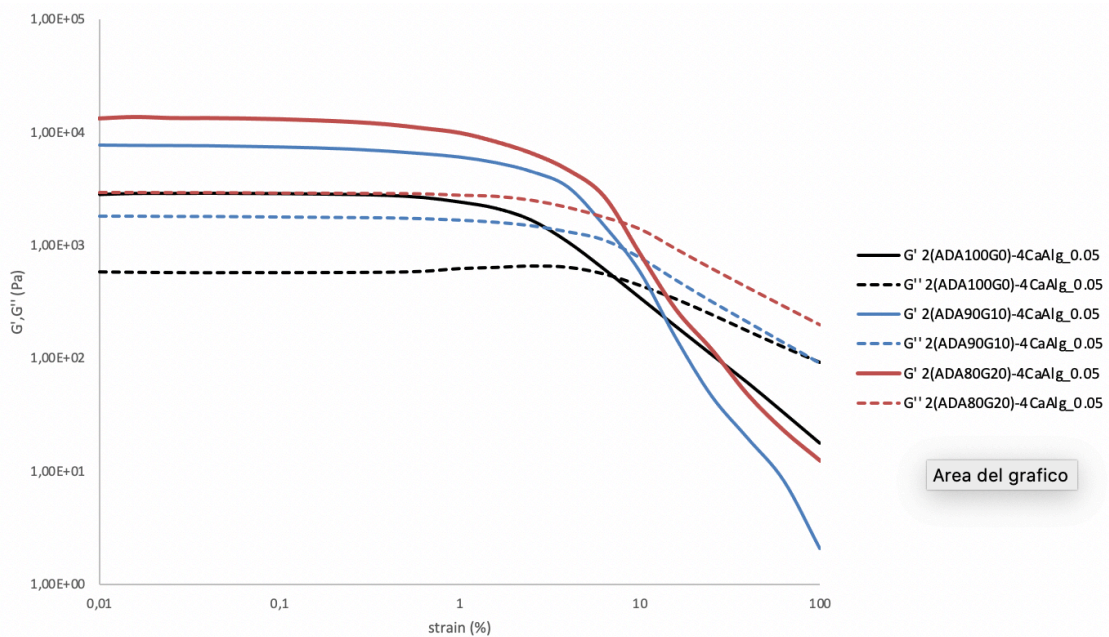


**Figure 4.24.** Results of oscillation strain test on ADAGEL/Ca<sup>2+</sup>-Alg hydrogels.

Furthermore, the values of G' and G'' in the LVE Region confirmed the gel-like behavior of the hydrogels, since for all the samples the value of G' was higher than the one of G''.

Time sweep tests have been performed to assess hydrogel formation and crosslinking kinetic. The results (Table 4.13) confirmed that the different biomaterials were adequately mixed at physiological temperature.

Sample	Gel formation	Stabilization time (min)
2ADA <sub>100</sub> G <sub>0</sub> -4CaAlg <sub>0.05</sub>	✓	7,6
2ADA <sub>90</sub> G <sub>10</sub> -4CaAlg <sub>0.05</sub>	✓	6,6
2ADA <sub>80</sub> G <sub>20</sub> -4CaAlg <sub>0.05</sub>	✓	5,6

**Table 4.13.** Results of oscillation time test performed on ADAGEL/Ca<sup>2+</sup>-Alg hydrogels.

The introduction of GEL component led to a progressive shortening of the time needed to complete the sol-to-gel phase transition. In agreement with previous studies, a stabilization time of about 8 minutes was confirmed for ADA/Ca<sup>2+</sup>-Alg hydrogels, whereas ADA/GEL-based hydrogels exhibited a faster reticulation kinetic.

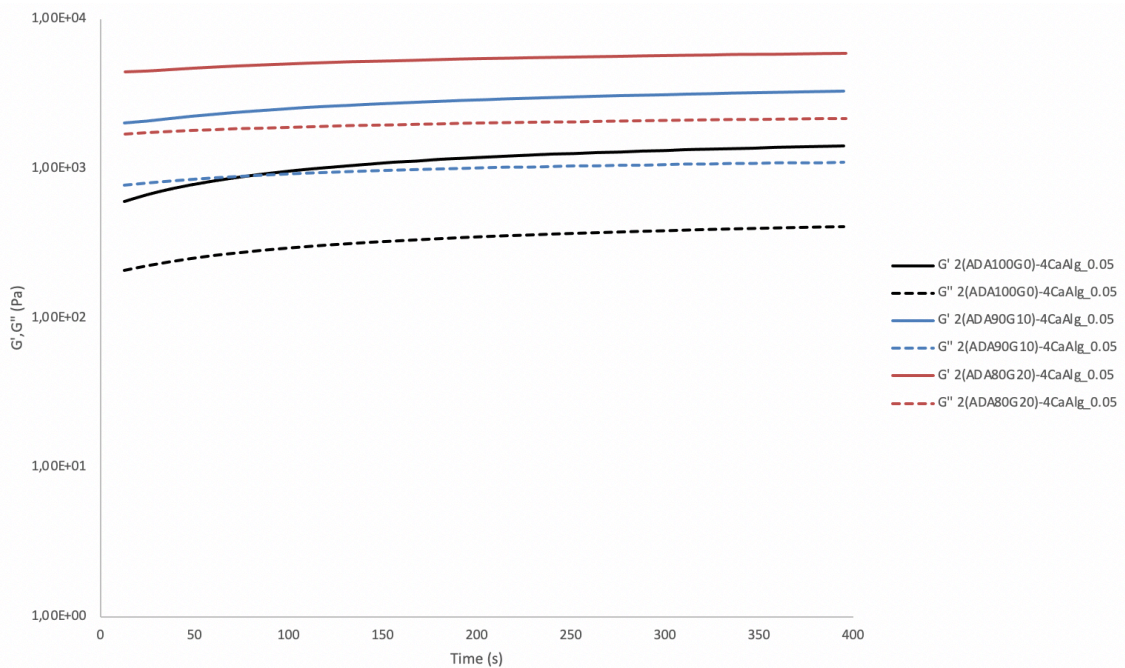


**Figure 4.25.** Results of oscillation time test on ADAGEL/Ca<sup>2+</sup>-Alg hydrogels.

As can be observed from the figure, ADA/GEL-based hydrogels followed a similar gelling pattern. However, the gelling trend related to ADA100:GEL0 ratio presented a higher slope, thus indicated that the onset of the sol-gel transition was delayed in time for gelatin-free hydrogels. Therefore, the influence of gelatin concentration on the gelling time was found to be particularly striking. Since the gelling time decreased with increase in the concentration of gelatin, it demonstrated that not only calcium ions, but the ability of ADA aldehyde groups to complex with amino groups could be responsible for the gelation.

Frequency sweep tests were carried out within the LVE Region of each hydrogel, thus determining the material frequency dependence, in the range of angular frequency between 0.1 and 100 rad/s. The results of the tests are reported in Figure 4.26.

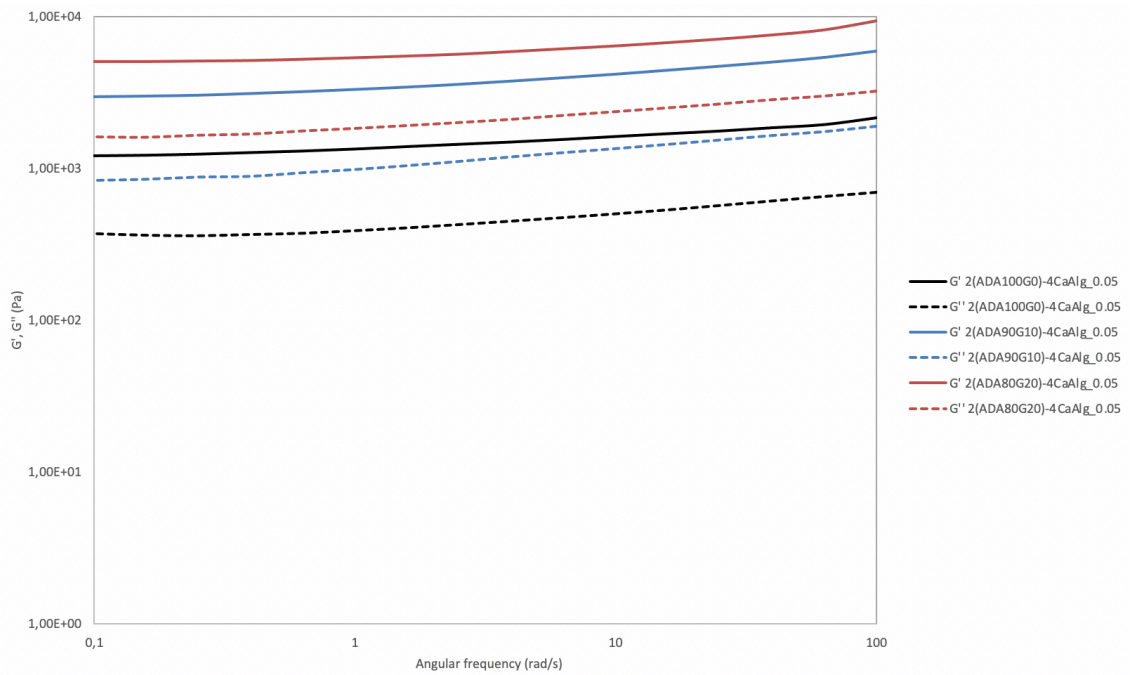


**Figure 4.26.** (A) Results of oscillation frequency test on ADAGEL/ $\text{Ca}^{2+}$ -Alg hydrogels.

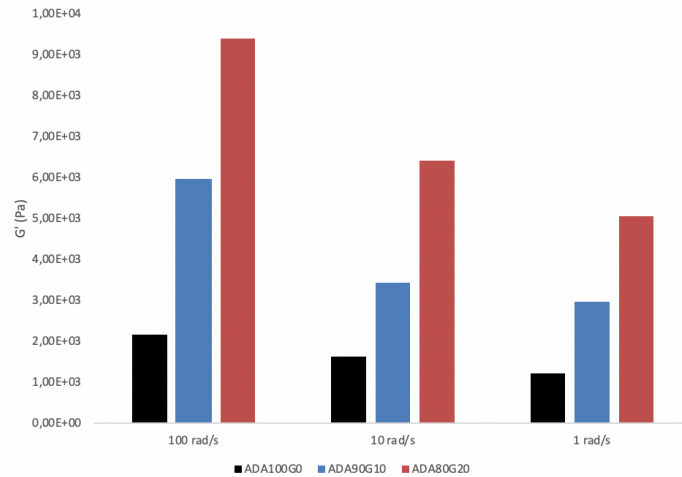


**Figure 4.26. (B)** Storage moduli of ADAGEL/ $\text{Ca}^{2+}$ -Alg hydrogels at a strain of 100%, 10% and 1%.

All the hydrogels presented  $G'$  always higher than  $G''$ , denoting a solid structure with a predominant elastic behavior. Furthermore, both  $G'$  and  $G''$  were poorly dependent on the applied frequency for all the hydrogel, thus indicating that for these samples the material response did not account for the viscous component. As the previous oscillation tests, frequency sweep measurements pointed out a positive correlation between gelatin content and storage modulus. As the  $\text{Ca}^{2+}$ -Alg<sub>0.05</sub> content was kept constant in all the formulations, the increase in  $G'$  was strictly related to the higher number of Schiff base bonds. Moreover, hydrogels were tested at physiological temperature, therefore the results were minimally affected by the thermogelling behavior of gelatin. Hence, ADA/GEL ratio fitted the number of the available aldehydic binding sites leading to the *in situ* formation of the expected hydrogel.

Under the tested conditions, the crosslinking process was found to be ascribed to both Schiff base formation between the free  $\epsilon$ -amino groups of lysine and hydroxylysine of GEL and the ADA aldehyde groups, and calcium-diol complexation between  $\text{Ca}^{2+}$ -Alg particles and the hydroxyl groups of ADA.



## V. CONCLUSION

---

Myocardial infarction is one of the leading causes of death all over the world. For the surviving patients, worsening of the disease will lead as well to fatal condition. To date, the only effective therapeutic approach to avoid heart failure is the heart transplantation. However, this strategy is limited by the lack of donors.

Currently, new regenerative strategies are under investigation. Among the ongoing studies, the European BIORECAR-ERC-2017-CoG project proposes a new regenerative approach based on cellular direct reprogramming by using an injectable hydrogel to *in situ* delivery therapeutic agents.

The present thesis project was carried out with the aim was to show that an injectable, *in situ* forming, biocompatible, and biodegradable polymer scaffold can be formulated starting from widely investigated biopolymers, such as oxidized alginate and gelatin. ADA was synthesized by partial periodate oxidation of sodium alginate. ATR-FTIR and  $^{13}\text{C}$  NMR analysis showed the successful formation of aldehyde groups. The synthesis was repeated in triplicate following the same protocol and yield of production and oxidation degree confirmed the reliability of the process.

ADA is characterized by the presence of aldehyde groups, which can form Schiff base bond with molecules containing amino groups, such of gelatin. ADA biodegradation was improved because of the lower  $M_w$  and the formed aldehyde groups which are susceptible to hydrolysis. In addition, as GEL contains RGD sequences, also ADA bioactivity and biocompatibility were enhanced because of the formation of cell-interacting regions for cell adhesion and proliferation.

GEL was added to the hydrogel composition not only to increase its bioactivity and biocompatibility, but also to enhance the mechanical properties of ADA-based

hydrogels. Therefore, chemical crosslinking between ADA and GEL was investigated. By employing ADA having appropriate  $M_w$  and oxidation degree, it is possible to achieve a rapid gelation between the polymers. However, gelation did not occur, due to the low oxidation degree obtained during ADA synthesis.

Thereafter, an extraneous crosslinking agent was employed to ionically crosslink ADA and GEL, thanks to the ADA property of undergo gelation in presence of divalent cations. Specifically, calcium alginate particles were used as  $Ca^{2+}$  source. Firstly, ADA: $Ca^{2+}$ -Alg ratio was assessed and the behavior of hydrogels obtained with higher ions concentration was investigated.

Generally, stiffer biomaterials exhibit good mechanical properties and can maintain their shape after the injection. However, breakage of the structure occurs for lower strain amplitude. On the other hand, the less the hydrogels stiffness the harder the mechanical strength to hold their structure. Hence, the aim was to obtain a hydrogel with the right balance between these two extremes. Rheological characterization and swelling and degradation study suggested 2ADA:4 $Ca^{2+}$ -Alg/6M as the most suitable composition. Then, GEL was added and different ADA:GEL ratio were tested using  $Ca^{2+}$ -Alg/3M. Gelation time and crosslinking degree of ADA-GEL hydrogels was successfully tailored by changing the ratio of ADA and GEL, which might also influence the degradation behavior of the hydrogels. Mechanical properties and shear modulus of the hydrogels were investigated by rheological measurements.

The aim was to obtain a hydrogel with mechanical stiffness resembling the one of Algisyl-LVR<sup>TM</sup> device or even higher, to better mechanically integrate with the cardiac tissue. Specifically, in normal patients shear elastic modulus is between 5 and 27 kPa during diastole and systole and increase two to eight times after MI.<sup>85</sup> The most suitable hydrogel was composition was 2(ADA<sub>80</sub>G<sub>20</sub>)-4CaAlg<sub>0.05</sub>/3M, with a shear elastic modulus of about 13 kPa.

Results obtained in this work may serve as a basis to make the process of ADA/GEL ionic crosslinking reproducible and reliable. This will be the starting point to put into practice the theoretical processes described in the thesis, therefore the

achievement of a cardiac tissue regeneration by recruiting resident cardiac fibroblasts and inducing their direct reprogramming into cardiomyocytes-like cells.

## VI. FUTURE PERSPECTIVES

---

Although the positive outcomes achieved during this thesis project several limitations emerged, and literature was revised to overcome them. Therefore, additional research was performed.

The first aim is to define improved and reproducible strategies for the biomaterial characterization, the formulation protocol to perform ionic crosslinking hydrogels. First of all, ADA molecular weight need to be defined to obtain a complete overview of the oxidation process. Then, a modulation of the parameters in ADA formulation protocol is required, aimed to achieving a higher oxidation degree. By knowing the molecular weight and changing the oxidation degree of ADA, the possibility to chemically crosslink ADA and GEL will be further investigated. Simultaneously, ionic crosslinking protocol will be optimized. The process to obtain  $\text{Ca}^{2+}$ -Alg particles was not reliable since experimental errors often occurred. Hydrogels formulated with this crosslinking agent exhibited high variability in their mechanical properties and swelling and degradation behavior. Therefore, other  $\text{Ca}^{2+}$  source will be investigated, for instance  $\text{CaCO}_3$  and glucono- $\delta$ -lactone (GDL).

Additional experiments are required to complete the characterization of blend hydrogels and identify the most suitable ADA:GEL ratio in terms of mechanical properties, degradation behavior and gelation time. Specifically, the previous formulation led to short gelation times which make the handling time shorter, and this is not feasible for intramyocardial injection.

NPs and miRNA release from the polymer matrix will be further evaluated. Specifically, NPs will be embedded also in ADA/GEL hydrogels and the release kinetic and their influence on the hydrogel dissolution will be investigated. By

analyzing the release media with DLS and ELS analysis, it will be possible to understand the release starting time point. Simultaneously, Qubit fluorometric analysis will quantify miRNA leakage from the NPs.

Once the hydrogel formulation will be defined and hydrogel and NPs characterization will be finished, it could be interesting to functionalize the injectable device with bioactive peptides such as thymosin  $\beta$ 4, in order to activate resident cells and recruit them to initiate self-repair process. In this way, NPs interaction and miRcombo release will be targeted towards cardiac fibroblasts.

The last goal will be testing the *in vitro* cytocompatibility and reprogramming efficiency of the NPs-loaded hydrogel. The outcomes of this last step will be presented in three groups. First, a comparative 2D *in vitro* cytocompatibility study among all compositions of ADA/GEL using human adult cardiac fibroblasts. Second, a comparative investigation of cardiac fibroblasts behavior during the interaction with ADA/GEL prepared by both chemical and ionic method. Third, analysis of the effect of miRNA-loaded NPs incorporation into ADA/GEL hydrogel on the reprogramming activity of human adult cardiac fibroblasts *in vitro*. If positive outcomes will be recorded, *in situ* direct reprogramming through injectable hydrogel will be further assessed *in vivo* condition using a 3D *in vivo* rat model.

In conclusion, the developed system is extremely promising for future application in the treatment of myocardial infarction.

## VII. BIBLIOGRAPHY

---

1. Sanchis-Gomar, F., Perez-Quilis, C., Leischik, R. & Lucia, A. Epidemiology of coronary heart disease and acute coronary syndrome. *Ann. Transl. Med.* **4**, 1–12 (2016).
2. MAGIDSON, O. Myocardial infarction. *Med. Press* **226**, 435–439 (1951).
3. Thygesen, K. *et al.* Fourth Universal Definition of Myocardial Infarction (2018). *J. Am. Coll. Cardiol.* **72**, 2231–2264 (2018).
4. Frangogiannis, N. G. Pathophysiology of myocardial infarction. *Compr. Physiol.* **5**, 1841–1875 (2015).
5. De Lemos, J. A., Newby, L. K. & Mills, N. L. A Proposal for Modest Revision of the Definition of Type 1 and Type 2 Myocardial Infarction. *Circulation* **140**, 1773–1775 (2019).
6. Paiva, L. *et al.* Universal definition of myocardial infarction: Clinical insights. *Cardiol.* **131**, 13–21 (2015).
7. Frangogiannis, N. G. The extracellular matrix in myocardial injury, repair, and remodeling. *J. Clin. Invest.* **127**, 1600–1612 (2017).
8. Manuscript, A. Fibroblasts in myocardial infarction: a role in inflammation and repair. 74–82 (2015) doi:10.1016/j.yjmcc.2013.11.015.Fibroblasts.
9. M. Christopher, A. M. L. S. The Biological Basis for Cardiac Repair After Myocardial Infarction: From Inflammation to Fibrosis. *Physiol. Behav.* **176**, 100–106 (2016).
10. Hashimoto, H., Olson, E. N. & Bassel-Duby, R. Therapeutic approaches for cardiac regeneration and repair. *Nat. Rev. Cardiol.* **15**, 585–600 (2018).
11. Ferrini, A., Stevens, M. M., Sattler, S. & Rosenthal, N. Toward Regeneration of the Heart: Bioengineering Strategies for Immunomodulation. *Front. Cardiovasc. Med.* **6**, (2019).
12. Scibona, E. & Morbidelli, M. Expansion processes for cell-based therapies.

- Biotechnol. Adv.* **37**, 107455 (2019).
13. Kuraitis, D., Giordano, C., Suuronen, E. J. & Ruel, M. *Cell therapy to regenerate the ischemic heart. Cardiac Regeneration and Repair* vol. 1 (Woodhead Publishing Limited, 2014).
  14. Machado-Júnior, P. A. B., Blume, G. G., Francisco, J. C. & Guarita-Souza, L. C. Cell-Based Therapies for Myocardial Regeneration in Heart Failure: 20 Years of Debate. *Brazilian J. Cardiovasc. Surg.* **35**, VIII–XI (2020).
  15. Ghiroldi, A. *et al.* Cell-based therapies for cardiac regeneration: A comprehensive review of past and ongoing strategies. *Int. J. Mol. Sci.* **19**, (2018).
  16. Isomi, M., Sadahiro, T. & Ieda, M. Progress and Challenge of Cardiac Regeneration to Treat Heart Failure. *J. Cardiol.* **73**, 97–101 (2019).
  17. Yu, H., Lu, K., Zhu, J. & Wang, J. Stem cell therapy for ischemic heart diseases. *Br. Med. Bull.* **121**, 135–154 (2017).
  18. Bar, A. & Cohen, S. Inducing Endogenous Cardiac Regeneration: Can Biomaterials Connect the Dots? *Front. Bioeng. Biotechnol.* **8**, (2020).
  19. Chen, Y., Yang, Z., Zhao, Z. A. & Shen, Z. Direct reprogramming of fibroblasts into cardiomyocytes. *Stem Cell Res. Ther.* **8**, 1–8 (2017).
  20. Cahill, T. J., Choudhury, R. P. & Riley, P. R. Heart regeneration and repair after myocardial infarction: Translational opportunities for novel therapeutics. *Nat. Rev. Drug Discov.* **16**, 699–717 (2017).
  21. Loscalzo, D. E. H. R. C. J. Direct Reprogramming of Fibroblasts into Functional Cardiomyocytes by Defined Factors. *Bone* **23**, 1–7 (2011).
  22. Kang, M. H. *et al.* Optimizing delivery for efficient cardiac reprogramming. *Biochem. Biophys. Res. Commun.* **533**, 9–16 (2020).
  23. Qian, L. *et al.* In vivo reprogramming of murine cardiac fibroblasts into induced cardiomyocytes. **485**, 593–598 (2012).
  24. Georgiadis, V., Knight, R. A., Jayasinghe, S. N. & Stephanou, A. Cardiac tissue engineering: Renewing the arsenal for the battle against heart disease. *Integr. Biol. (United Kingdom)* **6**, 111–126 (2014).
  25. Cassani, M. *et al.* Combining Nanomaterials and Developmental Pathways to Design New Treatments for Cardiac Regeneration: The Pulsing Heart of

- Advanced Therapies. *Front. Bioeng. Biotechnol.* **8**, (2020).
26. Muniyandi, P. *et al.* Poly(lactic- co -glycolic acid)/Polyethylenimine Nanocarriers for Direct Genetic Reprogramming of MicroRNA Targeting Cardiac Fibroblasts . *ACS Appl. Nano Mater.* **3**, 2491–2505 (2020).
  27. Breiding, M. J. A New Era of Cardiac Cell Therapy: Opportunities and Challenges. *Physiol. Behav.* **63**, 1–18 (2014).
  28. Fasbender, A. *et al.* Effect of co-lipids in enhancing cationic lipid-mediated gene transfer in vitro and in vivo. *Gene Ther.* **4**, 716–725 (1997).
  29. Mahato, R. I., Smith, L. C. & Rolland, A. Pharmaceutical Perspectives of Nonviral Gene Therapy. *Adv. Genet.* **41**, 95–156 (1999).
  30. Letizia Nicoletti, Camilla Paoletti, Giulia Tarricone, Ilaria Andreana, Barbara Stella, Silvia Arpicco, Carla Divieto, Clara Mattu, V. C. Lipoplexes for Effective In Vitro Delivery of MicroRNAs to Human Adult Cardiac Fibroblasts for Perspective Direct Cardiac Cell Reprogramming\_draft AHM 310521.
  31. Daniele Testore, Letizia Nicoletti, Clara Mattu, V. C. Design of bioartificial nanoparticles as microRNA delivery system. *Master Degree Thesis, Politec. di Torino* (2020).
  32. Cosco, D. *et al.* Delivery of miR-34a by chitosan/PLGA nanoplexes for the anticancer treatment of multiple myeloma. *Sci. Rep.* **5**, 1–11 (2015).
  33. Gascón, A. R. & Pedraz, J. L. Cationic lipids as gene transfer agents: A patent review. *Expert Opin. Ther. Pat.* **18**, 515–524 (2008).
  34. Catoira, M. C., Fusaro, L., Di Francesco, D., Ramella, M. & Boccafoschi, F. Overview of natural hydrogels for regenerative medicine applications. *J. Mater. Sci. Mater. Med.* **30**, (2019).
  35. Laftah, W. A., Hashim, S. & Ibrahim, A. N. Polymer hydrogels: A review. *Polym. - Plast. Technol. Eng.* **50**, 1475–1486 (2011).
  36. Hoffman, A. S. Hydrogels for biomedical applications. *Adv. Drug Deliv. Rev.* **64**, 18–23 (2012).
  37. Ahmed, E. M. Hydrogel: Preparation, characterization, and applications: A review. *J. Adv. Res.* **6**, 105–121 (2015).
  38. Radhakrishnan, J., Krishnan, U. M. & Sethuraman, S. Hydrogel based

- injectable scaffolds for cardiac tissue regeneration. *Biotechnol. Adv.* **32**, 449–461 (2014).
39. Saludas, L., Pascual-Gil, S., Prósper, F., Garbayo, E. & Blanco-Prieto, M. Hydrogel based approaches for cardiac tissue engineering. *Int. J. Pharm.* **523**, 454–475 (2017).
  40. Hasan, A. *et al.* Injectable Hydrogels for Cardiac Tissue Repair after Myocardial Infarction. *Adv. Sci.* **2**, 1–18 (2015).
  41. Carballo-Pedrares, N., Fuentes-Boquete, I., Díaz-Prado, S. & Rey-Rico, A. Hydrogel-based localized nonviral gene delivery in regenerative medicine approaches—an overview. *Pharmaceutics* **12**, 1–21 (2020).
  42. Wang, L. L. *et al.* Sustained miRNA delivery from an injectable hydrogel promotes cardiomyocyte proliferation and functional regeneration after ischaemic injury. *Nat. Biomed. Eng.* **1**, 983–992 (2017).
  43. Van Vlierberghe, S., Dubruel, P. & Schacht, E. Biopolymer-based hydrogels as scaffolds for tissue engineering applications: A review. *Biomacromolecules* **12**, 1387–1408 (2011).
  44. Peña, B. *et al.* Injectable Hydrogels for Cardiac Tissue Engineering. *Physiol. Behav.* **176**, 139–148 (2016).
  45. Nasr, S. M. *et al.* Biodegradable nanopolymers in cardiac tissue engineering: From concept towards nanomedicine. *Int. J. Nanomedicine* **15**, 4205–4224 (2020).
  46. Alagarsamy, K. N., Yan, W., Srivastava, A., Desiderio, V. & Dhingra, S. Application of injectable hydrogels for cardiac stem cell therapy and tissue engineering. *Rev. Cardiovasc. Med.* **20**, 221–230 (2019).
  47. Li, Y., Meng, H., Liu, Y. & Lee, B. P. Fibrin gel as an injectable biodegradable scaffold and cell carrier for tissue engineering. *Sci. World J.* **2015**, (2015).
  48. Urciuolo, A. & De Coppi, P. Decellularized tissue for muscle regeneration. *Int. J. Mol. Sci.* **19**, 1–11 (2018).
  49. Chiu, L. L. Y. & Radisic, M. Controlled release of thymosin  $\beta$ 4 using collagen-chitosan composite hydrogels promotes epicardial cell migration and angiogenesis. *J. Control. Release* **155**, 376–385 (2011).

50. Thottappillil, N. & Nair, P. D. Scaffolds in vascular regeneration: Current status. *Vasc. Health Risk Manag.* **11**, 79–91 (2015).
51. Sarker, B. Advanced Hydrogels Concepts Based on Combinations of Alginate , Gelatin and Bioactive Glasses for Tissue Engineering Entwicklung anwendungsspezifischer Hydrogelkonzepte basierend auf der Kombination von Alginat , Gelatine und bioaktivem Glas für das Tissue. 206 (2015).
52. Puscaselu, R. G., Lobiuc, A., Dimian, M. & Covasa, M. Alginate: From food industry to biomedical applications and management of metabolic disorders. *Polymers (Basel)*. **12**, 1–30 (2020).
53. Lee, K. Y. & Mooney, D. J. Alginate: Properties and biomedical applications. *Prog. Polym. Sci.* **37**, 106–126 (2012).
54. Smith, A. M. & Senior, J. J. Alginate Hydrogels with Tuneable Properties. (2021) doi:10.1007/10\_2020\_161.
55. Szekalska, M., Puciłowska, A., Szymańska, E., Ciosek, P. & Winnicka, K. Alginate: Current Use and Future Perspectives in Pharmaceutical and Biomedical Applications. *Int. J. Polym. Sci.* (2016) doi:10.1155/2016/7697031.
56. Ruvinov, E. & Cohen, S. Alginate biomaterial for the treatment of myocardial infarction: Progress, translational strategies, and clinical outlook. From ocean algae to patient bedside. *Adv. Drug Deliv. Rev.* **96**, 54–76 (2016).
57. Mchugh, D. J. Chapter 2 - Production, Properties and Uses of Alginates. *FAO Food Agric. Organ. United Nations* 1–42 (2013).
58. Cattelan, G. *et al.* Alginate Formulations: Current Developments in the Race for Hydrogel-Based Cardiac Regeneration. *Front. Bioeng. Biotechnol.* **8**, (2020).
59. Lee, R. J. *et al.* The feasibility and safety of Algisyl-LVR™ as a method of left ventricular augmentation in patients with dilated cardiomyopathy: Initial first in man clinical results. *Int. J. Cardiol.* **199**, 18–24 (2015).
60. Melvik, J.-E., Dornish, M., Onsoyen, E., Berge, Astrid, B. & Svendsen, T. Self-gelling alginate systems and uses thereof. (2006).
61. Frey, N. *et al.* Intracoronary delivery of injectable bioabsorbable scaffold (IK-5001) to treat left ventricular remodeling after ST-elevation myocardial

- infarction: A first-in-man study. *Circ. Cardiovasc. Interv.* **7**, 806–812 (2014).
62. Bialystok, E. Prognosis of Adults with Borderline Left Ventricular Ejection Fraction. *Physiol. Behav.* **176**, 139–148 (2017).
  63. Rao, S. V. *et al.* Bioabsorbable Intracoronary Matrix for Prevention of Ventricular Remodeling After Myocardial Infarction. *J. Am. Coll. Cardiol.* **68**, 715–723 (2016).
  64. Traverse, J. H. *et al.* First-in-Man Study of a Cardiac Extracellular Matrix Hydrogel in Early and Late Myocardial Infarction Patients. *JACC Basic to Transl. Sci.* **4**, 659–669 (2019).
  65. Lou, K.-J. VentriGel goes into pigs. *Sci. Exch.* **6**, 232–232 (2013).
  66. Reakasame, S. & Boccaccini, A. R. Oxidized Alginate-Based Hydrogels for Tissue Engineering Applications: A Review. *Biomacromolecules* **19**, 3–21 (2018).
  67. Balakrishnan, B., Lesieur, S., Labarre, D. & Jayakrishnan, A. Periodate oxidation of sodium alginate in water and in ethanol-water mixture: A comparative study. *Carbohydr. Res.* **340**, 1425–1429 (2005).
  68. Bouhadir, K. H. *et al.* Degradation of partially oxidized alginate and its potential application for tissue engineering. *Biotechnol. Prog.* **17**, 945–950 (2001).
  69. Srivastava, D. Making or Breaking the Heart: From Lineage Determination to Morphogenesis. *Cell* **126**, 1037–1048 (2006).
  70. Srivastava, D., Ieda, M., Fu, J. & Qian, L. Cardiac repair with thymosin  $\beta$ 4 and cardiac reprogramming factors. *Ann. N. Y. Acad. Sci.* **1270**, 66–72 (2012).
  71. Bollini, S., Riley, P. R. & Smart, N. Thymosin  $\beta$ 4: Multiple functions in protection, repair and regeneration of the mammalian heart. *Expert Opin. Biol. Ther.* **15**, 163–174 (2015).
  72. Gupta, S. *et al.* Thymosin  $\beta$ 4 and cardiac protection: Implication in inflammation and fibrosis. *Ann. N. Y. Acad. Sci.* **1269**, 84–91 (2012).
  73. Lei Ye, Pengyuan Zhang, Sue Duval, Liping Su, Qiang Xiong, and J. Z. Thymosin  $\beta$ 4 increases the potency of transplanted mesenchymal stem cells for myocardial repair. *Bone* **23**, 1–7 (2008).
  74. Paoletti, C. *et al.* MicroRNA-Mediated Direct Reprogramming of Human

- Adult Fibroblasts Toward Cardiac Phenotype. *Front. Bioeng. Biotechnol.* **8**, 1–9 (2020).
75. Sarker, B. *et al.* Evaluation of fibroblasts adhesion and proliferation on alginate-gelatin crosslinked hydrogel. *PLoS One* **9**, 1–12 (2014).
  76. Neira-Velázquez, M. G., Rodríguez-Hernández, M. T., Hernández-Hernández, E. & Ruiz-Martínez, A. R. Y. Polymer Molecular Weight Measurement. *Handb. Polym. Synth. Charact. Process.* 355–366 (2013)  
doi:10.1002/9781118480793.ch17.
  77. Masuelli, M. A. & Illanes, C. O. Review of the characterization of sodium alginate by intrinsic viscosity measurements . Comparative analysis between conventional and single point methods. *Int. J. Biomater. Sci. Eng.* **1**, 1–11 (2014).
  78. Sarker, B. *et al.* Fabrication of alginate-gelatin crosslinked hydrogel microcapsules and evaluation of the microstructure and physico-chemical properties. *J. Mater. Chem. B* **2**, 1470–1482 (2014).
  79. Emami, Z., Ehsani, M., Zandi, M. & Foudazi, R. Controlling alginate oxidation conditions for making alginate-gelatin hydrogels. *Carbohydr. Polym.* **198**, 509–517 (2018).
  80. Genç, H. *et al.* Differential responses to bioink-induced oxidative stress in endothelial cells and fibroblasts. *Int. J. Mol. Sci.* **22**, 1–21 (2021).
  81. Pettignano, A. *et al.* Self-healing alginate-gelatin biohydrogels based on dynamic covalent chemistry: Elucidation of key parameters. *Mater. Chem. Front.* **1**, 73–79 (2017).
  82. Distler, T. *et al.* Neuronal differentiation from induced pluripotent stem cell-derived neurospheres by the application of oxidized alginate-gelatin-laminin hydrogels. *Biomedicines* **9**, (2021).
  83. Larsen, B. E., Bjørnstad, J., Pettersen, E. O., Tønnesen, H. H. & Melvik, J. E. Rheological characterization of an injectable alginate gel system. *BMC Biotechnol.* **15**, 1–12 (2015).
  84. Clogston, J. D. & Patri, A. K. Zeta potential measurement. *Methods Mol. Biol.* **697**, 63–70 (2011).
  85. Pislaru, C., Urban, M. W., Pislaru, S. V., Kinnick, R. R. & Greenleaf, J. F.

Viscoelastic Properties of Normal and Infarcted Wave Method : Comparison With Pressure-Segment Length Method. *Ultrasound Med Biol* **40**, 1785–1795 (2014).